

Università
Ca'Foscari
Venezia

Ph.D. Course

in Science and Management of Climate Change

36th cycle

Research Thesis

Three essays on carbon cycle and land-atmosphere interactions

SSD: GEOS-04/C

Ph.D. Program Coordinator
Prof. Enrica De Cian

Supervisor
Prof. Davide Zanchettin

Ph.D. Candidate
Matteo Mastropierro
Matricola 956554

Acknowledgements

This thesis is dedicated to my family that has always nurtured my curiosity and supported my life choices, laying the foundations for the achievement of this goal.

I would like to thank my supervisor Prof. Dr. Davide Zanchettin, for his trust on my research ideas and for backing my work during these years.

I have to thank also my coauthors Dr. Daniele Peano and Dr. Katsumata Tanaka, for their fruitful feedbacks and discussions for the conceptualization of the chapters, and also a thank to Irina, for her trustful help during the first months of research.

I want to thank Prof. Dr. Enrica De Cian, coordinator of PhD program, for being always available to help us students and improving the PhD program.

I have to thank my colleagues MK, Laura and Marghe for the mutual support during the difficulties and challenges of this journey.

Finally, I very much need to say thank you to Giulia, for sharing the best moments of this PhD in Venice, and for helping me trust my capabilities.

Audentes Fortuna Iuvat

Abstract

This thesis characterizes the carbon cycle and land-atmosphere interactions through a multifaceted approach and perspective. It integrates insights from three distinct research studies, each one addressing a critical aspect influencing the modelling of the carbon cycle, its estimates and associated uncertainties. The first explores the role of non-CO_2 forcings in overshoot scenarios, investigating the carbon budget implications of the role of CH_4, as a short-lived climate pollutant. By adopting a newly developed conversion metric for CO_2-eq in overshoot scenarios, results of the first chapter indicate a misrepresentation of the temperature equivalency, particularly on long-term timescales and rapid mitigation pathways. In the second chapter, carbon-climate feedbacks within the Amazon basin ecosystem, a crucial component of the terrestrial carbon cycle, are examined. Taking advantage of CMIP6 generation Earth System Models, the influence of mean-state changes and interannual variability on ecosystem productivity are exposed, thus identifying the main drivers of future net carbon sink projections as well as factors of models uncertainties. The last chapter of the thesis explores the biophysical implications of a large-scale afforestation/reforestation LUMIP simulation, a land-based climate mitigation solution. Focusing on the surface energy balance reveals that higher mitigation potential, with respect to surface temperatures, is achieved in correlation with water-limited environments, despite the drawback of water resources depletion, due an enhancement of evaporative cooling.

Table of Contents

Acknowledgements 1

Abstract 2

Table of Contents 3

Introduction 6

Physical and policy perspectives on Carbon budget and net-zero 6

The role of tropical ecosystems in controlling CO_2 atmospheric accumulation 8

Biophysical effect of afforestation 10

Thesis structure and research contribution 11

1 Chapter 1: Testing GWP* to quantify non-CO_2 contributions in the carbon budget under overshoot scenarios 13

1.1 Abstract 13

1.2 Introduction 14

1.3 Data and Methods 18

1.3.1 Description of three reduced-complexity models 18

1.3.2 Carbon cycle parameters in ACC2 20

1.3.3 Emulating ACC2 to CMIP6 ESMs 22

1.4 Results and Discussion 25

1.4.1 Testing the temperature equivalency of GWP* under SSPs 25

1.4.2 Using GWP* to quantify the overshoot carbon-eq budget of overshoot scenarios 28

1.4.3 TCRE of the ramp-up and ramp-down phases of overshoot scenarios 36

1.5 Conclusions 40

Code and Data Availability: 41

Annex 42

2 Chapter 2: Drivers of Amazon carbon sink projections and uncertainty in CMIP6 models 55

2.1 Abstract 55

2.2 Introduction 56

2.3 Data and Methods 59

2.3.1 Data 59

2.3.2 Long-term mean-state climatic effects 61

2.3.3 Carbon fluxes sensitivity at inter-annual timescales 62

2.4 Results and Discussion 64

2.4.1 Intermodel uncertainties of carbon and climatic drivers 64

2.4.2 Long-term carbon sink sensitivity 66

2.4.3 Inter-annual variability of carbon fluxes 70

2.4.4 ENSO modulation 74

2.5 Conclusions 77

Code and Data Availability 79

Annex 81

3 Chapter 3: Emerging trade-offs in the deployment of large-scale Afforestation in a high CO_2 climate 93

3.1 Abstract 93

3.2 Introduction 94

3.3 Data and Methods 97
3.3.1 Data 97
3.3.2 Surface Energy Balance (SEB) decomposition 99
3.3.3 Intrinsic Biophysical Mechanism (IBPM) decomposition 100
3.3.4 Sensitivity of turbulent fluxes to changes in LAI 100
3.4 Results and Discussion 101
3.4.1 SEB and IBPM decomposition 101
3.4.2 Cooling mechanisms and hydrological implications 106
3.5 Conclusions 110
Code and Data Availability 111
Annex 112
Thesis Conclusion 120
4 Bibliography 123

Introduction

Physical and policy perspectives on Carbon budget and net-zero

At the end of 2023, CO_2 concentrations in the atmosphere at the Mauna Loa observatory have reached the annual mean value of 421.08±0.12 ppm (mole fraction in dry air) (Keeling *et al.*, 2001), leading to a Global Mean Surface Temperature of 14.98 °C , standing as 1.48 °C warmer than the 1850-1900 pre-industrial level (Copernicus Climate Change Service (C3S), 2017). This temperature level is worryingly close to the Paris Agreement (PA) temperature limit of 1.5 °C of anthropogenic warming, which aims to prevent widespread climatic impacts and socioeconomic consequences. This observed global warming is roughly linearly proportional to the cumulative amount of CO_2 emitted in the atmosphere, therefore making it possible to relate the two quantities defining the Transient Climate Response to Cumulative Emissions (TCRE) (Allen *et al.*, 2009; Matthews *et al.*, 2009). TCRE represents the ratio of CO_2 induced warming per unit of cumulative carbon dioxide emissions, and according to the most recent estimates from the IPCC AR6, it falls likely within the range of 1.0 – 2.3 °C per 1000 GtC (or 0.27 – 0.63 °C per 1000 $GtCO_2$), with a median estimate of 1.65 °C per 1000 GtC (0.45 °C per 1000 $GtCO_2$) (Canadell *et al.*, 2021). The TCRE relationship provides the basis for the concept of carbon budget, which is defined as the amount of carbon dioxide emissions that would be needed to limit global warming below a specific level. Similarly, a remaining carbon budget is the amount of CO_2 that can be emitted from present day before reaching a temperature target. Under the assumption that residual warming after CO_2 emission cease is negligible, a remaining carbon budget could be estimated directly from TCRE, with the precaution of accounting for sources of uncertainty (i.e. from non-CO_2 forcing and scenarios, unrepresented Earth system feedbacks, historical temperature uncertainty, zero emission commitment, see Table 5.8 in Canadell et al.,

(2021)(Canadell *et al.*, 2021) (Rogelj, Shindell, *et al.*, 2018; Rogelj, Forster, *et al.*, 2019; Matthews *et al.*, 2020; Damon Matthews *et al.*, 2021). From the physical perspective, given the prominent PA goals of limit global warming within 1.5 °C or "well below" 2 °C, two conditions are required and must be met to have high probabilities of achieving these targets. First, as reported before, the remaining carbon budget must not be exceeded, with the precaution of maintaining an emission buffer to account for the above-mentioned uncertainties. Second, another necessary condition is temperature stabilization, for which approximately net-zero CO_2 emissions must be reached to avoid further warming over multi-decadal timescales (Jenkins *et al.*, 2022). From the policy perspective net-zero is a very clear climatic ambition, with several national, international and private corporate pledges defining a date for the net-zero goal, up to the point that, at the moment, roughly 90% of all countries emissions are covered by net-zero CO_2 emissions plans (*Net Zero Tracker | NewClimate Institute*, no date). Still, the exact conditions for CO_2-induced temperature stabilization are still uncertain and may depend on the multi-century carbon and thermal cycle responses and, additionally, these do not guarantee that total warming is ceased, since non-CO_2 warming must be accounted for. Therefore, policy must focus on a urgent and drastic reduction of anthropogenic CO_2 emissions, at least of an order of magnitude compared to the current rates, to eventually halt global warming.

In a real world context with multiple GHGs, properly accounting for non-CO_2 warming is of paramount importance, given their role in the estimation of the remaining carbon budget. In particular, the impacts of non-CO_2 emissions on the remaining carbon budgets can be assessed with several methodologies (Jenkins *et al.*, 2018; Rogelj, Shindell, *et al.*, 2018; Matthews *et al.*, 2020; Damon Matthews *et al.*, 2021), but their applicability and uncertainties have not yet been explored in depth. Therefore, the focus of the first chapter of the thesis is to investigate on the potential applicability of a metric of conversion for non-CO_2 Short Lived Climate Pollutants (SLCP) into CO_2-equivalent emissions, with a specific emphasis on overshoot scenarios. The consideration of overshoot scenarios is justified by the

imminent chances of temperature overshooting 1.5 °C; indeed, the vast majority of scenarios compatible with meeting the PA targets are temperature overshoot scenarios.

The role of tropical ecosystems in controlling CO_2 atmospheric accumulation

Reaching approximately net-zero CO_2 emissions implies halting the net accumulation of carbon dioxide in the atmosphere, which is controlled and dampened by the dynamic exchange of carbon between multiple reservoirs in the atmosphere itself, in the ocean and on land. In particular, the terrestrial biosphere and its carbon sinks are influenced by climate and by atmospheric CO_2 concentrations, and modulate the rate at which carbon from anthropogenic emissions accumulates in the atmosphere, the so-called airborne fraction, by amplifying or dampening climate change signal (Allen *et al.*, 2009; Archer *et al.*, 2009; Ballantyne *et al.*, 2012). Terrestrial ecosystems have played a fundamental role in absorbing a large share of cumulative carbon emitted by anthropogenic activities since 1850, approximately 32%, corresponding to 3.3 $\pm$0.8 GtC $year^{-1}$ during 2013-2022 (Friedlingstein *et al.*, 2023). This modulation is the direct consequence of two major land carbon feedbacks: a negative carbon concentration feedback (due to the CO_2 fertilization effect) and a positive carbon-climate feedback (Gregory *et al.*, 2009). The former denotes a higher leaf-level photosynthesis as a direct consequence of increased atmospheric CO_2, due to a partial stomata closure effect and therefore reduced transpiration rates (denoted as an increased Water Use Efficiency, WUE). The latter, on the other hand, implies a predominantly negative impact of climate change on land carbon uptake, related to higher decomposition rates of soil carbon, increased droughts, fires and generally speaking extreme events, despite the high uncertainties in the magnitude and geographical extent of the feedback (Friedlingstein *et al.*, 2006; K. Arora *et al.*, 2020). As a consequence of the carbon-climate feedback magnitude uncertainty, the representation of the land carbon sink evolution during the historical period was the highest source of uncertainty in the global carbon cycle compared to observation-based estimates from the Global Carbon Project (Friedlingstein *et*

al., 2023). This is due in part to the current limitations in the Earth System Models (ESMs) representation of specific processes (e.g. land-use change, nutrient limitation, vegetation dynamics and disturbances), and for these reasons it will be very likely that land carbon will continue to dominate the overall uncertainty in the projected response of global carbon cycle to climate change (Canadell *et al.*, 2021). Here lies the first motivation for the second chapter of the thesis, which aims to investigate the Amazon ecosystem response in ESMs to a future high radiative forcing climate change scenario. The focus on the tropical Amazon is additionally motivated by mainly two other causes. First, because the adverse effects emerging from the carbon-climate feedback are expected to increasingly impact tropical ecosystems, and especially the Amazon. This, among other factors such as future deforestation rate, has eventually lead to hypothesize for the Amazon a climatic tipping point, with potential significant consequences for the Earth system. Second, the focus on the Amazon ecosystem is motivated by the reason that tropical land ecosystems dominate the interannual variability of atmospheric carbon dioxide, a process that is mainly modulated by temperature, and is influenced by the dynamics of climatic modes of interannual variability (Zhu *et al.*, 2017; Piao *et al.*, 2020). Therefore, it is of particular relevance and scientific interest to explore the evolution of the Amazon not only to long-term changes in climatic and environmental conditions, but also its response to potential changes in climatic variability under a future climate change scenario. As if the Amazon will continue to be a net carbon sink in future decades, it depends on the balance and interplay among the atmospheric CO_2 fertilization effect, even if the fractional productivity increase will diminish at high concentrations, the long-term climatic changes, and the cumulative impacts of climatic modes of variability, among which El Nino Southern Oscillation (ENSO) is the dominant one. Thus, given the relevance of the Amazon in the Earth system and for the global carbon cycle, the second chapter of the thesis aims to investigate its evolution as projected by ESMs participating in the Coupled Model Intercomparison Project Phase 6 (CMIP6).

Biophysical effect of afforestation

The broad scientific focus of the second chapter was on the natural vegetation carbon fluxes, which are influenced by long-term environmental conditions and interannual climatic variability. On another note, the last chapter of this thesis examines the climatic consequences of direct human interferences with terrestrial vegetation and ecosystems, which are commonly referred to as Land Use and Land Cover Changes (LULCC) activities, including deforestation, afforestation, crop intensification and urbanization. Despite changes in land-use until mid 19th century remained small at the global scale, at present day, about three quarters of ice-free global land is interested by some sort of human activities (Lawrence *et al.*, 2016; Venter *et al.*, 2016; Erb *et al.*, 2017). During the historical period, LULCC exerted two contrasting effects globally: a biophysical cooling as a consequence of increased albedo (due to widespread deforestation), and a biogeochemical warming due to GHG emissions deriving from deforestation and agricultural activities (Pongratz *et al.*, 2010; Boysen *et al.*, 2014). Overall, the Effective Radiative Forcing (ERF) derived from biophysical effects of LULCC in the 1850-2014 period is estimated to be -0.11 ± 0.09 Wm^{-2}, leading to a net cooling at the surface of 0.10 ± 0.15 °C (Jia *et al.*, 2019; Smith *et al.*, 2020). During the 21st century, different mitigation strategies with considerable land-use changes are expected and have to be made in order to achieve the reduction of emissions required to meet the PA goals. Given that the land sector is expected to deliver about 25% of the GHG mitigation pledges, as indicated in the countries Nationally Determined Contribution (NDC), and that a substantial share of this commitment is represented by large-scale afforestation/reforestation, it is of paramount importance to assess the potential biophysical consequences of these policies (Grassi *et al.*, 2017). Consequently, the goal of this chapter is to assess the biophysical impacts of an idealized factorial afforestation experiment from the Land Use Model Intercomparison Project (LUMIP), representing a sustainable land-use scenario implemented on top of a high radiative forcing background climate (Lawrence *et*

al., 2016). Understanding this potential impact is fundamental to correctly assess the local and global effects of afforestation when implemented in the context of global warming.

Thesis structure and research contribution

The dissertation is organized as follows. The first chapter focuses on the carbon budget and on the implications of adopting a newly developed metric (Global Warming Potential-star, GWP*) for the conversion of Methane emissions into CO_2-equivalent. Specifically, overshoot scenarios are investigated, in which the Paris Agreement temperature targets of 1.5 °C and 2 °C are temporarily exceeded, and emissions rise and fall in order to ensure a long-term warming below the targets. This chapter is motivated on the one hand by the need to correctly address and represent the effects of Short Lived Climate Pollutants (SLCP) within a carbon budget framework, an issue that is worsened by the widespread and incorrect application of conventional CO_2-eq conversion metrics, most notably the Global Warming Potential-100 (GWP100). On the other hand, as a consequence of inadequate emissions reduction policy commitments, the need to address overshoot scenarios is becoming essential to keep global temperatures within the PA goals, as the majority of future low-emission scenarios are, generally speaking, peak and decline scenarios.

In chapter two, the focus in on one of the main component of the carbon budget, in particular land ecosystems, which modulate atmospheric CO_2 concentrations by means of vegetation photosynthesis, autotrophic and heterotrophic respiration. At interannual time-scales, tropical ecosystems are responsible for controlling the biggest share of carbon exchanges between land and the atmosphere and, among those, the most critical and endangered one is the Amazon basin rainforest ecosystem. Considering its importance in the Earth system, up to being hypothesized as one of the future climate tipping points, its response to a high radiative forcing scenario (ssp585) is investigated. In particular, long-term mean state changes and interannual climatic variability, among which ENSO (El Nino Southern

Oscillation) effects on the productivity of the Amazon ecosystem at the end of the 21st century are examined by using the outputs of several ESMs simulations. Additionally, the uncertainty affecting the Inter-Annual Variability (IAV) projections of the regional net carbon sink across ESMs is addressed by exploring the contribution of the underlying physical processes, revealing the main factors responsible for the inter-model spread at the inter-annual time scale.

Lastly, chapter three shifts the attention from the biogeochemical to the biophysical interactions between land and atmosphere. Here, the contribution of Land Use and Land Cover Changes (LULCC) to surface climatic conditions are examined by considering ESMs simulations of an hypothetical future afforestation/reforestation (A/R) scenario, characterized by low anthropogenic pressure on the land system (low deforestation rates and increased forest expansion) implemented in a high radiative forcing scenario. The A/R consequences on surface temperature are assessed by disentangling the physical processes leading to the partitioning of Surface Energy Balance (SEB), and by exploring the modulation of background climatic regimes, specifically water and energy-limitation on evapotranspiration and vegetation productivity. Lastly, the consequences for local water availability are explored to reveal potential trade-offs in the long-term sustainability of large-scale A/R policies.

1 Chapter 1: Testing GWP* to quantify non-CO_2 contributions in the carbon budget under overshoot scenarios

1.1 Abstract

The Global Warming Potential-star (GWP*) approach is a way to convert the emissions of short-lived climate forcers to CO_2-equivalent emissions while maintaining consistency with temperature outcomes. Here we evaluate the performance of GWP* when it is used to account for non-CO_2 gases within the carbon budget framework. We convert methane (CH_4) emissions to CO_2-equivalent emissions via GWP* and calculate the temperature through simple climate models. We show that GWP* can accurately convert CH_4 emissions to reproduce the temperature until 2100 under a variety of scenarios, including overshoot scenarios, except those with a rapid decline in CH_4 emissions. Beyond 2100, however, the use of GWP* can lead to temperature overestimation since it extends beyond its calibration range. Furthermore, we find that under scenarios designed to achieve identical temperature targets but with varying overshoot profiles, cumulative CO_2-eq budgets (GWP*-basis) generally increase with overshoot length and magnitude. This is driven by the internal dynamics of our model, as characterized by its negative zero-emission commitment. While the use of GWP* enhances such effects with increasing overshoot length, it exerts opposite effects with increasing overshoot magnitude.

1.2 Introduction

Anthropogenic climate change is caused by emissions of a range of greenhouse gases (GHGs) that widely vary with respect to their radiative efficiency, atmospheric lifetime, and therefore impact on climate system (Myhre *et al.*, 2013). To deal with GHGs of different characteristics on a common scale, the impact of non-CO_2 GHG emissions on climate is sometimes expressed in terms of carbon dioxide (CO_2) equivalent (CO_2-eq) emissions. In doing so, the emissions of non-CO_2 GHGs are converted to CO_2-eq emissions using GHG emission metrics (Tanaka *et al.*, 2010). The most widely used metric is the 100-year GWP (GWP100), which is defined as the time-integrated radiative forcing over 100 years following a pulse emission of one ton of a GHG divided by the corresponding quantity of one ton of CO_2 (Lashof and Ahuja, 1990; UNFCCC, 2023). Similarly, other metrics often considered are the GWP20 (with a 20-year reference time period) and the 100-year Global Temperature change Potential (GTP100), which is defined as the global temperature change following a pulse emission of one ton of a GHG after the reference time period of 100 years divided by the corresponding quantity of one ton of CO_2 (Shine *et al.*, 2007).

International climate treaties, such as the Kyoto Protocol and the Paris Agreement, commonly address multiple GHGs with the use of these metrics (especially GWP100, which has been used as the standard one) to mitigate climate change cost-effectively (Manne and Richels, 2001; O'Neill, 2003; Tol *et al.*, 2012; UNFCCC, 2018; Tanaka *et al.*, 2021). However, these metrics may not accurately capture the impacts of different GHGs on global surface air temperatures owing to their diverse residence times in the atmosphere. GHGs fall into two categories: short-lived climate pollutants (SLCPs) and long-lived climate pollutants (LLCPs) (Allen *et al.*, 2022). There have been decades-long efforts to provide a more accurate emission metric in terms of the consistency with radiative forcing or temperature (Wigley, 1998; Shine *et al.*, 2007; Tanaka *et al.*, 2009, 2013; Allen *et al.*, 2018; Cain *et al.*, 2019). GWP100 is not able to differentiate between the contrasting behavior on temperature

change caused by LLCP and SLCP emissions (Fuglestvedt *et al.*, 2003; Tanaka *et al.*, 2010; Pierrehumbert, 2014; Allen *et al.*, 2022).

CO_2, a LLCP, once emitted, will largely remain in the atmosphere (the so-called airborne fraction) with slightly declining concentrations for centuries to millennia (Archer *et al.*, 2009; Eby *et al.*, 2009; Joos *et al.*, 2013). The slightly declining concentrations lead to a near-stable warming due to the thermal inertia of the ocean (Tanaka and O'Neill, 2018). It is thus possible to relate cumulative CO_2 emissions to the temperature rise in an almost linear fashion through the widely used transient climate response to cumulative emissions (TCRE) (Allen *et al.*, 2009; Matthews *et al.*, 2009). This provides the basis for the 'remaining carbon budget approach', which holds for LLCPs.

In contrast, methane (CH_4), a SLCP, is removed from the atmosphere due to atmospheric chemistry processes on faster time-scales, and thus has a smaller turnover time in this reservoir. It is currently an active research question how to determine the contribution of CH_4 and other SLCPs in the 'carbon budget' framework (Rogelj, Forster, *et al.*, 2019; Lynch *et al.*, 2020; Mengis and Matthews, 2020; Damon Matthews *et al.*, 2021; Jenkins *et al.*, 2021). Unlike CO_2, a pulse emission of CH_4 or other SLCPs does not result in a near-stable warming; a stable warming is the consequence of an increase in the rate of CH_4 emissions (or other SLCP emissions). In other words, a one-off emission of CO_2 is comparable to a permanent increase in the emission rate of CH_4 in terms of the temperature outcome (Smith *et al.*, 2012; Allen *et al.*, 2016).

A new metric, GWP*, that captures this fundamental relationship has been proposed, allowing an integration of SLCPs into the carbon budget framework (Cain *et al.*, 2019). Starting from the work of Allen et al. (2018), the GWP* metric was built by considering a 20-year time interval to assess the rate of changes in SLCP emissions. More recently, Cain et al. (2019) (2019) further improved GWP* by incorporating the small multi-centennial warming effect arising from SLCP emissions, with an additional term representing the "stock" effect (comparable to the behavior of CO_2) on top of the term for the "flow" effect

originally proposed. Therefore, GWP* can be defined by combining the effects from the emission itself (stock) and the change in emissions (flow), with the coefficients s and r, respectively, in equation (1). CO_2-eq emissions (E_{CO2e}) of SLCP emissions can be calculated as follows:

$$E_{CO2e} = GWP_H \times \left[r \times \frac{\Delta E_{SLCP}}{\Delta t} \times H + s \times E_{SLCP}\right] \quad (1)$$

Here, the term ΔE_{SLCP} represents the change in the rate of SLCP emissions with respect to the preceding time interval Δt, whereas E_{SLCP} is the emission of the SLCP for that year, and GWP_H is the GWP value of the SLCP over the time horizon H. Originally, by fixing the coefficients r and s to 0.75 and 0.25, respectively, it was possible to assure a good approximation of CH_4 impacts on temperatures over a range of emissions scenarios (RCP2.6, RCP4.5, and RCP6.0) until 2100 (Cain *et al.*, 2019; Lynch *et al.*, 2020). Subsequently, a further modification was put forward to scale the right hand side of equation (1) to ensure the forcing equivalency (Smith *et al.*, 2021). Finally, the GWP* equation adopted in the Sixth Assessment Report of the Intergovernmental Panel on Climate Change (IPCC AR6) (Forster *et al.*, 2021; Dhakal *et al.*, 2022), which is used in our analysis, is the following form:

$$\mathrm{E_{CO2e}(t)} = 0.28 \times \mathrm{E_{100}(t)} + 4.25 \times (\mathrm{E_{100}(t)} - \mathrm{E_{100}(t-20)}) \quad (2)$$

$E_{100}(t)$ denotes the emissions of an SLCP multiplied with its GWP100 value. The first and second terms on the right-hand side of equation (2) captures the stock and flow effects, respectively, with a much higher weight given on the flow effects. Equation (2) is a special case of equation (1) with the time interval Δt of 20 years (also modified with a scaling factor of 1.13 discussed above). Note that this formula is based on GWP100 values in Table 8.A.1 of the IPCC AR5 [a].

Although GWP* is often referred to as a metric, GWP* is not a single value: it is rather a more elaborated way of applying existing GWP100 values. In the traditional approach of using GWP100, the value of GWP100 for the non-CO_2 GHG of interest (for both SLCPs

and LLCPs) is simply multiplied with the non-CO_2 GHG emissions to calculate CO_2-eq emissions. In the GWP* approach, however, the value of GWP100 is multiplied with the emissions and the change in the rate of emissions for a non-CO_2 GHG as in equation (1). This approach allows for a more accurate translation of the temperature response of SLCP emissions to that of CO_2 emissions when calculating CO_2-eq emissions.

Scenarios that exceed the 1.5 °C or 2 °C warming target level temporarily, or so-called overshoot scenarios, in which temperatures rise and then fall, are becoming increasingly relevant in the face of inadequate emission reduction commitments in the policy arena. Although GWP* was proposed with the aim of obtaining a more accurate estimation of temperature changes from cumulative CO_2-eq emissions, the performance of GWP* with respect to declining emissions in overshoot scenarios was not fully assessed in IPCC AR6 (Canadell *et al.*, 2021) and, at the moment of writing this manuscript, has yet to be systematically tested in any peer-reviewed papers. This is particularly relevant to pathways achieving the 1.5 °C warming target, as around 90% of the scenarios considered in the IPCC Special Report on 1.5 °C (SR15) are either overshoot scenarios for the 1.5 °C target or, more generally, peak and decline scenarios (Rogelj, Shindell, *et al.*, 2018). Similarly, a large majority of low emissions scenarios developed from Integrated Assessment Models have been peak and decline scenarios (Tanaka and O'Neill, 2018), with newly developed stabilization scenarios with net-zero CO_2 emissions being an exception (Johansson, 2021; Riahi *et al.*, 2021). Lastly, given the current emission trajectory and the recent anomalous warming, overshooting the 1.5 °C target level seems to be in fact imminent (Bossy *et al.*, 2024; Schmidt, 2024).

Moreover, there is a growing interest in the Earth system modeling community to simulate very long-term overshoot scenarios over a few to several centuries (up to 2300 or 2500). Therefore, GWP* could be a convenient tool to assess the temperature implication of CH_4 emissions of such scenarios. Whereas GWP* may not be intended for such use, considering the calibration range to 2100, users of GWP* are not necessarily aware of the calibration

range. It is therefore useful to investigate how well GWP* works over multi-century time scales with different lengths and magnitudes of overshoot.

Previous studies have relied either on specifying the non-CO_2 warming response for a given scenario and determining the CO_2 contribution as a residual (Jenkins *et al.*, 2021; Tokarska *et al.*, 2020), or on assuming and exploiting a scenario-dependent relationship between cumulative CO_2 emissions and non-CO_2 climate forcers (Rogelj *et al.*, 2016). Another recent approach to consider the contributions of non-CO_2 climate forcers relies on the concept of CO_2 forcing equivalent (CO_2-fe) emissions (Jenkins *et al.*, 2018; Mengis and Matthews, 2020). However, implications of using GWP* to determine non-CO_2 contributions to the carbon budget for overshoot scenarios has not been systematically explored.

Therefore, in this paper, we aim to tackle the following scientific questions: Does the GWP* metric adequately ensure equivalent temperature responses when it is used to convert SLCP emissions to CO_2-eq emissions under multi-century scenarios with different lengths and magnitudes of temperature overshoot? Can this metric be used to include non-CO_2 contributions in the carbon budget approach if applied for overshoot scenarios?

1.3 Data and Methods

1.3.1 Description of three reduced-complexity models

Our analysis used three different reduced-complexity models as follows in the order of complexity: an Impulse Response Function (IRF) model of IPCC AR5 (Myhre *et al.*, 2013), the Finite Amplitude Impulse Response simple climate model (FaIR), and the Aggregated Carbon Cycle, Atmospheric Chemistry, and Climate (ACC2) Model (Tanaka *et al.*, 2007, 2021; Tanaka and O'Neill, 2018).

First, the IRF model is a simplified representation of the atmospheric response to a pulse emission of CO_2. It approximates the fraction of emitted carbon that remains in the atmosphere over time (Joos *et al.*, 2013), to estimate the temperature impact of GHG

emissions according to the radiative efficiencies of the single GHG. The IRF model used in our study is derived from the latest estimates summarized in the IPCC AR5. It is employed to estimate the temperature response of CH_4 derived CO_2-eq emissions using various conversion metrics, and to tune and optimize the parameters of the GWP* equation.

Second, the FaIR v1.3 (Finite Amplitude Impulse Response) emulator is a simple emissions-based impulse response and carbon cycle model (Millar *et al.*, 2017; Smith *et al.*, 2018), and has been extensively used for assessing the temperature impacts of different emissions pathways and mitigation scenarios (Jenkins *et al.*, 2018, 2021; Cain *et al.*, 2019; Lynch *et al.*, 2021). FaIR has a simple representation of the carbon cycle, and accounts for nonlinear feedbacks such as the temperature and saturation dependency of land and ocean carbon sinks. The model calculates both CO_2 and non-CO_2 GHG atmospheric concentrations by tracking their time-integrated airborne fraction from their initial emissions. From concentrations, Effective Radiative Forcing (ERF) for thirteen forcings, including land-use change, tropospheric and stratospheric O_3 as well as other GHG are computed; finally the temperature change is retrieved as the sum of its slow and fast components, representing temperature changes from a response to forcing from the upper ocean and the deep ocean, respectively.

Third, ACC2 is a simple climate-economy model composed of four modules: i) carbon cycle, ii) atmospheric chemistry, iii) physical climate, and iv) economy. The carbon cycle module is made of three ocean boxes, a coupled atmosphere-mixed layer box, and four land boxes. The physical climate module is the land-ocean energy balance model coupled with the heat diffusion model DOECLIM, which is used to calculate the temperature response to radiative forcing (Tanaka *et al.*, 2007). The radiative forcing is calculated for the following direct and indirect climate forcers: CO_2, CH_4, N_2O, O_3, SF_6, 29 halocarbon species, OH, VOC, CO, NO_x, stratospheric H_2O, sulfate aerosols, and carbonaceous aerosols (both direct and indirect effects). The changes in CH_4 and N_2O concentrations are given as a function of their atmospheric concentrations, the sum of anthropogenic and natural emissions, and their

lifetime. ACC2 accounts for nonlinear feedbacks such as the saturation of ocean CO_2 uptake under rising CO_2 concentration, CO_2 fertilization of the land biosphere, and increasing heterotrophic respiration of the land biosphere with rising temperatures. Furthermore, uncertain parameters in ACC2 are calibrated with a Bayesian approach (Tanaka *et al.*, 2009; Tanaka and O'Neill, 2018). The model is developed in the GAMS programming language and numerically solved using CONOPT3 and CONOPT4, two nonlinear optimization solvers included in the GAMS software package. When ACC2 is used as a simulator, the first three modules are used to calculate temperature changes based on prescribed emissions scenarios. On the other hand, when ACC2 is used as an optimizer, all four modules, including the economy module consisting of the marginal abatement cost curves for global CO_2, CH_4, and N_2O emissions, are used to derive least-cost emission pathways for a given climate target. ACC2 has participated in model intercomparison projects (Joos *et al.*, 2013; Nicholls *et al.*, 2020) and has been subject to comparison with other models in other studies (Melnikova *et al.*, 2023). This model has been applied to analyze pathways to achieve the targets of the Paris Agreement (Tanaka and O'Neill, 2018; Tanaka *et al.*, 2021; Xiong *et al.*, 2022). The performance of ACC2 configured for this paper with three EMSs was benchmarked against other simple climate models under commonly used scenarios RCP2.6 and RCP4.5 in the emission-driven mode (Nicholls *et al.*, 2020) (Figure S6 and Figure S7).

1.3.2 Carbon cycle parameters in ACC2

As in many simple climate and carbon cycle models, a steady state is assumed for the carbon cycle in the preindustrial period (Mackenzie and Lerman, 2006). In 1750, the preindustrial start year of ACC2, the Net Primary Production (NPP) is assumed to be constant and in balance with the heterotrophic respiration. The perturbation of the NPP and the resulting changes in heterotrophic respiration are described by the four-reservoir land box model. A change in atmospheric CO_2 concentration logarithmically influences the NPP (i.e., CO_2 fertilization), the strength of which is scaled with the BETA factor (Friedlingstein et al., 1995). On the other hand, the heterotrophic respiration is exponentially dependent on the

temperature as parameterized through a Q10 factor, at the rate of which the heterotrophic respiration increases with a temperature increase of 10 °C.

The governing equation for each of the four land reservoirs is:

$$\dot{c}_{ter,l}(t) = A_{ter,l}\tau_{ter,l}\left(\bar{f}_{NPP}^{pre} + \delta f_{NPP}(t)\right) - \frac{1}{\tau_{ter,l}}\left(\bar{c}_{ter,}^{pre} + c_{ter,l}(t)\right) q(t) \; with \; l = [1,2,3,4] \quad (3)$$

Here, the first term represents added carbon to the reservoir *l*: the increase in NPP of year *t* ($\delta f_{NPP}(t)$) combined with the preindustrial constant NPP ($\bar{f}_{NPP}^{pre}$). $A_{ter,}$ and $\tau_{ter,l}$ represent the coefficients and the overturning time constants of the IRF describing the temporal evolution of biomass for each reservoir. The second term represents released carbon from the reservoir *l*: the release of carbon from both preindustrial ($\bar{c}_{ter,l}^{pre}$) and fertilized storage ($c_{ter,l}(t)$), which can be enhanced under warming through $q(t)$, the Q10 factor, accounting for climate-carbon cycle feedbacks.

Furthermore, the BETA (β_{NPP}) and Q10 factor used to parameterize the CO_2 fertilization effect on photosynthesis and temperature control on heterotrophic respiration, respectively, are expressed in the two following equations:

$$\delta f_{NPP}(t) = \bar{f}_{NPP}^{pre}\beta_{NPP}\, ln\left(\frac{pCO_2(t)}{pCO_2^{pre}}\right) \quad (4)$$

$$q(t) = Q_{10}\frac{\delta T_{land-air}(t)}{10} \quad (5)$$

Note that the BETA factor is a commonly used parameter representing the CO_2 fertilization effect (more technically, a scaling parameter expressing the sensitivity of the change in NPP to the logarithmic change in atmospheric CO_2 concentrations) but importantly differs from another commonly used parameter β also representing a quantity including the CO_2 fertilization effect (a scaling parameter expressing the sensitivity of the carbon storage to the change in atmospheric CO_2 concentrations, expressed in GtC ppm^{-1}) (Friedlingstein *et al.*, 2006; Gregory *et al.*, 2009; Jones *et al.*, 2016; Melnikova *et al.*, 2021).

1.3.3 Emulating ACC2 to CMIP6 ESMs

ACC2 was emulated to five state-of-the-art ESMs (CanESM5, CNRM-ESM2-1, IPSL-CM6A-LR, MIROC-ES2L, and UKESM1-0-LL, see Table S6 for an overview of the ESMs) developed under the Coupled Model Intercomparison Project 6, CMIP6 (Eyring *et al.*, 2016). The emulation was performed using ssp534os, a high temperature overshoot scenario combining the high emission ssp585 scenario until 2040 with strong mitigation thereafter (O'Neill *et al.*, 2016). Data from the fully-coupled (COU) configuration of ESMs have been used. The emulation method focuses on just three key parameters: namely, the equilibrium climate sensitivity (ECS), BETA, and Q10. Overall, three configurations of ACC2 emulating IPSL-CM6A-LR, CNRM-ESM2-1 and MIROC-ES2L have been used for the analysis because relatively large number of scenarios were obtained from these three configurations for the range of temperature targets and overshoot profiles considered in this study. First, the ACC2 temperature response was calibrated with the temperature from ESM. By tuning the ECS parameter in ACC2 (Table 1), for each ESM was determined the value of ECS which yielded the closest projection to the temperature response (Figure S8 and Table 2). Then, BETA and Q10 values were tuned to reproduce NBP (Table 1). NBP was considered to capture carbon-concentration and carbon-climate feedback effects. NBP estimates of ACC2 were corrected to account for a lack of representation of land-use change (LUC) processes in ACC2. That is, LUC emissions data from the Global Carbon Budget (Friedlingstein *et al.*, 2021) from 1850 to 2014 and integrated assessment models (IAM) output from 2015 to 2100 for the SSP534OS (Ackerman *et al.*, 2009; Van Vuuren *et al.*, 2017) were used to make the ACC2 output comparable with ESMs. The best combination of BETA and Q10 values were identified for each ESM, for which the RMSE of the NBP estimates from ACC2 relative to the NBP from the ESMs is minimized.

Table 1: Parameter ranges considered in ACC2 emulations

ACC2 Parameter	Definition	Values
ECS	Equilibrium climate sensitivity	2.0 to 5.6 with intervals of 0.2
BETA	CO_2 fertilization effect on photosynthesis	0.1 to 1.0 with intervals of 0.1
Q10	Temperature effect on heterotrophic respiration	0.7 to 2.0 with intervals of 0.1

Table 2: Best estimates of the three main parameters in ACC2 to emulate ESMs. ECS values of ESM from Zelinka et al. (2020) are shown for comparison.

ESM	Ensemble member (COU)	Ensemble member (BGC)	ECS Zelinka et al. (2020)	ACC2 ECS	ACC2 BETA	ACC2 Q10
CanESM5	r1i1p1f1	r1i1p2f1	5.64	4.8	0.6	1.1
CNRM-ESM2-1	r1i1p1f2	r1i1p1f2	4.79	3.8	0.9	1.3
IPSL-CM6A-LR	r1i1p1f1	r1i1p1f1	4.56	4.0	0.6	1.2
MIROC-ES2L	r1i1p1f2	r1i1p1f2	2.66	2.4	0.9	2.0
UKESM1-0-LL	r4i1p1f2	r4i1p1f2	5.36	4.8	0.7	1.5

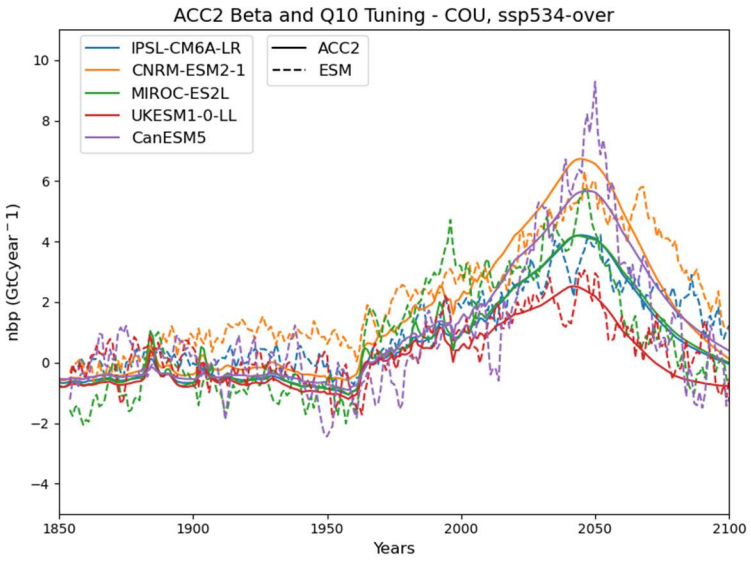


Figure 1 NBP projections of ACC2 emulated to each ESM. The BETA and Q10 values in ACC2 were adjusted to each ESM to best reproduce NBP.

The results of the emulation process are shown in Table 2 and Figure 1, and Figures S4-S7. Our emulation for ACC2 gives similar or systematically lower ECS values compared to those reported by Zelinka *et al.* (2020), with an average difference of 0.64 °C.

In Figure 1, NBP from ACC2 with the best combination of BETA and Q10 values for each ESM is compared with NBP from the respective ESM. Apart from the inter-annual variability, the emulation shows overall a good performance for both the ramp-up and ramp-down phases. The emulation of IPSL-CM6A-LR with ACC2 was further evaluated by using the optimal combination of ECS, BETA and Q10 parameters to simulate seven additional scenarios. Figure S9 to Figure S11 show the land carbon uptake, ocean carbon uptake, and temperature evolution from the emulated ACC2 and IPSL-CM6A-LR. The temperature change was reproduced very well overall for all the SSP scenarios considered. Some over-estimation of ocean carbon uptake, on the other hand, occurred in ACC2 when the ocean carbon uptake declines. This inconsistency may be related to a faster mixing of carbon from the surface to the deep ocean in simple climate models, as discussed in Melnikova *et al.* (2023)(Melnikova *et al.*, 2023). Land carbon uptake showed a significant misfit in the cases of medium to high forcing scenarios (ssp245, ssp460, ssp370, and ssp585), which gives >3 °C

warming at the end of this century. The largest warming level considered in the analysis using the ranges of overshoot scenarios (Figure 3 and Figure 4) is approximately 3 °C (or 1 °C overshoot of the 2 °C target level). Thus, the misfit found here is not a problem for the analysis, as it happens outside the range of our model application.

1.4 Results and Discussion

1.4.1 Testing the temperature equivalency of GWP* under SSPs

First, a simple Impulse Response Function (IRF) model (Myhre *et al.*, 2013) is used to simulate the temperature effect of CH_4 emissions under the ssp119, ssp126, ssp434, ssp460, ssp534os, and ssp585 scenarios, up to the year 2300. We then calculated the temperature effect of CO_2-eq emissions of such CH_4 emissions converted via different emission metrics. By comparing the two results from IRF, we assessed the temperature equivalency of using different emission metrics under SSPs.

The results in Figure 2 show that GWP100 ensures an imperfect but reasonably good temperature equivalency approximately up to the point of peak CH_4 emissions; however, its accuracy decreases substantially when CH_4 emissions decline, a well-known issue with GWP100. It is also shown that GWP100 performs better than GWP20 and GTP100 in terms of the temperature equivalency. GWP20 and GTP100 are in fact illustrative of emphasizing and de-emphasizing, respectively, the temperature effect of CH_4 emissions relative to GWP100 (Cherubini *et al.*, 2016; Levasseur *et al.*, 2016; Tanaka *et al.*, 2019). Thus, the results from GWP20 and GTP100 are opposite each other, relative to those from GWP100.

It is further shown that GWP* gives a nearly perfect temperature equivalency approximately until the end of the century under the range of emission scenarios. This result is rather expected, as GWP* is calibrated to do so under the three RCP scenarios. A notable exception is, however, that when CH_4 emissions drop sharply, GWP* overestimates the cooling effect, as shown most evidently for ssp534os (Figure 2e). This behavior reflects the

fact that none of the RCP scenarios used to train GWP* contain a large overshoot as in ssp534os. It should also be emphasized that, compared to GWP100, GWP* clearly shows superior performances for reproducing the temperature (Table S1). Over the longer run, however, the temperature equivalency provided by GWP* no longer holds. The cooling effect of CH_4 is underestimated or shown to be warming by this metric when CH_4 emissions decrease (in all SSPs). From the physical perspective, this is due to the fact that the "stock" parameter, as defined in Cain et al., (2019), emphasize too much the century-timescale response to earlier methane emission increases, leading to an overestimation of temperatures beyond 2100. These findings are robust since the deviations discussed here are generally confirmed by two other modeling approaches (Figure S12). These findings raise the question regarding whether the use of GWP* could be adequate for accounting for the contribution of CH_4 emissions in the carbon budget framework when it is applied for overshoot scenarios, in particular beyond 2100.

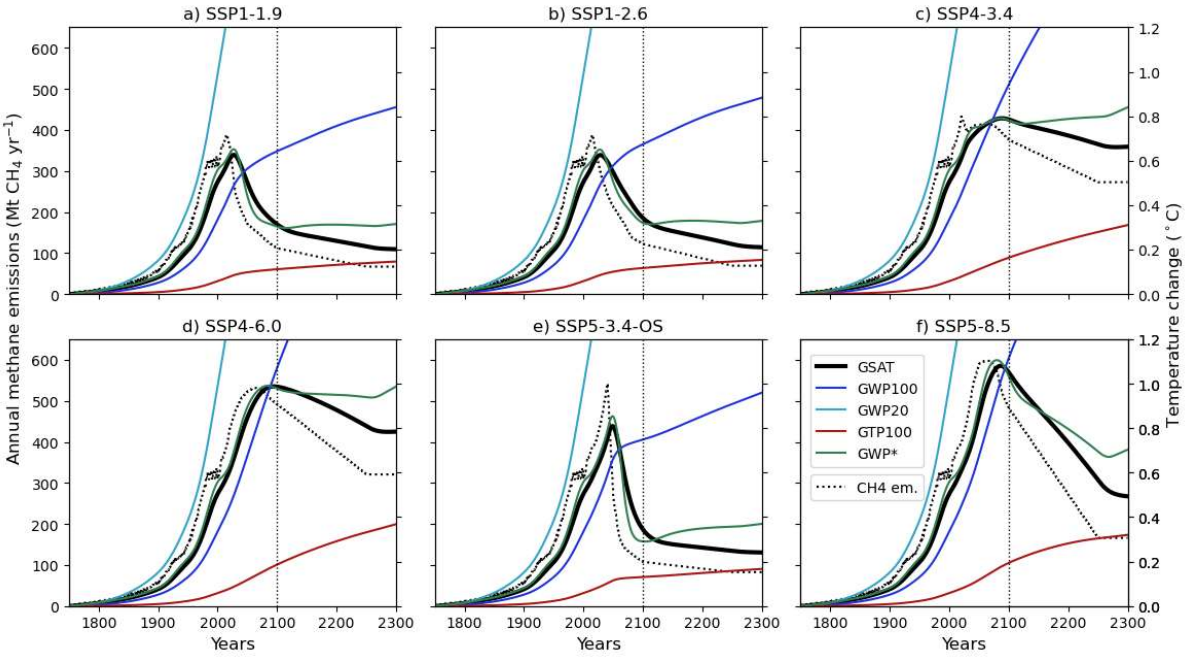


Figure 2 *The temperature response to CO_2-eq emissions computed from CH_4 emissions using different emission metrics, in comparison to the actual temperature response to CH_4 emissions, under six SSP scenarios. Dotted black lines indicate CH_4 emissions of each SSP. Thick black lines gives the estimates of temperature effect deduced from the cumulative CH_4 emissions reported, calculated with the IRF climate response model, without the application of any metric. Thin solid lines show temperature responses calculated from CO_2-eq emissions converted from CH_4 emissions using different metrics such as GWP100 and GWP*. Only CH_4 emissions or CO_2-eq emissions converted from CH_4 emissions are considered for temperature calculations here. The temperature calculation is based on the Impulse Response Function model of IPCC AR5. This figure mimics but extends the presentation of Figure 7.22 of IPCC AR6 WGI, which shows the outcome only till 2100.*

The sensitivity of the temperature equivalency to the parameters used to define GWP* has been then explored. First, it was changed the time interval (Figure S13a horizontal axis) considered between two pulse emissions in the flow term of equation 2 (20 years by default). By minimizing the Sum of Squared Errors (SSE) between the temperatures from original CH_4 emissions and that from CO_2-eq emissions based on the modified GWP* for all the scenarios, the optimal time interval was found to be 22 years (Figure S13a), which is close to the commonly used value of 20 years. Furthermore, the sensitivity of the temperature equivalency was investigated by substituting the default flow term taking the change in emissions 20 years apart (equation 2) with an alternative flow term taking the average change in emissions over the previous 5, 10, 20, 30, 40 or 50 years (Figure S13b horizontal

axis). These results show that the use of average emissions over the previous 40 years or longer leads to the best temperature equivalency (Figure S13b). Additionally, the use of average emissions over the previous 40 years yielded a slightly better temperature equivalency than the use of emissions 20 years apart. This outcome can be explained by the fact that the use of average emissions over 40 years, compared to the use of two end-point emissions 20 years apart, more closely resembles the exact CO_2-eq emissions that precisely reproduce the warming from original CH_4 emissions (i.e., the Linear Warming Equivalence emissions) as explained in Allen *et al.* (2021). However, even when the GWP* equation is modified in several different ways, the temperature misfit after the rapid drop in CH_4 emissions persists (Figure S14).

1.4.2 Using GWP* to quantify the overshoot carbon-eq budget of overshoot scenarios

The analysis based on the SSP scenarios has shown that the temperature equivalency of GWP* can be influenced by the rate of CH_4 emission reduction. To gain more insights, a further analysis was performed based on scenarios with different overshoot lengths and magnitudes. To generate a range of overshoot scenarios, we used the Aggregated Carbon Cycle, Atmospheric Chemistry, and Climate (ACC2) model (Tanaka *et al.*, 2007, 2021; Tanaka and O'Neill, 2018). ACC2 is a simple climate model (Nicholls *et al.*, 2020) that resolves many GHGs and aerosols, accounting for primarily important nonlinearities in the global earth system such as CO_2 fertilization of the land biosphere, saturation of ocean CO_2 uptake under rising atmospheric CO_2 concentrations, and climate-carbon cycle feedback. The interaction between CH_4 and tropospheric ozone through the OH chemistry is parameterized in ACC2. The temperature is calculated by using a land-ocean energy balance model coupled with a heat diffusion model (see Methods for details). The simple climate model ACC2 can be further coupled with a climate mitigation module consisting of a set of marginal abatement cost functions (Tanaka *et al.*, 2021; Xiong *et al.*, 2023) to calculate

least-cost emission pathways for a specified climate target. ACC2 then works as an optimizing climate-economy model, and we took advantage of this model feature to generate sets of overshoot pathways systematically for our metric analysis. ACC2 was used to generate a range of pathways that reach the 1.5 or 2 °C target level after overshoot of varying lengths and magnitudes. Least-cost CO_2 and CH_4 emission scenarios have been computed to keep the temperature below a target level throughout the simulation period (temperature *stabilization* pathways). If the temperature target is applied only after a certain year, the model yields least-cost CO_2 and CH_4 emission scenarios that lead to temperature *overshoot* pathways. In this case, the temperature exceeds the target level before that year, since it is less costly to invest in mitigation efforts later in the cost-effectiveness framework as also pointed out by previous studies (Emmerling *et al.*, 2019; Rogelj, Huppmann, *et al.*, 2019). The length and the magnitude of the temperature overshoot are determined by ACC2's internal least-cost calculations reflecting assumptions on the maximum rates of emission abatements and the discounting rate. Target years have been varied between 2060 and 2180 with an interval of 10 years and tested for each temperature goal (1.5 °C and 2 °C). For each target year, discount rate was varied between 2% and 6%, compared to the original 4% by default, to generate different overshoot magnitudes, while keeping the same overshoot length. Emissions of all climate forcers other than CO_2 and CH_4 are assumed to follow ssp119 and ssp126 in the case of the 1.5 and 2 °C target, respectively.

For each pathway, the overshoot carbon-eq budget was defined as the cumulative net CO_2-eq emissions (GtC-eq) from 2020 till the year when the temperature stabilizes at or returns to the 1.5 or 2 °C warming target level after temperature overshoot. The overshoot carbon-eq budget discussed in this paper implicitly assumes that positive and negative emissions can be equally balanced, although the validity of this assumption will be explored later in this paper. The carbon budget for this time frame is referred to as the threshold return budget elsewhere (Rogelj, Popp, *et al.*, 2018; Rogelj, Forster, *et al.*, 2019), but non-CO_2 contributions were included in the threshold return budget using the emission metric

approach: GWP* for SLCPs and GWP100 for LLCPs. For the sake of analysis, the overshoot carbon-eq budget considers only CO_2 and CH_4, which are largely representative of the entire carbon-eq budget because these two gases are usually most important for climate change mitigation. Results calculated from ACC2 emulating IPSL-CM6A-LR are presented and further discussed, but qualitatively similar results can be found from ACC2 emulating other ESMs, as in Figure S15 and Figure S16 for MIROC-ES2L and CNRM-ESM2-1.

First multi-gas optimization experiments are presented, where both CO_2 and CH_4 emission pathways are optimized simultaneously via the ACC2 least-cost scheme, while all other gases and pollutants are assumed to follow ssp119 and ssp126 in the case of the 1.5 and 2 °C target, respectively. Panels a) and b) of Figure 3 show the overshoot CO_2-eq budget (with CH_4 converted via GWP*) for different 1.5°C and 2°C stabilization years, respectively, with ranges of overshoot magnitude and length. For both the 1.5°C and 2°C target year simulations, we found that the longer the temperature overshoot is, the larger the overshoot CO_2-eq budget is. Furthermore, for the same overshoot length, the higher the overshoot is, the larger the overshoot CO_2-eq budget is (the 2 °C case with the 2060 target year is an exception because the target lengths and magnitudes are not clearly separated) (Table 3). The increasing total overshoot carbon-eq budget with increasing overshoot lengths and magnitudes reflects both the model behavior of ACC2 and the conversion of CH_4 emissions to CO_2-eq emissions via GWP*. The contribution of CH_4 in the overshoot carbon-eq budget becomes particularly important for 1.5 °C pathways, in which the total overshoot carbon-eq budget is so small that the carbon-eq budget from CH_4 can even determine the sign of the total overshoot carbon-eq budget. This indicates that how to account for CH_4 contributions to the carbon-eq budget is particularly crucial for mitigation pathways aiming at the 1.5 °C target level. The overshoot carbon-eq budget is in fact already negative in about a half of the cases for the 1.5 °C target level. The overshoot CO_2-eq budgets calculated with our default version of ACC2 are generally low because this version of ACC2 was configured to IPSL-CM6A-LR, which exhibits a high climate sensitivity (Table 2, Figure S6 and Figure

S7). The overshoot CO_2-eq budget is in fact already negative in about a half of the cases for the 1.5 °C target level, specifically for scenarios with target years in 2090 and 2120. These negative overshoot CO_2-eq budgets reflect deep CO_2 mitigation that is required to compensate for the limited CH_4 mitigation (Figure S17 for simulations for the target year of 2120 with three different overshoot profiles), as well as the unmasked warming from decreasing emissions of air pollutants (following SSP1-1.9 for 1.5 °C target scenarios).

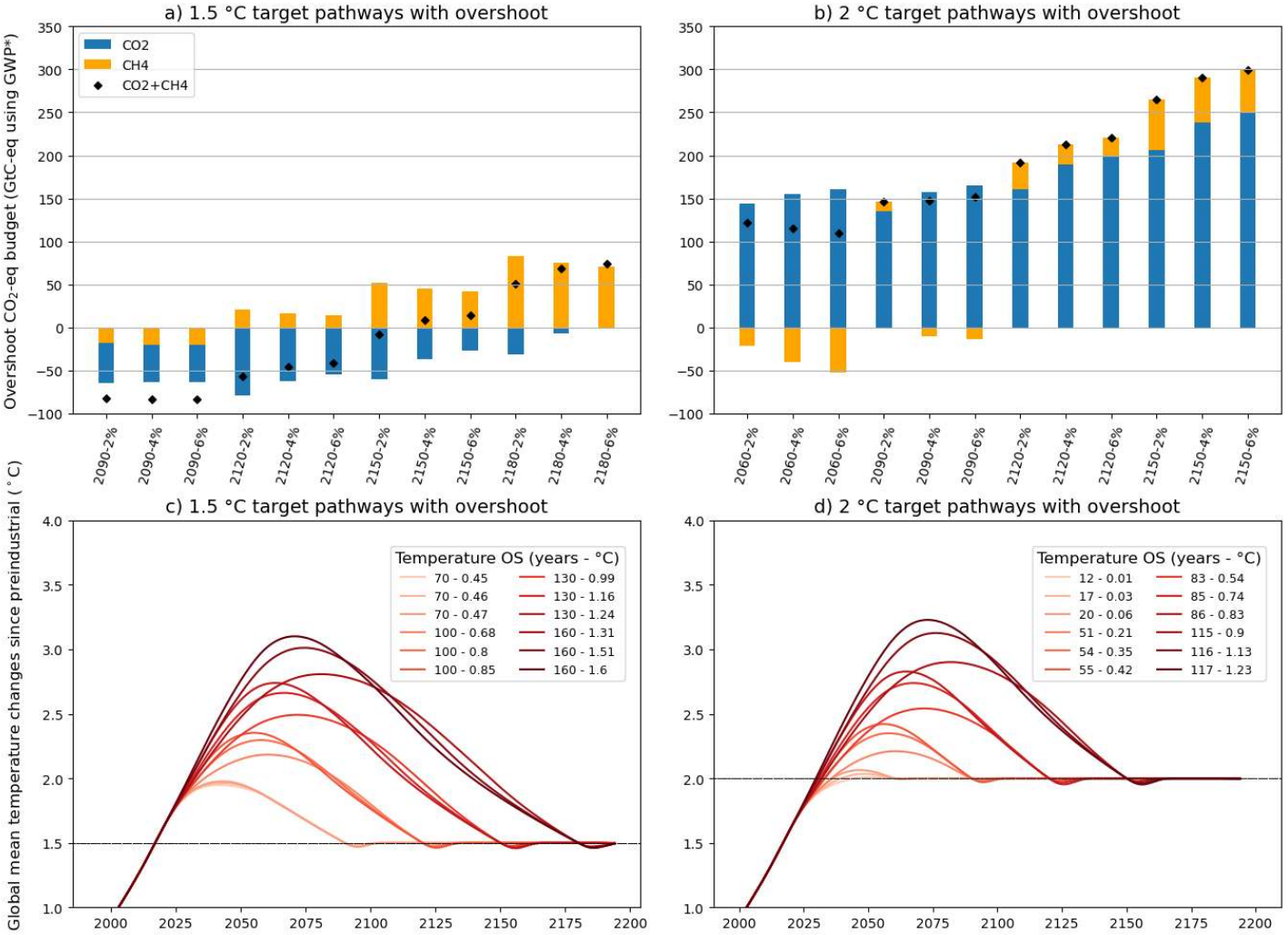


Figure 3: Overshoot carbon-eq budgets of least-cost pathways for the 1.5 and 2 °C target levels with temperature overshoot of varying lengths and magnitudes (multi-gas optimization experiment). Both CO_2 and CH_4 emission pathways were optimized using ACC2 (emulating IPSL-CM6A-LR) for each target level and year with different discounting, with all other gases and pollutants following respective SSPs (SSP1-1.9 and SSP1-2.6 for the 1.5 and 2 °C target level, respectively). The figure shows the results of a combination of four different overshoot lengths and three different overshoot magnitudes for each temperature target level. The overshoot carbon-eq budgets account for contributions from CO_2 and CH_4. The contributions of CH_4 in the carbon-eq budget were determined using GWP. Legends in panels c) and d) represent the duration and magnitude of temperature overshoot relative to the 1.5 °C or 2 °C target level, respectively.*

Table 3: The effect of different overshoot profiles on the CO_2-eq budget under multi-gas, CO_2-only, and CH_4-only optimization scenarios for the 1.5 and 2 °C targets. This table summarizes how the overshoot length and magnitude can generally affect the overshoot CO_2-eq budget for scenarios aiming for identical long-term temperature targets (1.5 or 2 °C warming) as derived by ACC2. See text for further details and discussions.

	Multi-gas optimization scenarios	**CO_2-only optimization scenarios**	**CH_4-only optimization scenarios**
Increasing overshoot length	*Increase* in CO_2-eq budget	*Increase* in CO_2-eq budget	*Increase* in CO_2-eq budget
Increasing overshoot magnitude	*Increase* in CO_2-eq budget	*Increase* in CO_2-eq budget	*Decrease* in CO_2-eq budget

Single-gas optimization experiments are then presented (Figure 4 and Figure S18). In this case, only the emission pathway of one of the two gases (CO_2 or CH_4) is optimized to reach the target temperature with lowest cost, while the emission pathways of all other gases and pollutants are kept at the respective SSP scenario (ssp119 or ssp126) corresponding to the target temperature (1.5 or 2 °C target level). This experiment is useful to isolate the relative contribution of CO_2 and CH_4 to the total carbon-eq budget. That is, unlike the previous experiments, in which emission reductions of CO_2 and CH_4 can be traded to yield a least-cost solution, emission reductions of only one gas can change with varying overshoot lengths and magnitudes in these experiments. In the case of CO_2-only optimization experiment (Figure 4a), the longer the temperature overshoot is, the larger the overshoot carbon-eq budget (CO_2-only optimization) is. This finding is in contrast to the general belief that the carbon budget is reduced with increasing overshoot lengths (Zickfeld *et al.*, 2016; Tokarska *et al.*, 2019). Qualitatively similar results are found for the CH_4-only optimized experiment as well (Figure 4b). Caution must be taken in drawing conclusions from this, as it could be interpreted that a late mitigation is preferred compared to early mitigation actions. It should be noted that this finding is dependent on the model assumptions such as CO_2 fertilization effect (Figure S19). The results for overshoot magnitudes provide a further insight: the higher the overshoot is for the same overshoot length, the larger the overshoot carbon-eq

budget (CO_2-only optimization) is from the CO_2-only optimization experiment, but the smaller the overshoot carbon-eq budget (CH_4-only optimized) is from the CH_4-only optimized experiment (in most cases). The results of the CO_2-only optimization experiment reflect the dynamic behavior of ACC2. Those of the CH_4-only optimized experiment, on the other hand, not only reflects the model characteristics of ACC2 but also the conversion of CH_4 emissions to CO_2-eq emissions via GWP*. This indicates that the use of GWP* can decrease the apparent carbon-eq budget under very long-term overshoot scenarios. Below are further investigated how these factors play out separately in the ramp-up and ramp-down periods of overshoot scenarios. Note that the carbon-eq budget (CH_4-only optimized) is higher in the 1.5 °C target case than that in the 2 °C target case, which appears counterintuitive first, since a lower temperature target usually implies stricter emission limits. This phenomenon is due to the higher relative contribution on radiative forcing of the prescribed CO_2 baseline scenario ssp126 (used for the 2 °C target simulations) compared to the ssp119 in the 1.5 °C target. Because the ssp126 CO_2 scenario contributes more to radiative forcing in the 2 °C

target simulations, there is less room for additional warming from CH_4, hence its lower carbon-eq budget with respect to the 1.5 °C target simulation.

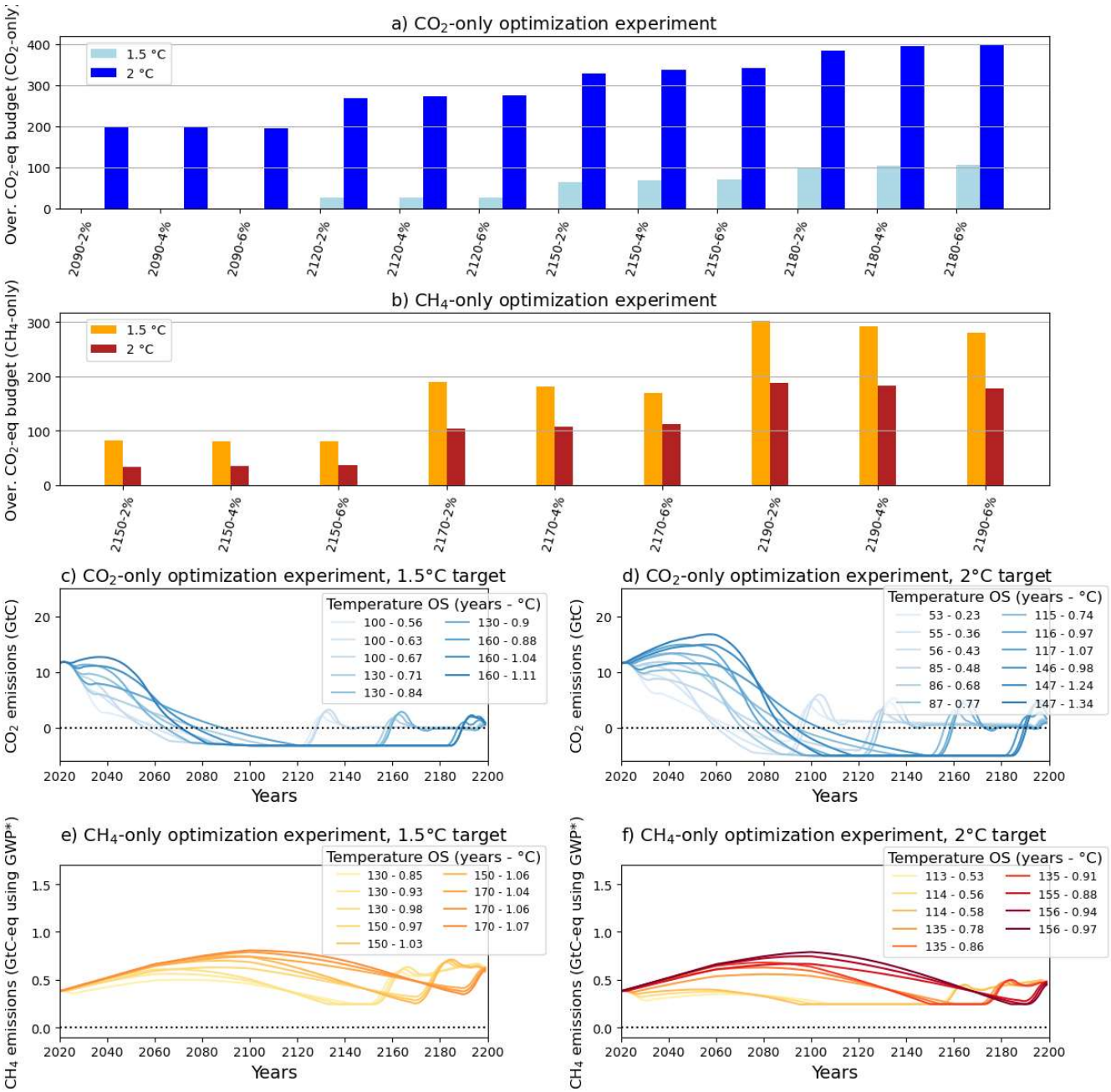


Figure 4: Overshoot carbon-eq budgets of least-cost pathways for the 1.5 and 2 °C target levels with temperature overshoot of varying lengths and magnitudes (single-gas optimization experiment). Either CO_2 or CH_4 emission pathways were optimized using ACC2 (emulating IPSL-CM6A-LR) for each target level and year with different discounting, with all other gases and pollutants following respective SSPs (SSP1-1.9 and SSP1-2.6 for the 1.5 and 2 °C target level, respectively). The contributions of CH_4 in the carbon-eq budget were determined using GWP. Legends in panels c) to f) represent the magnitude of temperature overshoot relative to the 1.5 °C and or 2 °C target level, respectively.*

1.4.3 TCRE of the ramp-up and ramp-down phases of overshoot scenarios

To gain insight into how the overshoot carbon-eq budget distributes between ramp-up and ramp-down phases of overshoot scenarios, the TCRE behavior is explored separately for both phases. TCRE is computed, for each single-gas optimization experiment, as the ratio of the temperature change over the cumulative carbon-eq emissions (one gas (CO_2 or GWP*-weighted CH_4) or the sum of CO_2, GWP*-weighted CH_4, and GWP100-weighted N_2O) over the relevant period. TCRE between the ramp-up (from year 1750 to the year of peak emissions) and the ramp-down phases (from the year of peak emissions to the year when the temperature target is met after overshoot) are distinguished as TCRE+ and TCRE−, respectively. It is unclear from the current literature to what extent the linear relationship between cumulative CO_2 emissions and temperature changes holds in case of negative emissions (Keller *et al.*, 2018). As reported in Chapter 5 of IPCC AR6 WGI, there is no clear agreement among models for the relationship between TCRE+ and TCRE− (Canadell *et al.*, 2021).

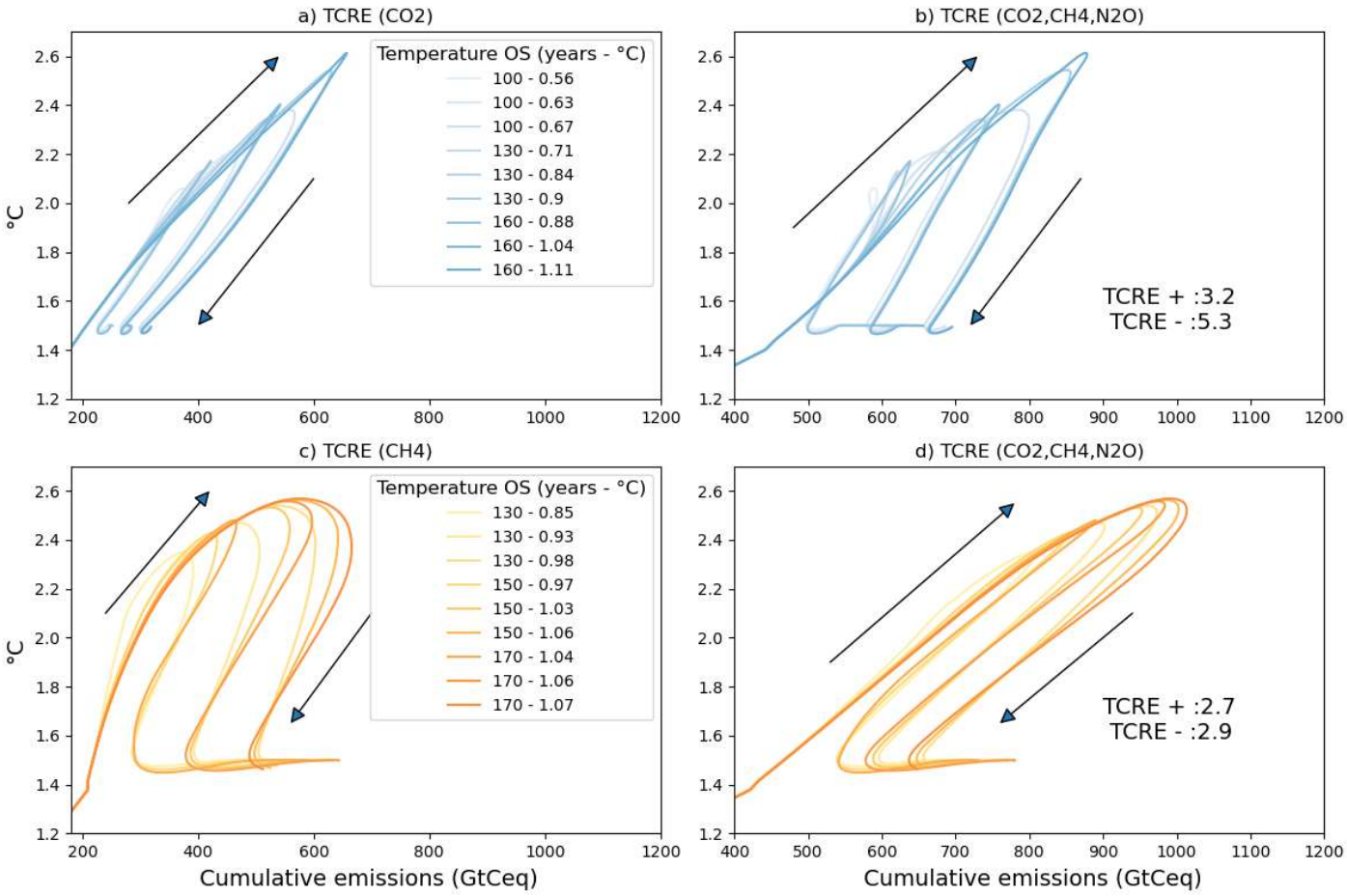


Figure 5: The TCRE obtained from the single-gas optimization experiment using ACC2 emulating IPSL-CM6A-LR for the 1.5 °C target. Panels a) and b) show the relationship between the temperature change and the cumulative emissions considering only CO_2 and the sum of CO_2, CH_4, and N_2O, respectively, for the period 2020-2200 from the CO_2-only optimization experiment. Panels c) and d) show the relationship between the temperature change and the cumulative emissions considering only CH_4 and the sum of CO_2, CH_4, and N_2O, respectively, also for the same period but from the CH_4-only optimized experiment. CH_4 emissions were converted to CO_2-eq emissions with GWP, whereas N_2O emissions were converted to CO_2-eq emissions with GWP100. Arrows indicate the direction of time.*

Figure 5 shows the results from both the CO_2-only optimization and CH_4-only optimized experiments for the 1.5 °C target. In Figure 5a, c, cumulative emissions consider only one gas, but the warming is calculated by the emissions of all gases, indicating that the cumulative emissions are not necessarily consistent with the simulated warming. In Figure 5b, d, on the other hand, cumulative emissions consider three major gases, which is thus approximately consistent with the simulated warming, but the effects from individual gases

cannot be separated. The values of TCRE+ and TCRE− (°C/1000GtCeq) reported in panels b) and d) represent the mean from all TCRE+ and TCRE− values of the scenarios presented in the panels. The general indication of Figure 5 is that TCRE− is larger than TCRE+, which is consistent with the finding from Figure 3 and Figure 4: the longer or higher the temperature overshoot is, the larger the overshoot carbon-eq budget is. An exception is the decreasing TCRE− with increasing overshoot magnitudes from the CH_4-only optimized experiments. By taking the average of TCRE+ and TCRE− across the overshoot scenarios for discount rates of 2%, 4%, and 6%, the TCRE− values are indeed decreasing with increasing discounting rates, which are 3.1, 2.9, and 2.7, respectively (mean value 2.9, as reported in Figure 5d). This can be confirmed with our earlier finding that the overshoot carbon-eq budget decreases with increasing overshoot magnitudes in the CH_4-only optimized experiment owing to the use of GWP*.

The relatively large TCRE− from the CO_2-only optimization experiment can be further confirmed with the Zero Emission Commitment (ZEC) parameters of this model. Following the ZEC Model Intercomparison Project (ZECMIP) framework described in Jones et al. (2019), the B.1, B.2, and B.3 experiments as in MacDougall et al. (2020) were performed to compute the ZEC parameters (Figure S20). These three experiments consist of 100 years bell-shaped CO_2 emissions of 1000 GtC, 750 GtC and 2000 GtC respectively, starting from pre-industrial conditions, aiming to assess the model specific climate inertia (i.e. temperatures) in the decades after a complete cessation of emissions. We report the estimates of ZEC25, ZEC50, and ZEC90, representing the temperature change respectively 25, 50, and 90 years after the start of zero emissions. Table 4 shows that all three ZEC parameters are negative, which supports the large TCRE− relative to TCRE+. We further note that the ZEC parameters for different configurations of ACC2 (emulated to CNRM-ESM2-1 and MIROC-ES2L used for sensitivity analyses) also present negative values (Figure S20).

It should be emphasized that there is generally no consensus for the relationship between TCRE+ and TCRE− among models, as demonstrated, by previous studies (Zickfeld *et al.*,

2016, 2021; Tachiiri *et al.*, 2019; Tokarska *et al.*, 2019; Melnikova *et al.*, 2021; Canadell *et al.*, 2022). The lack of consensus is also evident from the analysis of 1pctCO_2-cdr idealized experiment (Keller *et al.*, 2018), where MIROC-ES2L and CanESM5 report larger TCRE− whereas UKESM1-0-LL and ACCESS-ESM1-5 show smaller TCRE+ (Figure S21).

Table 4: ZEC values for ACC2 and other ESMs and EMICs participating at the ZECMIP framework(Jones et al., 2019). Shown are the results computed from the ZECMIP data repository (http://terra.seos.uvic.ca/ZEC/) for the B.1 simulations described in Jones et al., (2019) and MacDougall et al., (2020). ACC2 emulating IPSL-CM6A-LR is used as default in our analysis, while those emulating CNRM-ESM2-1 and MIROC-ES2L are used for sensitivity analyses.

Model	Model type	ZEC_{25} (°C)	ZEC_{50} (°C)	ZEC_{90} (°C)
ACC2 (emulating IPSL-CM6A-LR (default))	Simple climate model	-0.154	-0.282	-0.427
ACC2 (emulating CNRM-ESM2-1 (sensitivity))	Simple climate model	-0.168	-0.285	-0.403
ACC2 (emulating MIROC-ES2L (sensitivity))	Simple climate model	-0.136	-0.229	-0.322
Bern3D-LPX-ECS2K	EMIC	-0.057	-0.118	-0.158
DCESS1.0	EMIC	-0.050	-0.117	-0.212
GFDL-ESM2M	ESM	-0.154	-0.221	0.075
IAPRAS	EMIC	-0.060	-0.210	-0.420
LOVECLIM	EMIC	-0.002	0.102	0.001
MESM	ESM	-0.029	-0.113	-0.158
MIROC-lite-LCM	EMIC	-0.041	-0.056	-0.081
PLASIM-GENIE	EMIC	-0.151	-0.480	-0.684
UVicESCM2.10	EMIC	-0.034	-0.030	0.001

1.5 Conclusions

This study examined how the emissions of non-CO_2 GHGs, in particular CH_4, can be accounted for in the carbon-eq budget framework. A key requirement for including non-CO_2 contributions in the carbon-eq budget framework is to ensure the temperature equivalency. That is, non-CO_2 emissions should be converted to CO_2-eq emissions in such a way that the implied temperature outcome remains the same. Recently, the GWP* approach has received attention; however, this approach has not been extensively evaluated for overshoot scenarios or, more generally, peak and decline scenarios in a long time scale.

The analysis using the SSP scenarios confirmed that GWP* does a reasonably good job of ensuring a temperature equivalence for a range of pathways up to 2100. An exception is that when the temperature drops sharply in the ramp-down phase of overshoot, the use of GWP* leads to an overestimation of cooling. Over a longer time scale up to 2300, when the temperature decreases moderately, the use of GWP* can lead to an underestimation of cooling or indicate a slight warming instead. These findings are related to the fact that GWP* was tuned to certain pathways up to 2100, and the results indeed showed that the deviation tends to become more evident after 2100. These findings suggest that GWP* should be cautiously used for scenarios with strong decline in temperatures and longer-term peak and decline scenarios beyond 2100. Nevertheless, GWP* is still far superior to the standard and most widely used metric GWP100 in terms of the temperature equivalency under all scenarios. An attempt has been made to improve GWP* by modifying the parameters in the GWP* equation, but this did not result in any substantial improvement in temperature equivalence. It should be noted that the IRF was used for temperature calculations here to be consistent with the underlying methods that were used to derive metric values in AR5 and the GWP* formula in AR6. When ACC2 and FaIR are used for temperature calculations, our general findings hold; however, the quantitative results become different particularly from ACC2, reiterating the fact that the GWP* formula is model-dependent or reflects certain model assumptions, a point that deserves more attention.

The study further investigated how the overshoot carbon-eq budget for the 1.5 and 2 °C target levels, including the contribution of CH_4, can be affected by the temperature overshoot of varying lengths and magnitudes. Results generally showed that the overshoot carbon-eq budget increases with the length and magnitude of overshoot. This finding is mainly related to the model property of ACC2 that it takes larger cumulative CO_2 emissions in absolute terms to produce a given amount of warming than it takes to produce the same amount of cooling in absolute terms. In other words, TCRE+ is smaller than TCRE− in ACC2, which is also consistent with the negative ZEC. Furthermore, this finding is modified by the conversion of CH_4 emissions into CO_2-eq emissions via GWP*. The application of GWP* on CH_4 has an effect of decreasing the apparent overshoot carbon-eq budget.

To summarize, the use of GWP* to include CH_4 in the carbon-eq budget framework in case of overshoot scenarios works in most scenario until 2100, except for cases with a rapid decline in CH_4 emissions. Over a longer run beyond 2100, the use of GWP* can overestimate the warming effect of CH_4 emissions and consequently may lead to an inaccurate evaluation of carbon-eq budget. However, these results depend on the model configuration used for the analysis, requiring further studies based on different modeling approaches, including uncertainty analyses of Earth system feedbacks.

Code and Data Availability:

The data and the codes used for replicating the analysis and the figures presented in this work can be found in the following GitHub repository: https://github.com/Matteo-Mastro/GWP_overshoot.git.

Annex

Table S5: Performance of GWP100 and GWP temperature equivalency, expressed as RMSE, with respect to the projected temperature of the six SSP scenarios considered in Figure 1. We estimated the metrics performance until 2100 and until 2300.*

Scenario	RMSE $_{GWP100}$ 1750-2100	RMSE $_{GWP*}$ 1750-2100	RMSE $_{GWP100}$ 1750-2300	RMSE $_{GWP*}$ 1750-2300
ssp119	4.69	1.14	19.95	3.24
ssp126	4.5	1.06	20.82	3.32
ssp434	3.4	0.85	30.32	4.43
ssp460	3.77	0.98	35.36	4.95
ssp534os	5.1	1.59	22.73	3.83
ssp585	3.99	1.11	36.63	5.03

Table S6: ESMs used for the ACC2 emulation (from Melnikova et. al, 2021)

ESM	**IPSL-CM6A-LR**	**CNRM-ESM2-1**	**CanESM5**	**UKESM1-0-LL**	**MIROC-ES2L**
Reference	(Boucher et al., 2020)	(Séférian et al., 2019)	(Swart et al., 2019)	(Sellar et al., 2019)	(Hajima et al., 2020)
SSP534OS period	2040–2300	2015–2300	2040–2300	2040–2300	2015–2100
Land carbon	ORCHIDEE, br.2.0	ISBA-CTRIP	CLASS-CTEM	JULES-ES-1.0	VISIT-e
Nitrogen cycle	No	Implicit	No	Yes	Yes
Permafrost	No	No	No	No	No
Fires	No	Yes (natural)	No	No	No
Dynamic vegetation	No	No	dynamic wetlands	Yes	No
Ocean carbon	PISCES-v2	PISCESv2-gas	CMOC	MEDUSA-2.1	OECO2

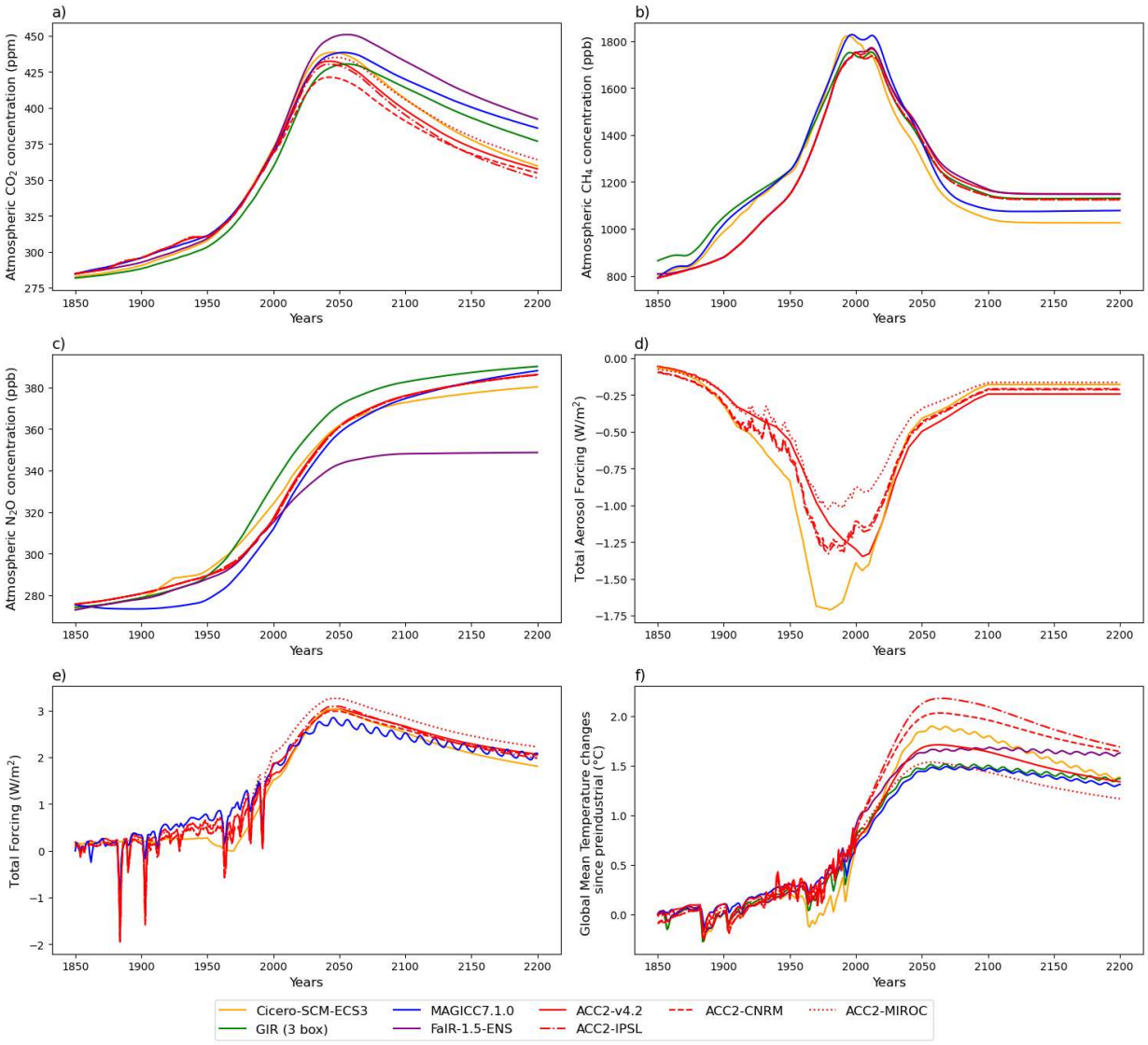


Figure S6: Emission-driven simulations performed by climate emulators using RCP2.6. Data are from Nicholls et al. (2020). Results from GHG emission-driven runs are available from the following emulators as presented: CICERO-SCM-ECS3, GIR (3 box), MAGICC7.1.0, FaIR-1.5-ENS, and ACC2 v4.2. ACC2 also contributes with the three versions emulating IPSL-CM6A-LR, CNRM-ESM2-1 and MIROC-ES2L. Only available models are shown for each of the following variables: atmospheric CO_2, CH_4, and N_2O concentrations (ppm, ppb, ppb, respectively), total aerosol forcing (W/m2), total forcing (W/m2), and global temperature changes (°C) (panels a to f, respectively). The number of models shown for the radiative forcing terms (panels d and e) is limited because some models report only effective radiative forcing. The temperature data were adjusted for the 1850-1900 reference.

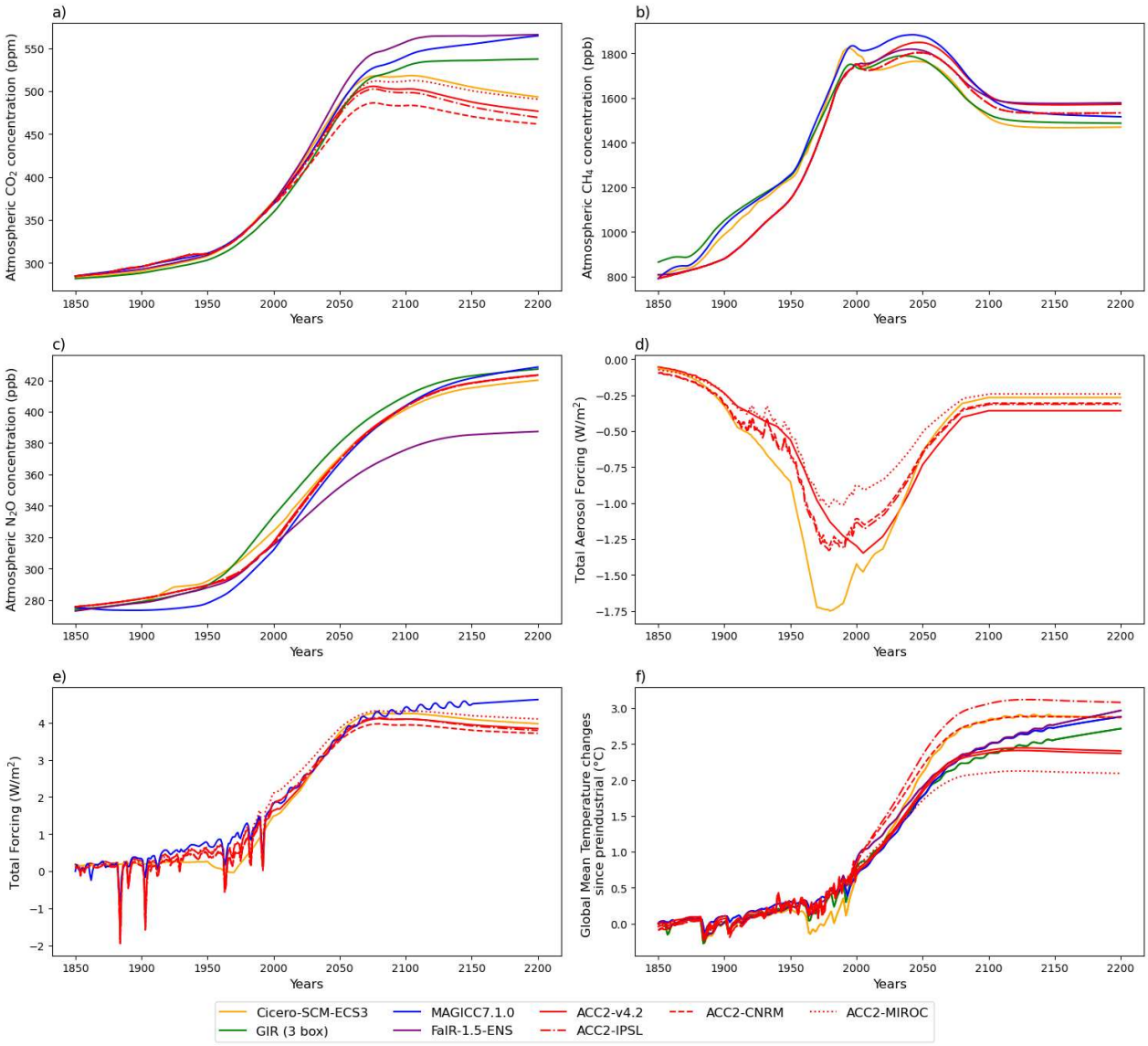


Figure S7: Emission-driven simulations performed by climate emulators using RCP4.5. Data are from Nicholls et al. (2020). Results from GHG emission-driven runs are available from the following emulators as presented: CICERO-SCM-ECS3, GIR (3 box), MAGICC7.1.0, FaIR-1.5-ENS, and ACC2 v4.2. ACC2 also contributes with the three versions emulating IPSL-CM6A-LR, CNRM-ESM2-1 and MIROC-ES2L. Only available models are shown for each of the following variables: atmospheric CO_2, CH_4, and N_2O concentrations (ppm, ppb, ppb, respectively), total aerosol forcing (W/m2), total forcing (W/m2), and global temperature changes (°C) (panels a to f, respectively). The number of models shown for the radiative forcing terms (panels d and e) is limited because some models report only effective radiative forcing. The temperature data were adjusted for the 1850-1900 reference.

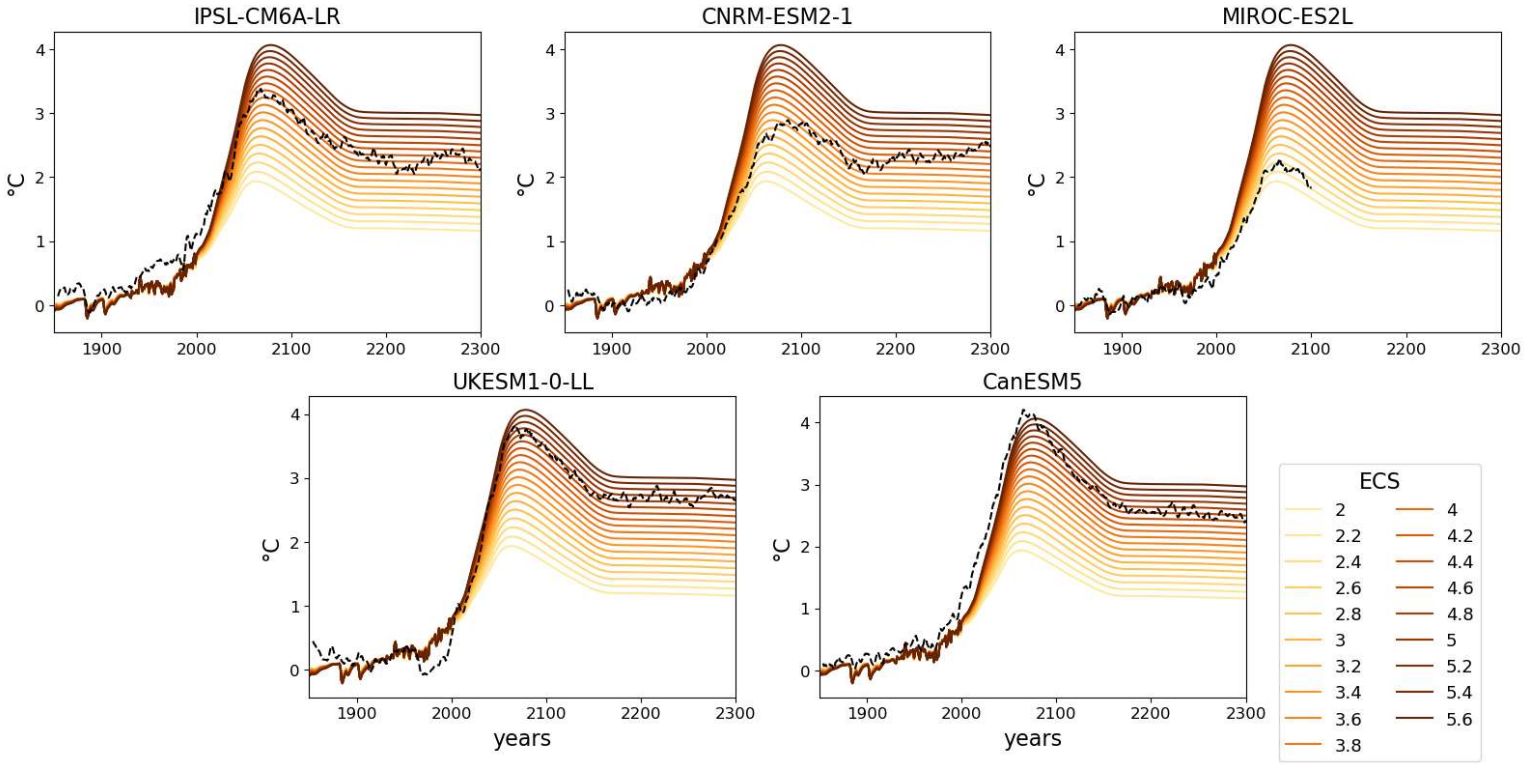


Figure S8: Results of the emulation process for the five ESM considered. GSAT values from ESM and ACC2 for different value of ECS are compared.

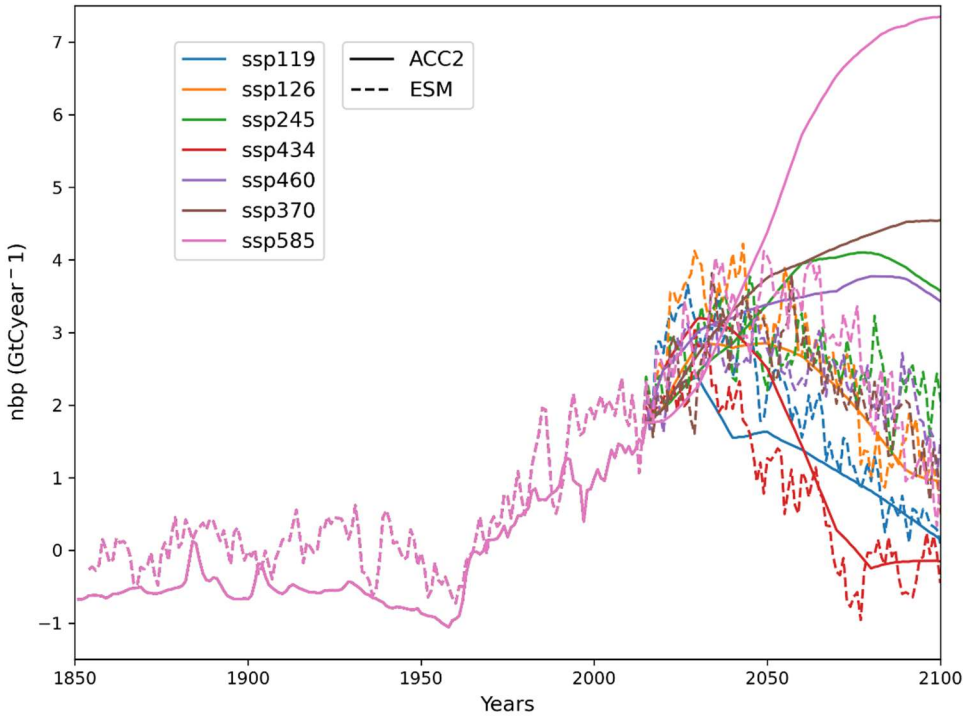


Figure S9: Results of the validation process for the emulation of IPSL-CM6A-LR. NBP values for seven SSP scenarios from ACC2 emulator are shown with respect to the CMIP6 simulation results of the considered model.

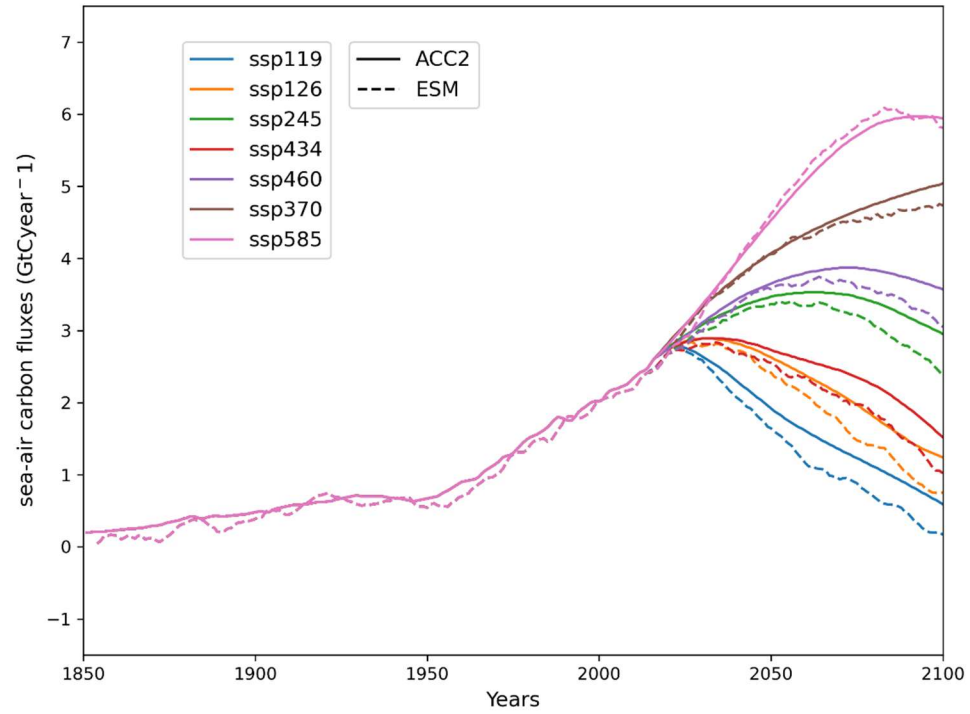


Figure S10: Results of the validation process for the emulation of IPSL-CM6A-LR. Sea-air carbon fluxes values for seven SSP scenarios from ACC2 emulator are shown with respect to the CMIP6 simulation results of the considered model.

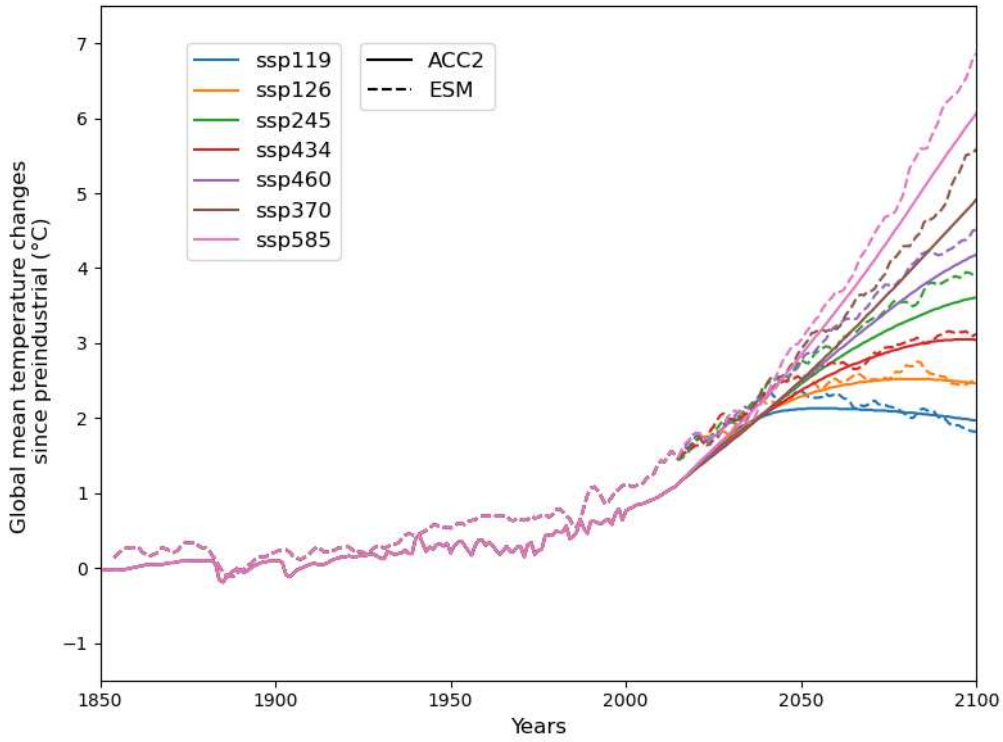


Figure S11: Results of the validation process for the emulation of IPSL-CM6A-LR. GSAT values for seven SSP scenarios from ACC2 emulator are shown with respect to the CMIP6 simulation results of the considered model.

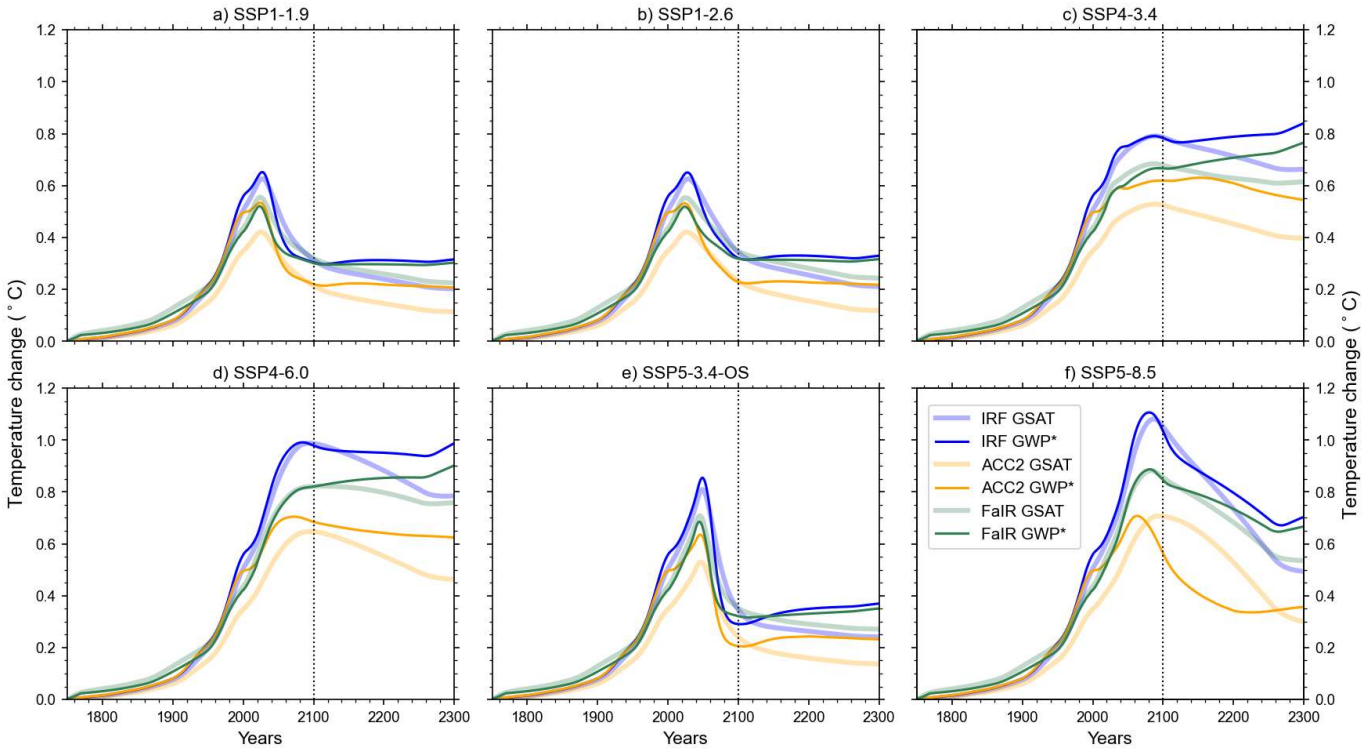


Figure S12: Intercomparison of the Impulse Response Function (IRF) model in AR5, ACC2, and FaIR simulating SSP scenarios. In Lighter lines represent the temperature responses directly calculated from CH_4 emissions using the AR5 IRF, ACC2 and FaIR models. Darker lines represent the temperature responses calculated from the CO2eq emissions converted from CH_4 emissions using GWP.*

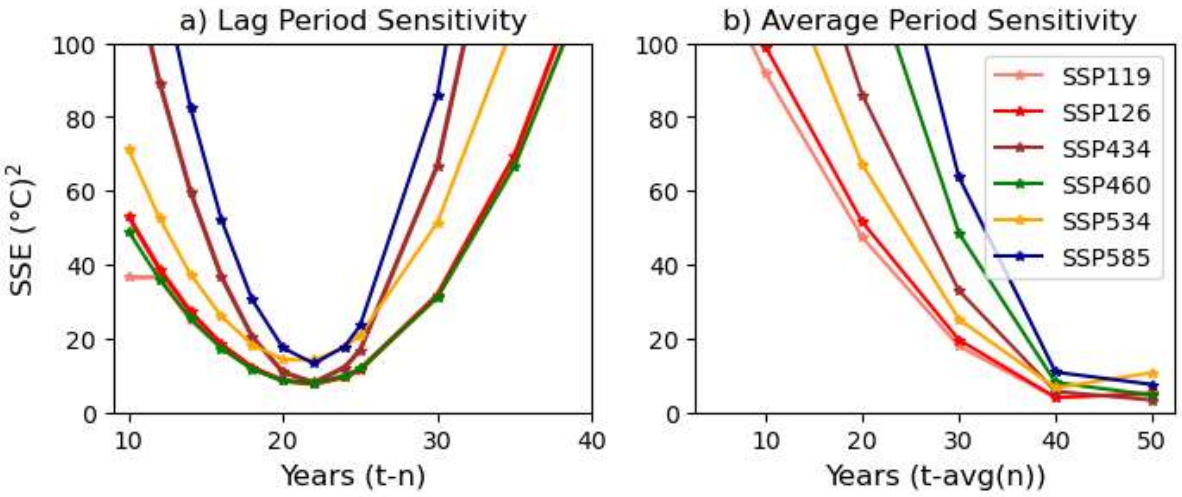


Figure S13: Sensitivity of the temperature equivalency to the parameters used to define GWP under six SSP scenarios. Panel a shows the relationship between the time interval of CH_4 emissions at two points in time in the GWP* flow term (20 years in default, t-n) and the goodness of fit (Sum of Square Error, SEE, y-axis) of the resulting temperature projection relative to the original projection calculated with the Impulse Response Function model directly from CH_4 emissions without using a metric. Panel b shows the relationship between the number of years averaged to calculate the emission trend in the flow term and the goodness of fit (Sum of Square Error, SEE, y-axis) of the temperature projection relative to the original (t-avg(n)).*

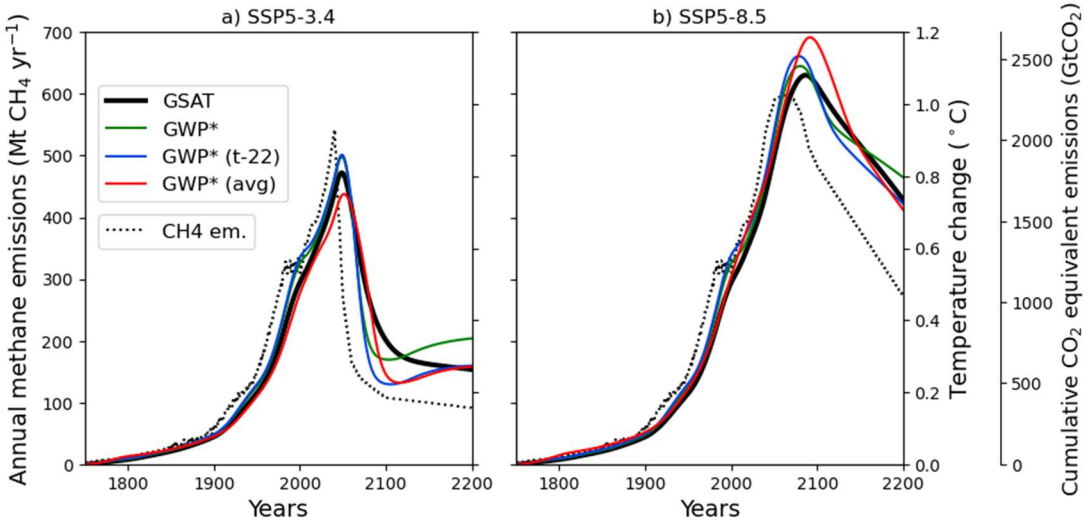


Figure S14: Temperature equivalency of using GWP and its variants under ssp534os and ssp585. GWP* (t-22) is our modified GWP* with the time interval of 22 years (best estimate from Figure 2 panel a) instead of 20 years. GWP* (avg) is another modified GWP*, in which the flow term uses the average change in emissions over the past 40 years (as done in Figure 2, panel b). Panels a and b present the outcome under ssp534os and ssp585, respectively.*

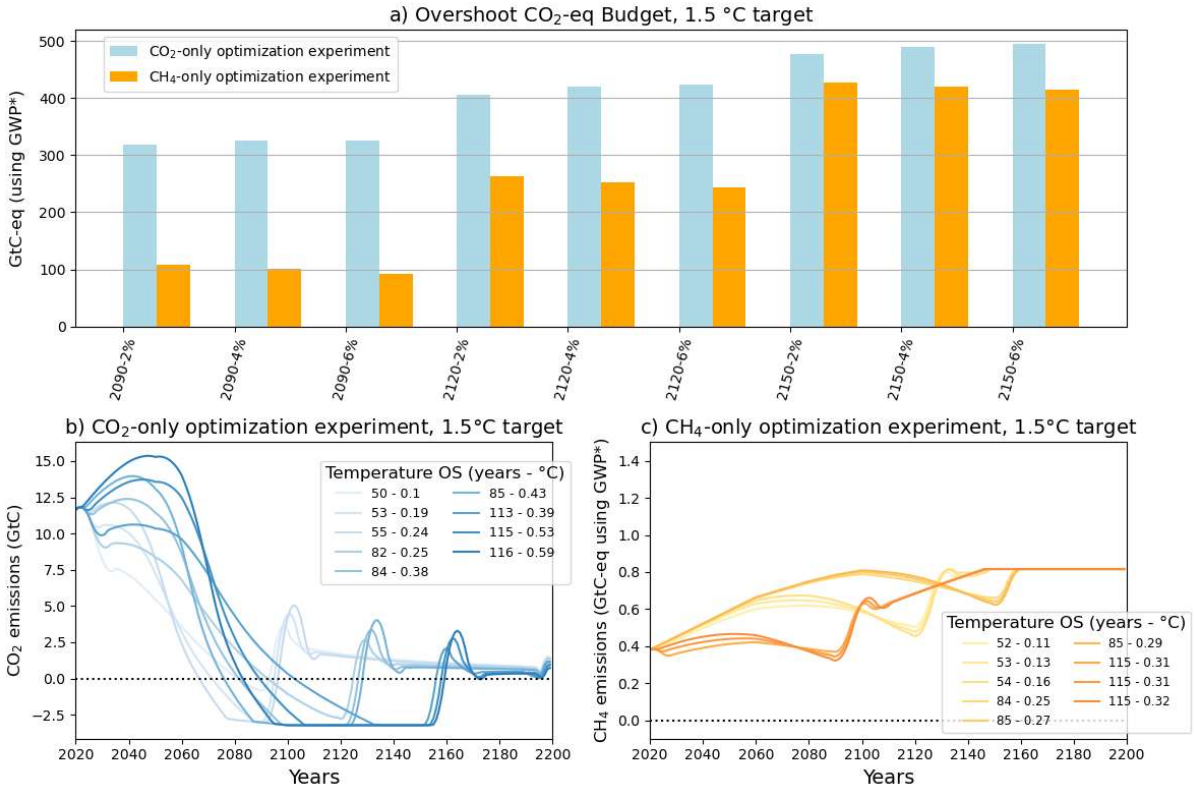


Figure S15: MIROC-ES2L emulation of carbon budget from 2020 to 2200 under 1.5 °C scenarios with a range of temperature overshoot

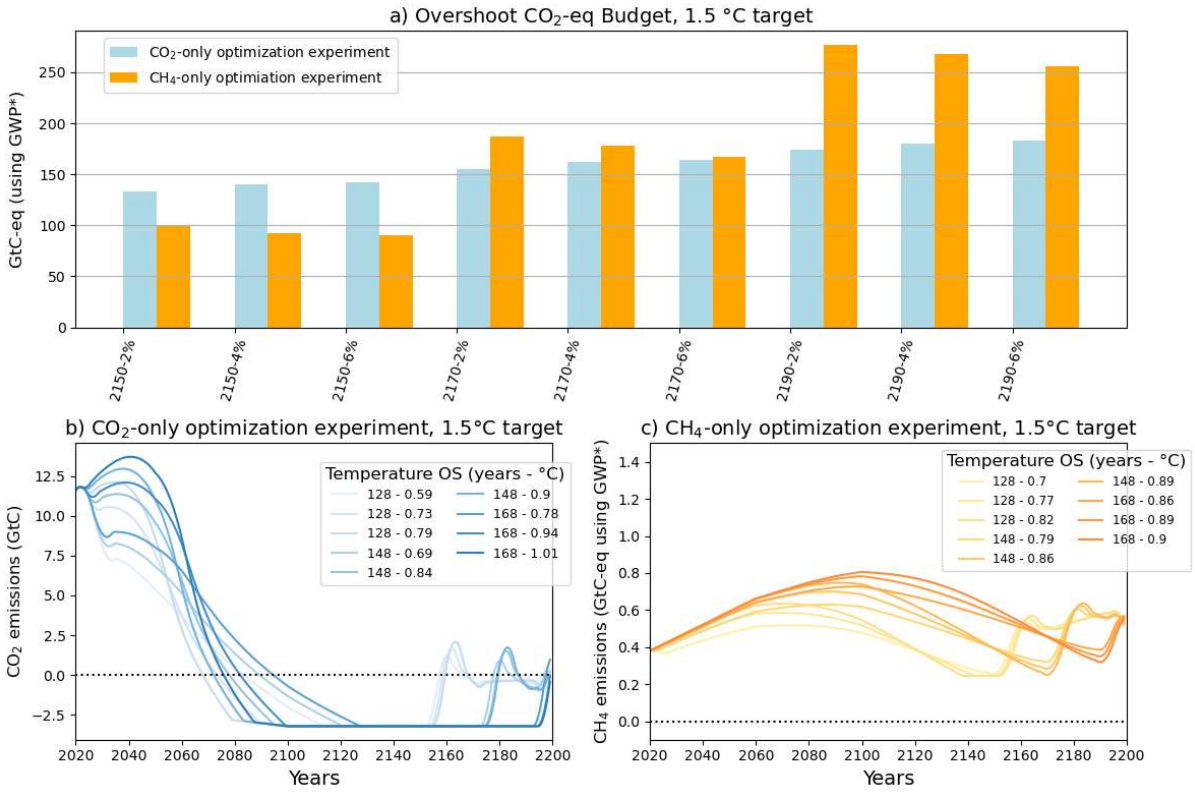


Figure S16: CNRM-ESM2-1 emulation of carbon budget from 2020 to 2200 under 1.5 °C scenarios with a range of temperature overshoot.

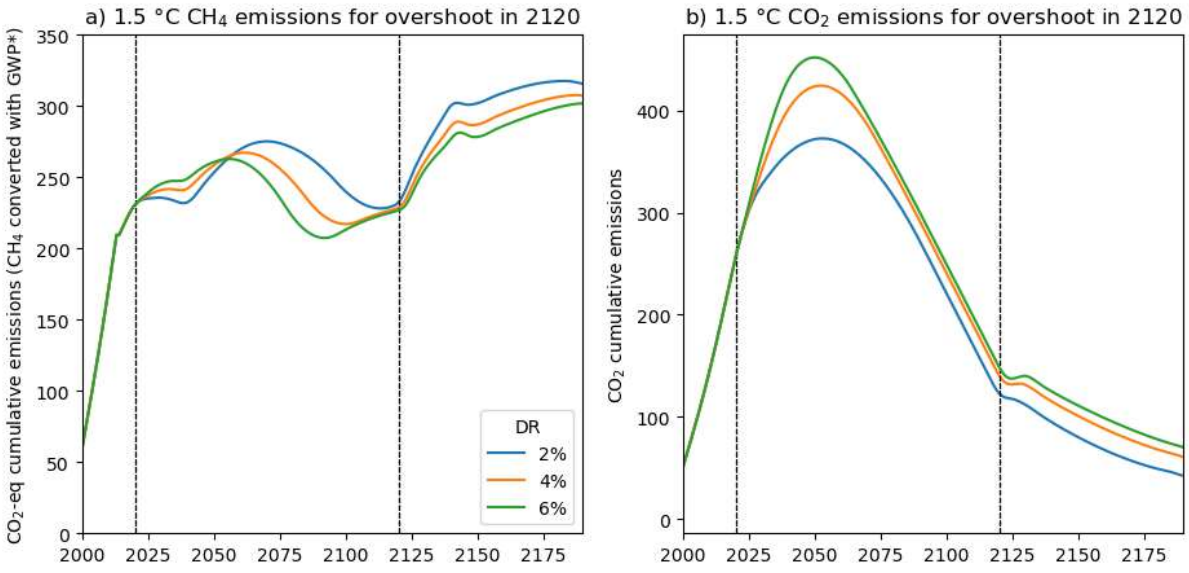


Figure S17 CH_4 and CO_2 emission pathways for scenarios towards the 1.5 °C target with overshoot till 2120 calculated with ACC2 emulating IPSL-CM6A-LR. Panel a) shows CO_2-eq cumulative emissions (from CH_4 emissions converted with GWP), whereas panel b) shows the CO_2 cumulative emissions for meeting the 1.5 °C target in 2120, for the three discount rates considered. Vertical dashed black lines represent the start (2020) and the end (2120) of the period in which the overshoot CO_2-eq budget is calculated. These emissions are used to calculate the overshoot CO_2-eq budgets for the target year 2120 as reported in panel a) of Figure 2.*

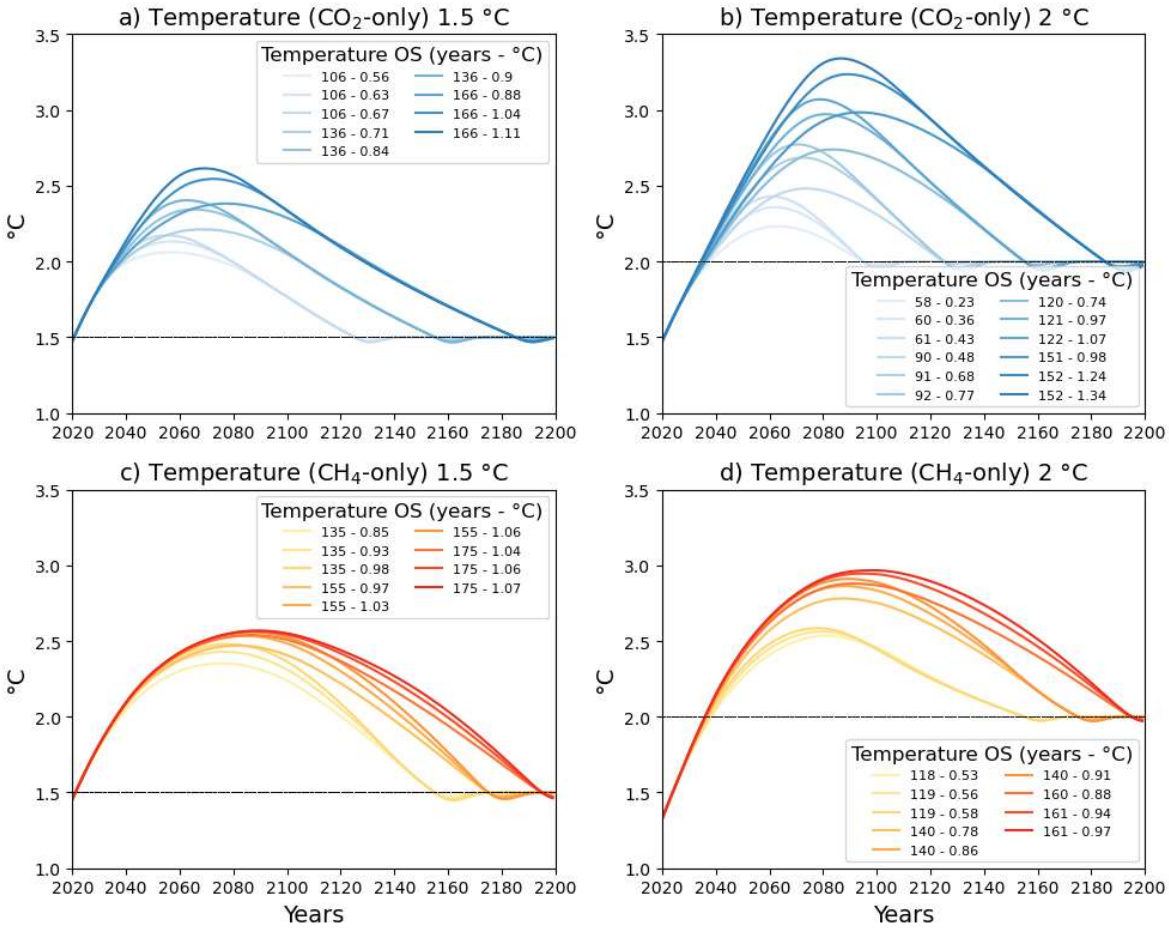


Figure S18: Temperature pathways of CO_2 and CH_4 for the 1.5 °C and 2 °C target levels with ACC2 emulating IPSL-CM6A-LR.. Panel a) and b) show the temperature pathways for CO_2 for meeting the 1.5 and 2°C target, panel c) and d) show the temperature pathways for CH_4 for meeting the 1.5 and 2°C target. Numbers in the legends indicate carbon-eq budget exceedance of each simulation, as derived from the year of the temperature target expressed in the labels of bar-charts of panels a) and b) of Figure 5.

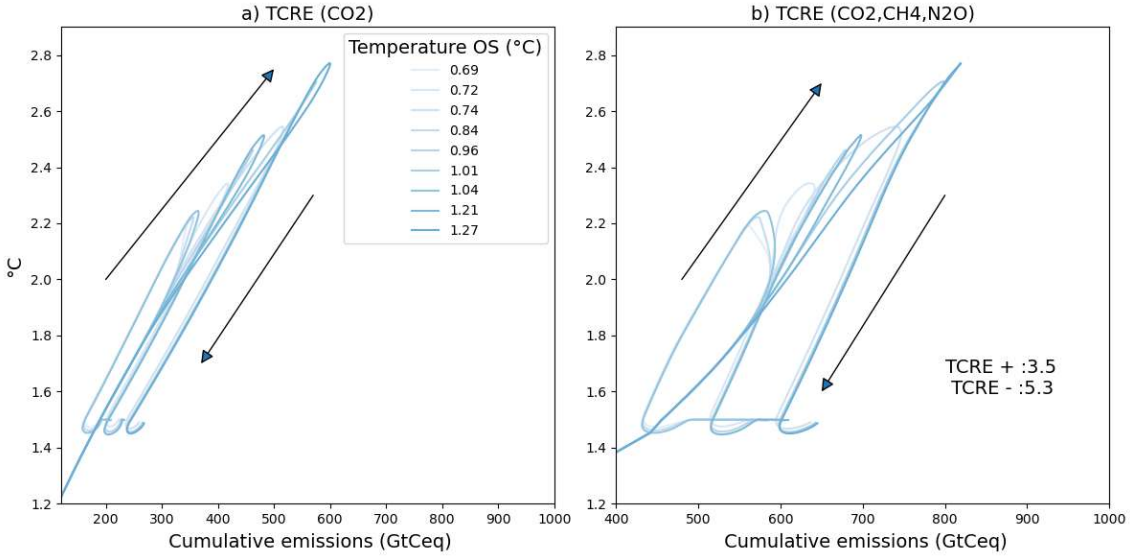


Figure S19: TCRE results for 1.5 °C target and CO_2 simulations with reduced CO_2 fertilization. The BETA factor is equal to 0.3, compared to 0.6 of the ACC2 version emulating IPSL-CM6A-LR (Table 2 in main text). As a consequence of the reduced CO_2 fertilization, TCRE- and TCRE+ values are different, therefore impacting the overshoot net-carbon-eq budget.

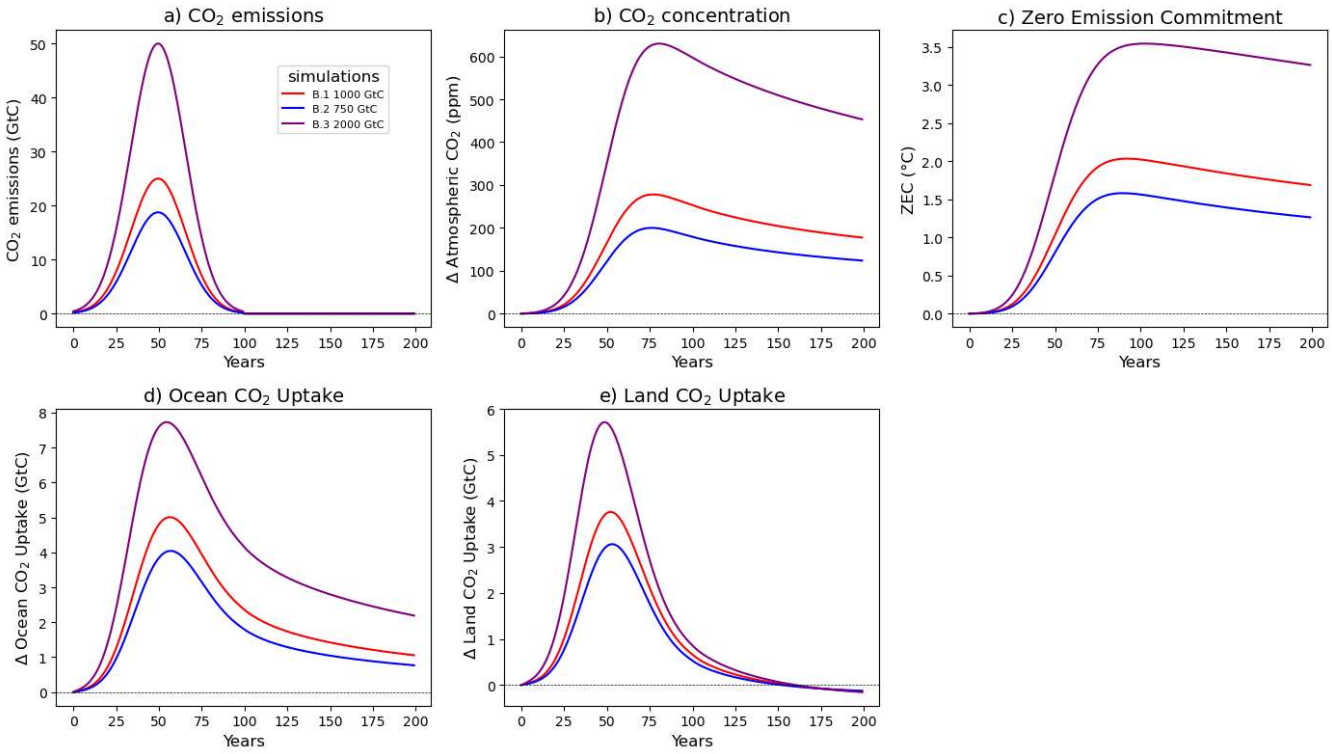


Figure S20: Results of three idealized experiments derived from ACC2 emulating IPSL-CM6A-LR, corresponding to gaussian-shaped CO_2 pathways for different magnitude of cumulative emissions (panel a). Panels b) and c) show the evolution of atmospheric CO_2 concentrations and temperature, while panels d) and e) display the pathways of ocean and land CO_2 uptake. We refer to the work of MacDougall et al., (2020) for the details of the experiments.

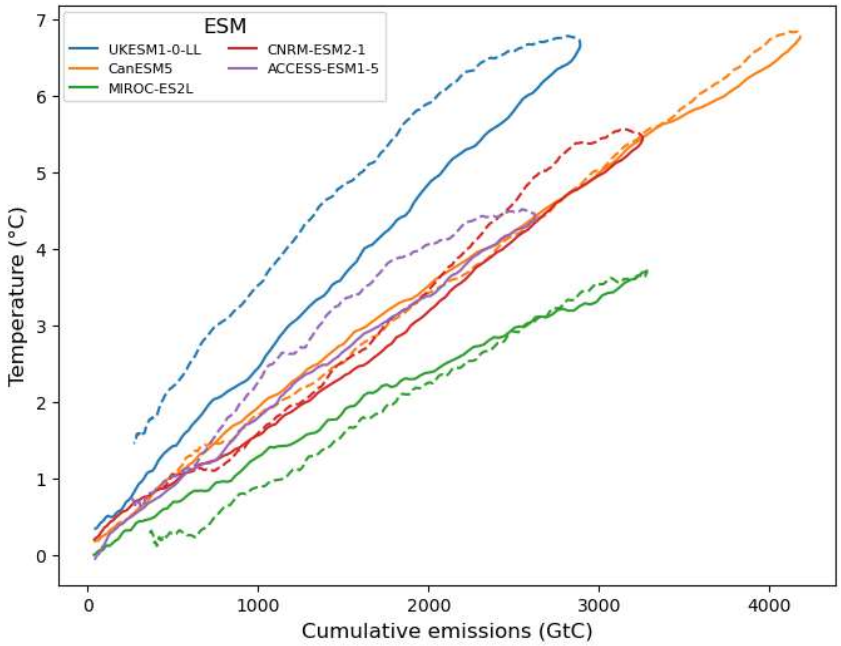


Figure S21: TCRE results for 1pctCO_2-cdr simulation experiments for different ESM

2 Chapter 2: Drivers of Amazon carbon sink projections and uncertainty in CMIP6 models

2.1 Abstract

The Amazon basin rainforest is a critical component of the climate system, currently representing 25% of terrestrial carbon gains and storing 150 to 200 billion tons of carbon. If and by which extent the Amazon rainforest will remain a net carbon sink is an open scientific question, motivated by the unexplained diversity across ESMs results. Specifically, divergent responses are observed in Amazon vegetation productivity projections, especially under sustained global warming scenarios. The inter-model diversity in projected Amazon vegetation is explored using C4MIP and ScenarioMIP simulations with eleven ESM by explicitly accounting for long-term mean state changes and climatic influence at interannual variability. CO_2 fertilization is identified as the main driver determining the future strength of the net carbon sink in a long-term high radiative forcing scenario. At the same time, results show that the impact of ENSO on NBP at interannual timescales is expected to strengthen, a consequence of the higher temperature sensitivity to the climatic mode of variability. Increased focus from modelling groups towards a more accurate and consistent representation of land carbon processes is therefore highly hoped and recommended to allow a more constrained prediction of future environmental changes in the Amazon region.

2.2 Introduction

The Amazon basin rainforest plays a fundamental role in the climate system, serving as a prominent actor in the land carbon cycle and by exerting a significative influence on the global energy budget and hydrological cycle (Davidson *et al.*, 2012). At the same time, the land carbon sink represents one of the crucial uncertainties affecting climate change future evolution (Friedlingstein *et al.*, 2006; K. Arora *et al.*, 2020; Canadell *et al.*, 2021). Indeed, projections of the Amazon climate and carbon sink are still poorly constrained by state-of-the-art Earth System Models (ESMs), indicative of persisting gaps of knowledge regarding this critical aspect of the Earth system (Ahlström *et al.*, 2012; Zhu *et al.*, 2019; Xu *et al.*, 2020; Baker *et al.*, 2021; Koch, Hubau, *et al.*, 2021; Lin *et al.*, 2023; Raoult *et al.*, 2023). In this research, a high-radiative forcing climate-change scenario is considered to assess the drivers of the Amazon net carbon sink variability and characterize some of the key uncertainties affecting inter-model discrepancies in vegetation productivity projections.

The Amazon ecosystem has been a long-term carbon sink during the past decades contributing to approximately 25% of terrestrial carbon gains, estimated in 0.42-0.65 Gt C yr^{-1} for the period 1990–2007, a trend mainly driven since the 1980s by the CO_2 fertilization effect from rising CO_2 concentrations in the atmosphere (Phillips *et al.*, 2009; Pan *et al.*, 2011; O'Sullivan *et al.*, 2019; Walker *et al.*, 2021). Nevertheless, recent estimates have demonstrated a slow-down of net carbon sequestration and consequently a saturation and declining trend in the Amazon carbon sink, with increase in carbon losses due to drought events and increased temperatures (Brienen *et al.*, 2015; Hubau *et al.*, 2020). Both CO_2 concentrations in the atmosphere and climatic conditions affect terrestrial carbon fluxes. Higher atmospheric CO_2 concentrations exert mainly a positive direct effect on photosynthesis through plants stomatal closure and the associated negative carbon-concentration feedback (Boer and Arora, 2009; K. Arora *et al.*, 2020), while they can indirectly increase Ra and Rh (Gao *et al.*, 2020). Climatic conditions, on the other hand, mainly affect vegetation carbon fluxes through temperature and water availability, with a

positive (negative) relationship between temperature (water availability) and changes in respiration rates (Humphrey *et al.*, 2018; Gentine *et al.*, 2019; Green *et al.*, 2019; Liu *et al.*, 2020; Canadell *et al.*, 2021). Additionally, the climatology of the Amazon forest influences the physical constraints on vegetation productivity: wetter parts of the forest (western and central Amazon) are primarily energy-limited, while those with a marked dry season (e.g., the Cerrado region) tend to be limited by water availability (Huete *et al.*, 2006). Interannual variations of water availability and temperature in the region are mainly related to El Niño-Southern Oscillation (ENSO), which is responsible for a vast part of the climatological and net land CO_2 observed interannual variability in tropical biomes (Jones *et al.*, 2001; Kim *et al.*, 2016; Zhu *et al.*, 2017; Bastos *et al.*, 2018; Piao *et al.*, 2020; Mcphaden *et al.*, 2021a). ENSO anomalies typically peak in boreal winter, coincident with the wettest portion of the year over the Amazon region (Cai *et al.*, 2020). Accordingly, some of the most severe droughts observed in the Amazon basin in recent decades and the associated reduction of the net land CO_2 sink were forced by strong warm ENSO events (or El Niños), most prominently including the 1997/1998 and 2015/2016 ones (Jiménez-Muñoz *et al.*, 2016; Koren *et al.*, 2018; Zhang *et al.*, 2019). Current explanations identify the increase of local temperatures forced by El Niño as the main process underlying the ENSO-Amazon connection, with potential consequences on the vegetation long-term state (Jiménez-Muñoz *et al.*, 2016; Liu *et al.*, 2017; Bastos *et al.*, 2018; Zhang *et al.*, 2019).

Given these promises, at least three factors will contribute to determining whether, and to which extent, the Amazon ecosystem will remain a net carbon sink in the future decades under sustained positive radiative forcing: mean-state climatic changes, nutrient limitation, and ENSO. First, a significant increase in surface air temperature and a marked decline in water availability in the Amazon basin as simulated for increased greenhouse gas emission scenarios will most likely result in a less effective carbon sink by the end of the 21st century (Parsons, 2020). In particular, coupled climate models suggest that the reduction in precipitation is given by reduced evapotranspiration resulting from stomatal closure response

to increased CO_2, which lead to changes in local surface energy balance and atmospheric circulation patterns (Kooperman *et al.*, 2018; Langenbrunner *et al.*, 2019). Then, Nitrogen and Phosphorous will likely more strongly limit tropical forests productivity (Fleischer *et al.*, 2019), partly counterbalanced by the positive effect exerted by the increasing atmospheric CO_2 concentrations (Huntingford *et al.*, 2013; Koch, Brierley, *et al.*, 2021). Lastly, an increased Amazon vegetation sensitivity to ENSO is expected under a range of global warming scenarios (Kim *et al.*, 2017; Park *et al.*, 2020; Uribe *et al.*, 2023). In particular, projected changes in the ENSO-Amazon connection may arise from both changes in ENSO properties (amplitude, skewness, spectrum) and from variations in the ENSO teleconnection mechanism with the Amazon region (Chen *et al.*, 2017; Zheng *et al.*, 2017; Yeh *et al.*, 2018; Beobide-Arsuaga *et al.*, 2021; Cai *et al.*, 2021; Mcphaden *et al.*, 2021b). Notably, ENSO amplitude is slightly yet significantly enhanced under future global warming scenarios (Beobide-Arsuaga *et al.*, 2021; Cai *et al.*, 2022), and regional patterns of precipitation and temperature anomalies over South America associated with ENSO teleconnections are projected to be amplified in warmer climates (Perry *et al.*, 2020; McGregor *et al.*, 2022). In this research the Amazon carbon sink variability is investigated in historical and ssp585 scenario conditions by means of CMIP6 ESMs simulations (Eyring *et al.*, 2016; O'Neill *et al.*, 2016) to separate the relative contributions of long-term changes and interannual variability under sustained global warming. Specifically, throughout the paper, one question that remains underexplored in the literature is tackled: what are the relative contributions of interannual variability and long-term climatic changes to uncertainty in the projected Amazon net carbon sink evolution? In doing that, an attempt is performed to identify the local factors contributing to inter-model diversity in Amazon vegetation productivity.

2.3 Data and Methods

2.3.1 Data

The research entails the use of simulations from eleven CMIP6 generation ESMs that contributed to C4MIP 1pctCO_2-bgc, 1pctCO_2-rad, ssp585-bgc, ssp585-rad and ScenarioMIP historical and ssp585 experiments (Eyring *et al.*, 2016; Jones *et al.*, 2016; O'Neill *et al.*, 2016) (Table 7). Those ESMs for which at least one realization is available for 1pctCO_2 experiments and that have all the prognostic variables needed for the analysis available (or computable indirectly) are considered. Table 7 presents an overview of the experiments considered and the methodologies adopted for each experiment. For the historical and ssp585 simulations, the first five realizations of each model were used, when more than one is available, with the caution of having the same simulation members for the historical and ssp585 scenarios to make a pairwise comparison. The details of the ESMs used are reported in Table S9. In these simulations, the analyses have been performed on single realizations, and have been aggregated by model solely for the presentation of the results. The evolution of the land carbon-cycle is investigated by considering monthly NBP values, which represent the balance of Gross Primary Productivity (GPP) due to photosynthesis at the net of autotrophic respiration (Ra), heterotrophic respiration (Rh) and disturbances, as fire dynamics (for those model having a fire module) and Land Use Change (LUC). Overall, the following variables have been considered in the study: sea-surface temperature (SST), Net Biome Productivity (NBP*)*, Gross Primary Production (GPP*)*, autotrophic respiration (Ra), heterotrophic respiration (Rh) , precipitation (Pr), soil moisture (mrso), air surface temperature (T), and shortwave incoming radiation (SWin).

Table 7: Overview of the experiments and methodologies used in the research. We refer to the work of Jones et al., (2016) and O'Neill et al., (2016) for more information on the C4MIP and ScenarioMIP experiments reported in this table.

Project	Experiments	Reference years	ESMs (n°)	Coupling	Effect estimated
C4MIP	1pctCO_2-rad	36-150	11	Radiative-only	Long-term, Climate
	ssp585-rad	2015-2100	7	Radiative-only	Long-term, Climate
	1pctCO_2-bgc	36-150	11	Biogeochemically-only	Long-term, CO_2 fertilization
	ssp585-bgc	2015-2100	7	Biogeochemically-only	Long-term, CO_2 fertilization
ScenarioMIP	historical	1750-2014	11	Coupled	Inter-annual variability (IAV)
	ssp585	2015-2100	11	Coupled	Inter-annual variability (IAV)

Zonal statistics computed within the Amazon basin and presented throughout the results are obtained by considering the grid-cells of interest within the Amazon basin shapefile downloaded from the SO HYBAM service (INPE, 2019, https://hybam.obs-mip.fr/).

The ESMs performances in representing ENSO properties, the Amazon basin climatology, carbon and energy fluxes are evaluated against observational and quasi-observational products. HadISST dataset is used for assessing ESMs sea surface temperatures (Rayner *et al.*, 2003), while ERA5 and ERA5-Land products are used to validate temperature, precipitation and soil moisture (Hersbach *et al.*, 2020; Muñoz-Sabater *et al.*, 2021). Finally, the FLUXCOM-RS+METEO dataset, specifically the one forced with the WFDEI meteorological dataset (Weedon *et al.*, 2014), is used as a reference for both carbon fluxes

(GPP, NEP, Total Ecosystem Respiration, TER) and energy fluxes (shortwave incoming radiation) (Jung *et al.*, 2019, 2020).

To evaluate ESMs against the reanalysis products, as well as to compute multi-model means across variables, a conservative remapping algorithm is applied to all the data to get a regular 1° longitude x 1° latitude grid, with the exception of SST from ESMs with a curvilinear grid (Table S9), for which a distance weighted (nearest-neighbor) average remapping is applied. The validation procedure refers to the climatological period 1979-2013. When comparing the carbon fluxes from ESMs with FLUXCOM data, the total ecosystem respiration is obtained by summing the contributions of Ra and Rh. An overview of the ESMs evaluation performances is available in the supplementary material (Figure S30 to Figure S33).

2.3.2 Long-term mean-state climatic effects

Increasing trends of atmospheric CO_2 concentrations affect terrestrial carbon sinks directly through a fertilization effect on vegetation (carbon-concentration feedback) and indirectly by forcing changes in the physical climate via a strengthened greenhouse effect, which in turn affects vegetation (carbon-climate feedback). A common approach to disentangle the two effect is by taking advantage of the carbon-cycle feedback framework, by which it is possible to estimate the magnitude of the carbon-concentration feedback and the carbon-climate feedback (Jones *et al.*, 2016; K. Arora *et al.*, 2020). The contribution of these two feedbacks is estimated with the following linear equations:

$$\beta = \frac{\Delta NBP_{cum,B}}{\Delta ppm_{BGC}} \tag{6}$$

$$\gamma_T = \frac{\Delta NBP_{cum,R}}{\Delta T_{RAD}}; \quad \gamma_{mrso} = \frac{\Delta NBP_{cum,R}}{\Delta mrso_{RAD}}; \quad \gamma_{SW_{in}} = \frac{\Delta NBP_{cum,RAD}}{\Delta SWin_{RAD}} \tag{7}$$

Carbon sink is represented here by the cumulative NBP, whose long-term sensitivity to CO_2 ppm (β), and climate (γ), is estimated from biogeochemically only coupled simulations (1pctCO_2-bgc and ssp585-bgc) and radiative only coupled simulations (1pctCO_2-rad and ssp585-rad) respectively. Within the former, the increased CO_2 atmospheric concentration

is uniquely exerting a biogeochemical effect which interests the terrestrial and ocean carbon cycle processes, whereas in the radiative simulation only the radiative transfer processes in the atmosphere are affected by the changing atmospheric CO_2 concentrations, with no consequences for biochemical processes. Changes (Δ) are expressed with respect to the first year the simulations; for 1pctCO_2 experiments only the years with atmospheric CO_2 ranges similar to ssp585 (400-1135 ppm, resulting in 104 years) have been considered. Carbon-climate feedback has been further computed with respect to surface atmospheric temperatures (T), soil moisture (mrso) and shortwave incoming radiation (SWin), to represent the variety of mean-state climatic changes affecting the cumulative carbon fluxes within the Amazon basin.

2.3.3 Carbon fluxes sensitivity at inter-annual timescales

The evolution of carbon fluxes within the Amazon basin has been assessed at interannual timescales to explore the short-term variability contribution of different climatic factors. With this respect, two additional analysis have been performed. A first analysis aimed at assessing the relative contribution of temperature, soil moisture and shortwave-incoming radiation on NBP, GPP, Ra and Rh by adopting a multivariate predictive regression model as in the following equation, for every ESMs considered:

$$\Delta NBP = \frac{\delta NBP}{\delta T}\Delta T + \frac{\delta NBP}{\delta mrso}\Delta mrso + \frac{\delta NBP}{\delta SW_{in}}\Delta SW_{in} + \epsilon \qquad (8)$$

The usage of temperature, soil moisture and shortwave incoming radiation is justified by their primary control on carbon fluxes interannual variability (Jung *et al.*, 2017); specifically, soil-moisture rather than precipitation was used as a proxy for water availability due to its stronger control on terrestrial carbon fluxes (Humphrey *et al.*, 2018). All the variables considered have been averaged over the calendar year, as the focus of the analysis is on interannual variability. In equation 8, NBP (as well as GPP, Ra and Rh) have been linearly detrended to remove the influence of CO_2 fertilization and other long-term climatic changes, while the three independent variables have been detrended and standardized (divided by

their standard deviation) to obtain comparable coefficients. Therefore, the standardized coefficients represent the quantitative contribution of temperature, soil-moisture and shortwave incoming radiation considering the simultaneous confounding impacts of the other variables. Specifically, a 5-fold cross-validation ridge regression model has been adopted, because the penalty score in the cost function of ridge regression helps to account for the collinearity among the predictors themselves. The best performing regularization parameter among a set of values spaced evenly on a log scale has been chosen. The multivariate model derives from the Scikit-Learn package, available for the Python scripting language (Pedregosa *et al.*, 2012). Given the predominant modulation of carbon fluxes IAV by means of ENSO within the Amazon basin (Mcphaden *et al.*, 2021a), a second analysis investigated its contribution on vegetation productivity within the Amazon basin mediated by either temperature and water-availability (using soil moisture as a proxy). For this, an annual time series of ENSO is obtained for each historical and ssp585 realization by computing the canonical Nino3.4 index, defined as the 5-months moving average of spatially-averaged sea surface temperatures over the region 170-120°W and 5°S-5°N, subsequently detrended by means of a 1st order polynomial and normalized. By taking the univariate sensitivities of temperature and soil-moisture with respect to ENSO, and accounting for the partial derivatives of NBP with respect to temperature and soil-moisture as in Equation 8, it is possible to estimate the contribution of ENSO driven by the two mechanisms as below:

$$dNBP_{n34,T} = \frac{\delta NBP}{\delta T} \frac{dT}{dn34} \quad (9)$$

$$dNBP_{n34,mrso} = \frac{\delta NBP}{\delta mrso} \frac{dmrso}{dn34} \quad (10)$$

Using the partial derivatives $\frac{\delta \mathrm{NB}}{\delta \mathrm{T}}$ and $\frac{\delta \mathrm{NBP}}{\delta \mathrm{mrs}}$ ensures that the contribution of temperature and precipitation accounts for the confounding factor of the other mechanism, a condition not met if the univariate estimates $\frac{\mathrm{dNBP}}{\mathrm{dT}}$ and $\frac{\mathrm{dNBP}}{\mathrm{dmrso}}$ would have been applied. A Mann-Whitney U-test of independence with Bonferroni correction was used to assess whether the zonal values of the regression coefficients within the Amazon basin are significantly different between the historical period and ssp585 scenario.

2.4 Results and Discussion

2.4.1 Intermodel uncertainties of carbon and climatic drivers

Amazon basin vegetation productivity and climatology shows substantial agreement across models during the historical period but strongly diverging trends during the ssp585 scenario, with individual models differing in magnitude and sign of projected changes (Figure 22). The multi-model ensemble yields a cumulative NBP mean of by the end of the 21st century of 59.3 ± 62 $kgCm^{-2}$. With respect to projections of the cumulative carbon sink in Figure 22a and carbon fluxes in Figure S34, the inter-model uncertainty is much higher compared to the intra-model uncertainty (which stems from the intrinsic climatic variability expressed in each realization and is represented by the ±1 standard deviation spread in the plots). On the other hand, considering the climatological variables in Figure 22b-e, intra-model uncertainty is considerably higher as it stems from the internal climate variability intrinsic in each simulation. These considerations already highlight that part of the divergence across carbon cycle predictions is related to differences in the land sensitivity to climatic forcings, other than uncertainties in the evolution of the climate itself. Overall, the climatological variables present a stronger agreement and coherence in the sign of projected changes among ESMs. A multi-model mean reduction of -21.13 mm $year^{-1}$ and -128.93 kgm^{-2} is projected for precipitation and soil moisture, respectively (Figure 22c,d), while an increase is observed for temperature and incoming shortwave radiation (+7.08 °C and +9.23 Wm^{-2}, Figure 22b,e). Still, the multi-model ensemble spread at the end of the 21st century remains substantial for all these variables. Differences among models of one or even two orders of magnitude could be seen for instance between MRI-ESM2-0 and CanESM5 for shortwave incoming radiation or for MIROC-ES2L and IPSL-CM6A-LR regarding soil moisture projections. For some models, divergent carbon sink projections cannot be easily attributed to similar deviations projected for the individual climatic drivers. For instance, ACCESS-ESM1-5 and NorESM2-LM projects similar end-of-the-century temperature and soil-moisture changes, but strongly diverging trends of cumulative NBP. Regarding the intra-model spread, the highest influence

of internal climatic variability (±1 standard deviations) is observed in precipitation and shortwave incoming radiation, followed by soil-moisture (spreads in Figure 22c,e and d). This indicates that within the Amazon basin, the highest source of ESMs uncertainty deriving from internal climate variability is associated to cloud formation and coverage, which is causally linked to the amount of precipitation (thus soil moisture content) and shortwave incoming radiation within the regional domain. All the carbon fluxes from which NBP is derived (GPP, Ra and Rh) depict an increasing trend throughout the 21st century (Figure S34), with the notable exception of GPP and heterotrophic respiration for ACCESS-ESM1-5. Among those, Rh presents the highest end of 21st century uncertainty (186.74 gCm^{-2}, z-score std-dev of 1.62), followed by GPP and Ra (753.59 and 548.71 gCm^{-2}, z-score std-dev of 1.12 and 0.76 respectively). This demonstrates that uncertainty in cumulative NBP does not solely stem from single climatic factors; instead, it arises from inconsistencies and differences in how models represent photosynthetic activity, autotrophic and heterotrophic respiration. Overall, inconsistencies in projected Amazon carbon sink cannot be simply understood as a consequence of discrepancies in the climatic factors affecting vegetation. A point that deserves attention is therefore how the projected carbon sink in the Amazon basin is sensitive to mean-state changes in environmental factors and climatic variability at the interannual timescale.

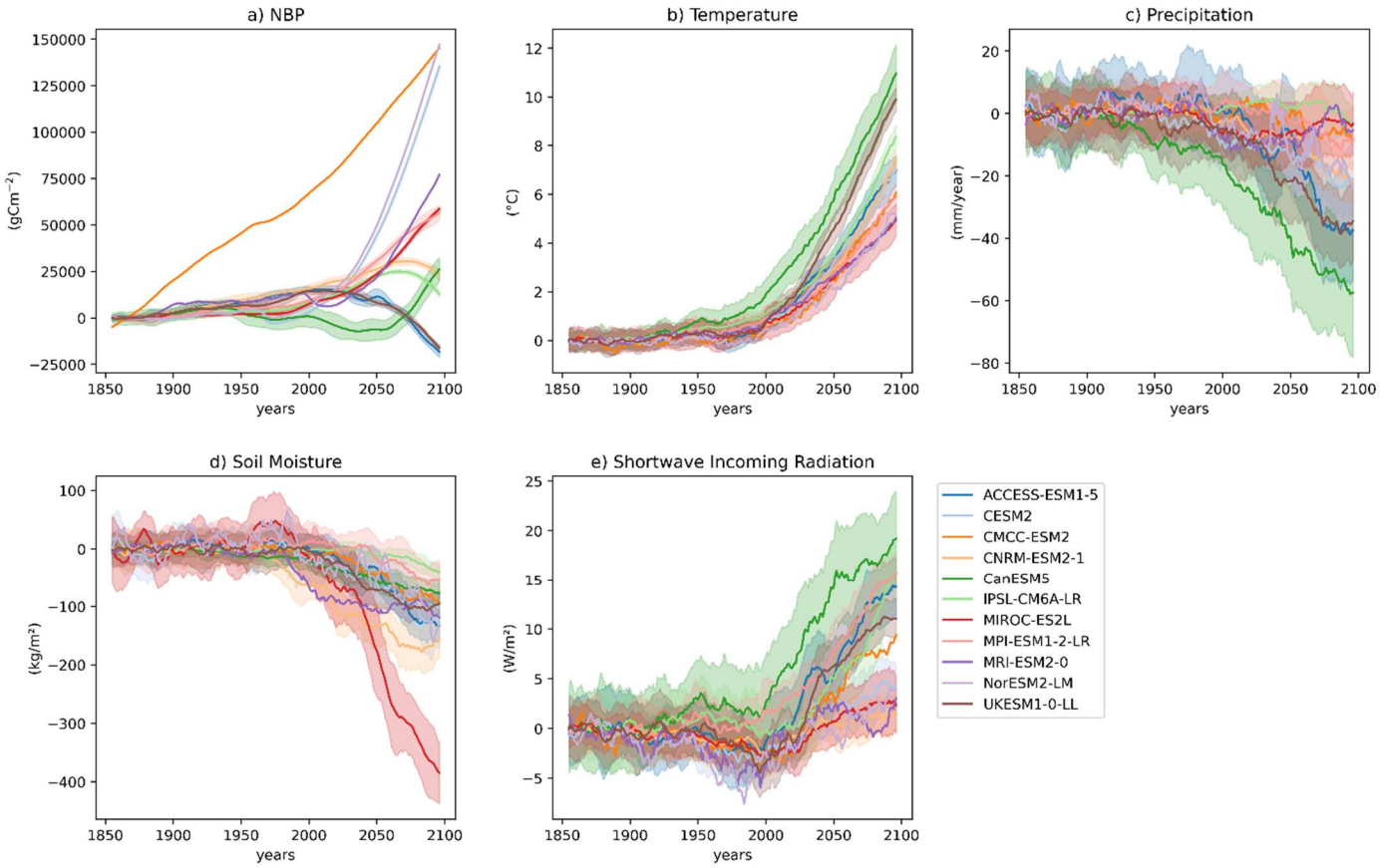


Figure 22: Long-term trends of (a) cumulative NBP, (b) temperature, (c) precipitation, (d) soil-moisture, (e) shortwave incoming radiation in the Amazon basin for the historical and ssp585 experiments. Trends are computed with respect to the first 30-year mean of the historical period (1850-1880), and are visualized as a 10-year moving average for clarity. For the models with more than one realization, both the model-ensemble mean (line) and the spread (±1 standard deviation, shading) are shown.

2.4.2 Long-term carbon sink sensitivity

Amazon carbon sink evolution under a high radiative forcing scenario as the ssp585 with respect to the historical period can be attributable either to an increased CO_2 concentration in the atmosphere, which exerts an effect on terrestrial ecosystems by modulating the plants stomatal conductance, or to changes in mean state climatic conditions. By applying the carbon-cycle feedback framework (see the methods in Paragraph 2.3), the net carbon sink (cumulative NBP) response is explained by the factor β (CO_2 fertilization) and by the factor γ (climate effect). Below, the magnitude of β derived from the 1pctCO-bgc simulation is

showed in Figure 23. All of the ESMs project a positive CO_2 fertilization effect within the Amazon basin for the range of CO_2 atmospheric ppm forcing the ssp585 scenario, despite considerable variability could be observed across the models. CESM2 and NorESM2-LM present the higher vegetation sensitivity to atmospheric CO_2, reasonably due to the fact that both the models share the same land module CLM5 (Table S9). CMCC-ESM2 also presents high β values, but these are restricted to the most forest-dense pixel cells, as it is evident from the sharp decline in the southern and south-eastern part of the basin, a pattern which is even more drastic in ACCESS-ESM1-5.

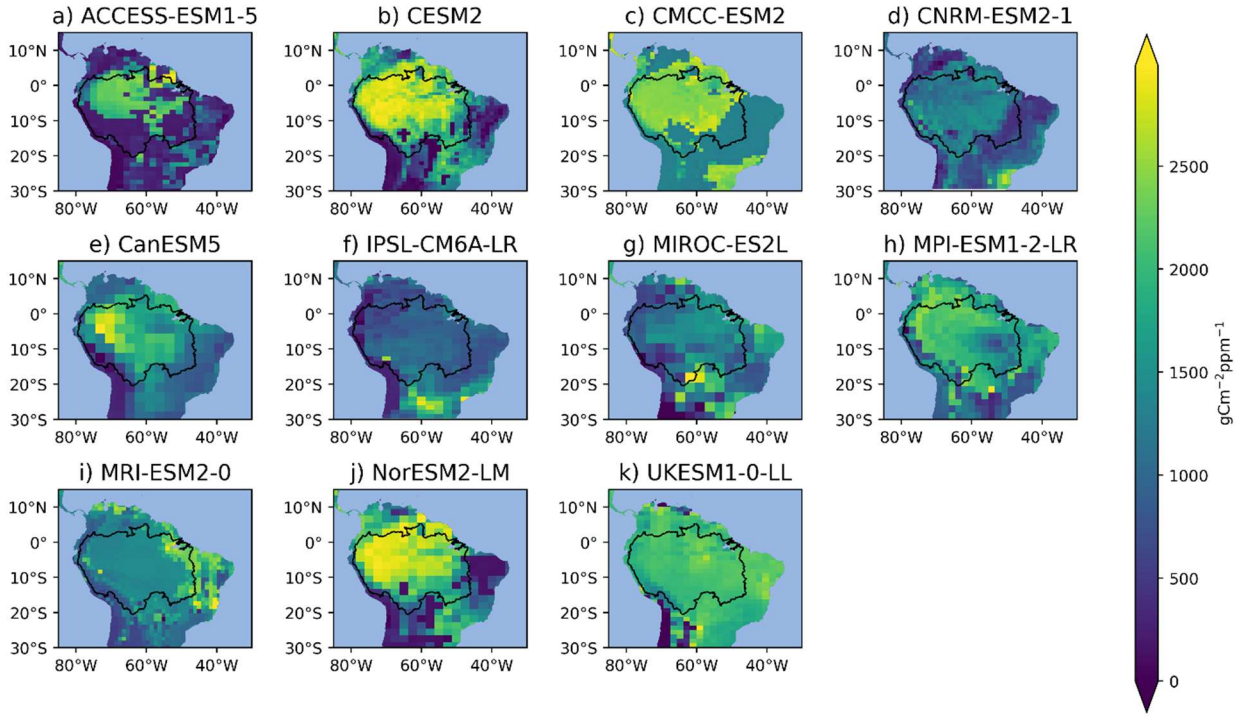


Figure 23: Estimates of the carbon-concentration feedback (β) for the ESMs considered The Amazon basin, obtained from the SO HYBAM service (https://hybam.obs-mip.fr/), is also represented.

Despite the carbon cycle feedback framework entails to describe the positive (to be intended here as reinforcing) carbon-climate feedback with surface air temperature, the values of the standardized γ and β values are reported in Figure S36 with the purpose of providing a

quantitative comparison of the ESMs sensitivity to atmospheric CO_2 and climate, thus γ_{tas}, γ_{mrso} and γ_{rsds} are not to be intended as cumulative long-term impacts. Remarkable negative effects on Amazon carbon sink are associated with long-term increasing temperatures, and partially with less intensity, with rising trends in shortwave incoming radiation. The positive co-variability of the carbon sink with soil-moisture is almost specular of the cumulative NBP sensitivity to shortwave incoming radiation, a consequence of the strong inverse correlation among the two factors, reflecting a reduction of cloud coverage in the Amazon basin with increasing atmospheric CO_2 and climate warming.

Overall, the long-term cumulative NBP in the coupled 1pctCO_2 simulation is reconstructed by means of its sensitivity to mean-state changes in temperature (from 1pctCO_2-rad simulation) and atmospheric CO_2 (from 1pctCO_2-bgc simulation). As a consequence, CO_2 fertilization effects on vegetation productivity are expected to dominate and overcome the climatic influence on the long-term carbon sink evolution in a high-CO_2 future scenario, as reported in Figure 24. This analysis reaffirms for state-of-the-art CMIP6 models and for the specific geographical domain of the Amazon region what pointed out by Huntzinger et al. (2017), despite the different research assumptions, that showed the predominant role of CO_2 sensitivity in shaping the net carbon sink variability across land models.

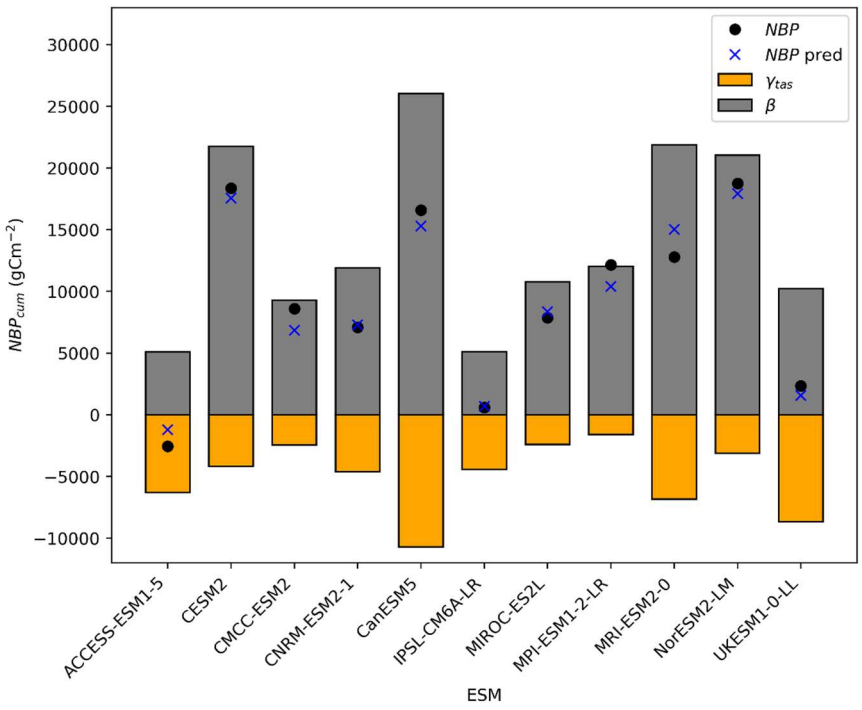


Figure 24: Contribution of carbon-concentration (β) and carbon-climate feedbacks (γ_{tas}) to net carbon sink projections at the end of the 1pctCO₂-bgc and 1pct CO₂-rad simulations. Black dots represent the net cumulative NBP resulting from the arithmetic sum of cumulative NBP from 1pctCO₂-bgc and 1pctCO₂-rad simulations, whereas the blue crosses are the result of the arithmetic sum of the estimated cumulative NBP by adopting the univariate $\boldsymbol{\beta}$ and $\boldsymbol{\gamma_{tas}}$ coefficients. Values are averaged within the Amazon basin domain.

The ESMs variability in the long-term climate-driven trend of net carbon sink in the Amazon region emerges from a very strong correlation between its sensitivity to temperature γ_{tas} and soil-moisture γ_{mrso}, reported in Figure 25 and Figure S37 for both 1pctCO$_2$-rad and ssp585-rad simulations. As a consequence, ESMs Amazon carbon sensitivity to long-term climate variability is not only discernible by the negative temperature effect, but it is also proportional in a positive fashion to soil-moisture, despite temperature plays a slightly stronger control on the net carbon sink (Figure S36).

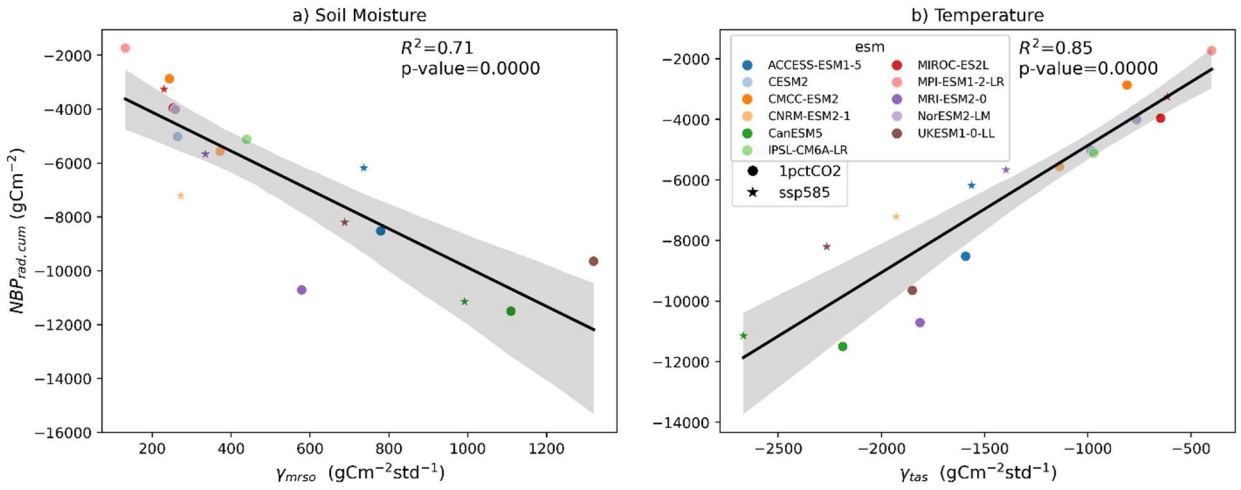


Figure 25: Intermodel uncertainty in climate-driven cumulative NBP as explained by differences in ESMs representation of temperature (γ_{tas}) and soil moisture (γ_{mrso}) impacts in 1pctCO₂-rad and ssp585-rad simulations. Values are averaged within the Amazon basin domain.

2.4.3 Inter-annual variability of carbon fluxes

Amazon carbon sink variability on shorter (interannual) timescales in the historical and ssp585 scenario is assessed with respect to the modulation of temperature, soil moisture and shortwave incoming radiation anomalies, following a multi-linear ridge regression predictive model (see Methods). The skills of the model optimized with the 5-fold cross-validation procedure are reported in Figure S38. Overall, a multi-model mean coefficient of determination of 0.55 is obtained, despite with substantial differences across ESMs. Remarkably lower values of variance explained (R^2<0.4) are found for CESM2, CMCC-ESM2 and NorESM2-LM, whereas CanESM5, MIROC-ES2L and UKESM1-0-LL stand out as the models with the highest goodness of fit and predictive capability (R^2>0.6) (Figure S38a). Undoubtedly, we acknowledge the limitations that arise from the adoption of a linear ridge regression model. As we didn't account for interactive and non-linear effects among the predictors influencing NBP IAV, we are not able to capture a portion of the unexplained variance in our regression model. The results in Figure S38 reflects this fact, suggesting that other factors, as well as the effects emerging from the interaction of temperature, soil-

moisture and shortwave incoming radiation, are likely having an important influence on NBP IAV, especially for CESM2, NorESM2-LM and partly CMCC-ESM2. Nevertheless, we opted for this modelling framework, as it still allows our results to be compared with prior works (Jung *et al.*, 2017; Humphrey *et al.*, 2018).

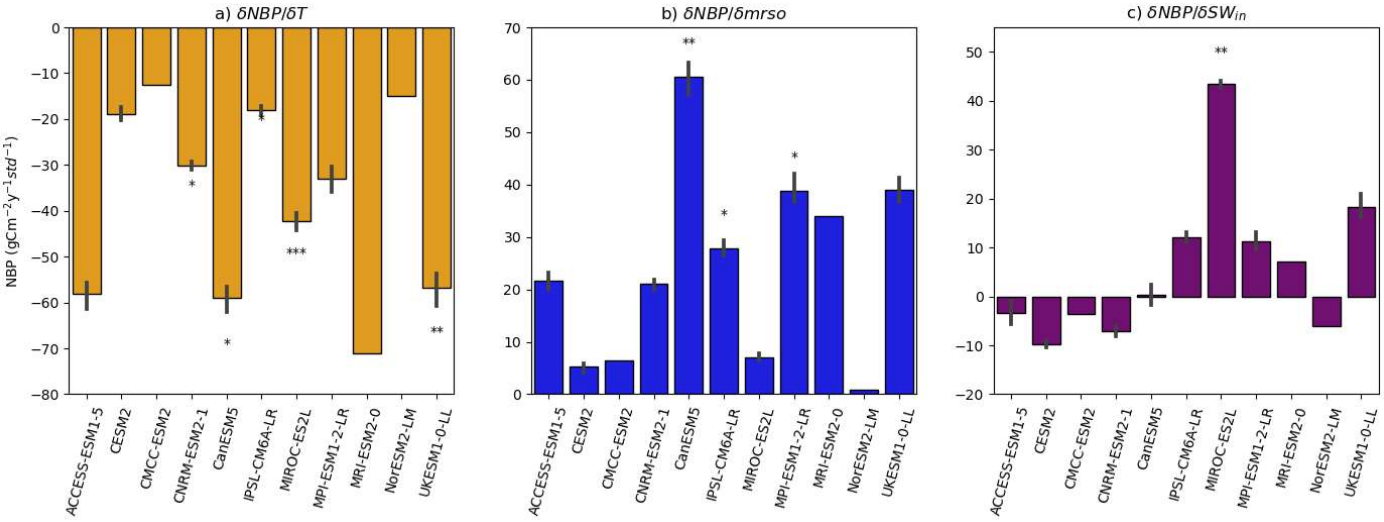


*Figure 26: Partial derivatives explaining the contribution of temperature (a), soil moisture (b) and shortwave incoming radiation (c) to interannual NBP, averaged across the Amazon basin. The black vertical bars represent the spread in the predictors coefficients for models with more than one realization available, whereas the stars indicate the level of significance (p-value), averaged over the Amazon basin, associated to every coefficient. Statistical significance refers to the following convention: *: 1.00e-02 < p <= 5.00e-02; **: 1.00e-03 < p <= 1.00e-02; ***: 1.00e-04 < p <= 1.00e-03; ****: p <= 1.00e-04*

The relative importance of the three variables in explaining the NBP interannual variability is reported in Figure S39 for both the historical period (panel a) and the ssp585 scenario (panel b), revealing the dominant regulation of temperature for all the ESMs except CanESM5, IPSL-CM6A-LR and MPI-ESM1-2-LR, that have primarily a soil-moisture driven variability and MIROC-ES2L, which stands out for the particularly high variance explained by shortwave incoming radiation and the low contribution of soil-moisture.

The standardized coefficients estimated for NBP in the ssp585 scenario, reported in Figure 26, point to an intermodel agreement with respect to the contribution of temperature (negative effect) and soil-moisture (positive effect), despite with remarkable inter-model

differences in the magnitude of the drivers contribution. Lower net carbon sink variability, on the other hand, is associated with shortwave incoming radiation, with ESMs diverging on the sign of the partial correlation (Figure 26c). Also, similar results are found for the multilinear regression estimation in the historical period, with the only difference regarding the magnitude of the standardized coefficients: a general increase in the sensitivity, in absolute terms, is found for temperature and soil moisture effects (Figure S40), mainly a consequence of increased interannual NBP variability in the future ssp585 scenario compared to the historical period. For seven out of eleven models, temperature is the first NBP predictor, while for CanESM5, IPSL-CM6A-LR and MPI-ESM1-2-LR soil moisture results to be more important, and MIROC-ES2L predicts shortwave incoming radiation as most important factor driving NBP interannual variability. The multi-model averaged coefficients for NBP are reported in Figure 27, with hatches delimiting those pixel cells where eight out of 11 ESMs agree in the sign of the partial derivative. Temperature impacts are particularly evident in the northern part of the Amazon, whereas the positive influence of soil moisture presents high agreement almost everywhere but in the north western part of the basin. Given the almost specular multi-model agreement in the positive value of shortwave incoming radiation coefficients in that specific domain, this could denote that the majority of the ESMs present an energy limited regime in the area, with shortwave incoming radiation (rather than water availability) being the main limiting factor constraining ecosystem productivity at interannual timescales.

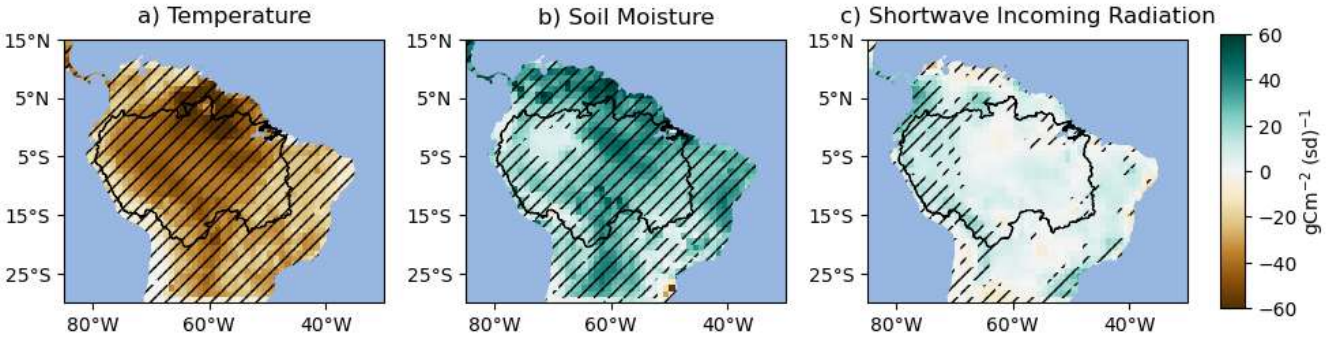


Figure 27: Multi model ensemble mean of the coefficient values for the climatic drivers obtained by the multi-linear regression, for the ssp585 scenario. Hatches represent those grid cells for which at least 8 out of 11 ESMs agree in the sign of the predictor value. The Amazon basin, obtained from the SO HYBAM service (https://hybam.obs-mip.fr/), is also represented.

As observed for long-term effects in Figure 25, the intermodel differences in the projection of net carbon sink variability at interannual timescales are characterized by an inverse relationship between temperature and soil moisture influence: as expected, high NBP interannual variability is driven by both higher (in absolute terms) temperature and soil moisture contributions (Figure S41).

To ultimately understand which process variable is associated to the largest source of uncertainty, the variability across the estimated coefficients have been compared, and are reported in Table 8 for each dependent variable (NBP, GPP, Ra and Rh). Please note that for this procedure the coefficients obtained from the multivariate regression model have been additionally standardized, thus divided by the std.-dev. of the respective dependent variable, to ensure an accurate comparison of coefficients across models.

Table 8: Inter-model uncertainty within the Amazon basin, expressed as std.dev. of the partial derivative values across all the ESMs. Rows represent the partial derivatives of temperature, soil moisture and shortwave incoming radiation, with respect to the dependent variables reported in the columns (carbon fluxes).

	NBP	**GPP**	**Ra**	**Rh**
$\frac{\delta X}{\delta T}$	0.14	0.15	0.34	0.42
$\frac{\delta X}{\delta mrso}$	0.24	0.25	0.31	0.45
$\frac{\delta X}{\delta SW_{in}}$	0.28	0.36	0.30	0.30

First, the high disagreement in the sign of the shortwave incoming radiation coefficients found for NBP originates from GPP sensitivity to shortwave incoming radiation $\frac{\delta GPP}{\delta SW_{in}}$ (panels c in Figure 26 and Figure S42 and Table 8). Uncertainties in net carbon sink projections across ESMs, for a high CO_2 future scenario like the ssp585, are therefore to be found, on the one hand, mainly in the different representation of photosynthesis modulated by light availability. Uncertainties in net carbon sink projections across ESMs therefore arise, on the one hand, mainly from differences in photosynthesis modulation by light availability. On the other hand, heterotrophic respiration sensitivity to soil moisture and temperature represents another prominent source of uncertainty across ESMs (see also panel a, b in Figure S43 showing the disagreement across ESMs coefficients), whereas autotrophic respiration shows median contributions to net carbon sink uncertainty (Table 8 and Figure S44).

2.4.4 ENSO modulation

Given the predominant role of large-scale climatic modes of variability in influencing local climate and the terrestrial carbon cycle, the NBP response to ENSO has been investigated. ENSO is the most important climatic mode affecting and modulating net tropical carbon sink variability at interannual timescales, and changes in key properties of ENSO could significantly impact the Amazon basin region. For example, an increase in the frequency or in the occurrence of El Nino and La Nina events under global warming, a possibility explored in previous studies (Cai *et al.*, 2014, 2015; Berner *et al.*, 2020; Brown *et al.*, 2020; Fredriksen *et al.*, 2020), could have important implications especially for the Amazon ecosystem due to a stronger inhibition of the tropical teleconnection pathway that regulates the influence of the equatorial Pacific. The ESMs in the considered ensemble largely overestimate the observed ENSO amplitude in the interannual-to-decadal band, with the associated spectra typically featuring a narrow peak around the 3-year periodicity (Figure S45). The ESMs also

yield a diversity of changes in ENSO spectral characteristics under the warming scenario: generally, all the models represents a shift of ENSO signal toward higher frequencies, with weaker amplitude at decadal time scales and stronger amplitude at interannual time scales (Figure S45). Changes in the amplitude of the ENSO signal, represented by the Nino3.4 index standard deviation, between the ssp585 scenario (orange dots) and the historical period (light-green crosses) are shown in Figure S46. Nine out of eleven ESMs show an increased ENSO variability under the ssp585 scenario, whereas CESM2 do not project any relevant changes, and UKESM1-0-LL predicts a slight decrease in ENSO amplitude. Consequently, the NBP variability related to ENSO is estimated by considering both the sensitivity of NBP to temperature and soil moisture, as well as the sensitivity of temperature and soil moisture to the Nino3.4 signal (Paragraph 2.3.3), therefore allowing to decompose the impacts associated to the two different mechanisms. First, all the models represent bigger carbon sink losses related to temperature-driven anomalies compared to soil moisture ones (Figure S46). Second, temperature and soil moisture impacts driven by ENSO are expected to increase in magnitude during the future ssp585 scenario with respect to the historical period, with the increase in $\delta NBP_{n34,}$ appearing to be statistically significant for all the models but MPI-ESM1-2-LR and NorESM2-LM. Regarding $\delta NBP_{n34,mrso}$, on the contrary, most of the ESMs (seven out of eleven) project either a not-significant change, or a low statistical significance (0.05<p-value<0.01). While the carbon cycle response to ENSO within the Amazon region presented here is well in agreement with previous research (Kim *et al.*, 2017; Betts *et al.*, 2020; Le *et al.*, 2021; Le, 2023), this study furtherly decouples the mechanism by which ENSO could influence the Amazon carbon fluxes in a high radiative forcing future scenario by attributing the biggest share of impacts to temperature. Specifically, the higher temperature-mediated ENSO impacts arise on the one hand from the higher (lower) co-variability observed in the ESMs between temperature (soil moisture) anomalies and ENSO, both during the historical period as well as in ssp585 projections (Figure S47). Additionally, this is accentuated by the simulated response of NBP to

temperature changes, which, as pointed out before, is stronger than the soil moisture control for the majority of ESMs (Figure 26).

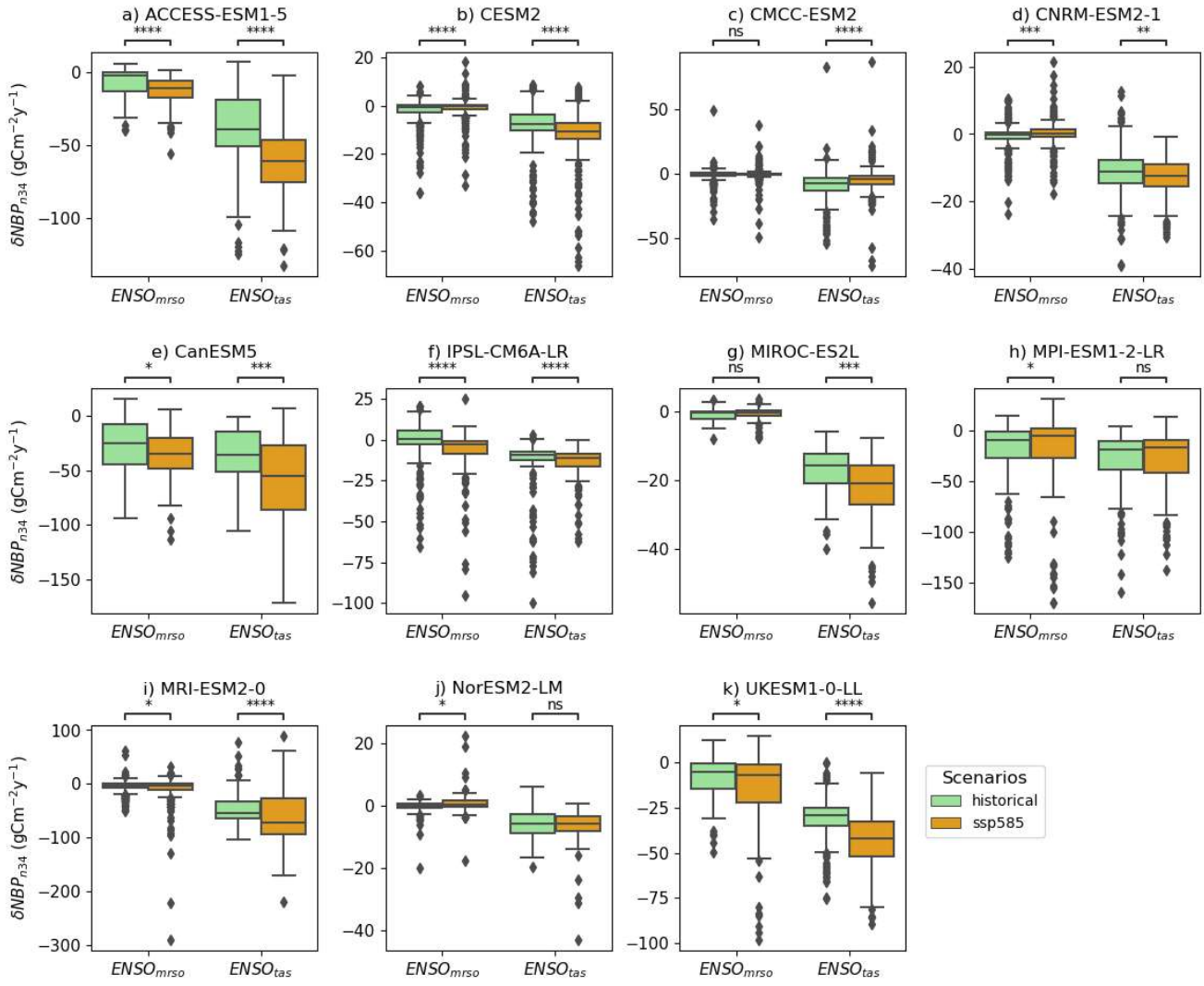


*Figure 28: Variability of NBP at interannual timescales associated to ENSO (y-axis), and mediated by either soil moisture or surface air temperature (x-axis), for every ESM. Reported are the distribution of the values within the Amazon basin, for the historical period (light-green) and the ssp585 scenario (orange). Statistical difference among the distribution of the coefficients for the two periods are tested by means of a Mann-Whitney U-test and is reported in the stars above the plots with the following convention: *: 1.00e-02 < p <= 5.00e-02; **: 1.00e-03 < p <= 1.00e-02; ***: 1.00e-04 < p <= 1.00e-03; ****: p <= 1.00e-04*

The influence of ENSO by means of temperature and soil moisture anomalies is additionally examined considering the multi-model mean of $\delta NBP_{n34,T}$ and $\delta NBP_{n34,mrso}$. To do so, the

ESMs coefficients reported in Figure 28 have been re-gridded to a common 1x1 grid using bilinear interpolation. As discernible from Figure 29, the temperature-driven impacts of ENSO are expected to be clearly stronger in the future ssp585 scenario, both compared to the historical period (panel a), as well as with respect to soil moisture related impacts (panel b). Considering that climatic variability associated to ENSO in the Amazon basin in not expected to significantly change in the ssp585 scenario compared to historical simulation for all the models (Figure S47), results in Figure 29 indicate that climate change will significantly amplify the NBP sensitivity to temperature anomalies in the Amazon, while its influence on NBP sensitivity to soil moisture anomalies will be less pronounced.

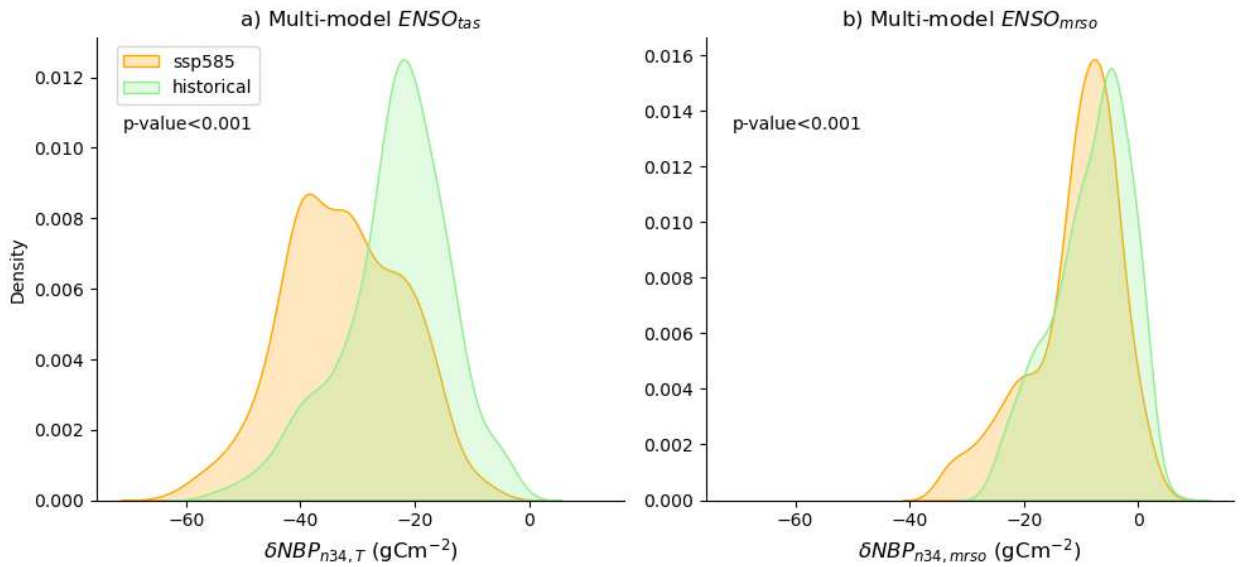


*Figure 29: Only grid-cells within the Amazon basin are included. Statistical significance, tested by means of a Mann-Whitney U-test, is reported in the stars above the plot, and refers to the following convention: *: 1.00e-02 < p <= 5.00e-02; **: 1.00e-03 < p <= 1.00e-02; ***: 1.00e-04 < p <= 1.00e-03; ****: p <= 1.00e-04*

2.5 Conclusions

In this chapter, the main environmental drivers affecting the long-term and IAV projections of Amazon basin carbon sink have been assessed considering the ssp585 high radiative forcing scenario with respect to eleven CMIP6 ESMs. Several important outcomes have been

identified and confirmed. Specifically, we recognized CO_2 fertilization as the predominant mechanism determining the long-term Amazon carbon sink trend and uncertainty under the range of atmospheric CO_2 concentrations of the ssp585 scenario (400-1135 ppmv). These results reaffirm, for the CMIP6 generation of ESMs, what reported in a previous study by Huntzinger et al. (2017), that under different research assumptions showed the predominant role of vegetation sensitivity to CO_2 in shaping the net carbon sink variability across CMIP5 generation Land Surface Models (LSMs). Additionally, we disentangled the fundamental physical processes behind net carbon sink discrepancies across ESMs, highlighting dominant mechanisms affecting simulated carbon fluxes uncertainty for the Amazon basin ecosystem. Particularly, we show that the ensemble divergence of NBP under future warming scenario is largely determined by GPP modulation by shortwave incoming radiation and uncertainty in the representation of heterotrophic respiration sensitivity to both soil moisture and temperature. Our multi-model ensemble approach expands the results obtained in previous researches (Ma *et al.*, 2021) by allowing for an explicit consideration of model uncertainty. By showing the strong uncertainties across the driving factors of heterotrophic respiration, we suggest that not only ESMs differ in the positive modulation of temperature on Rh (controlled by the Q_{10} equation), but also largely disagree in the association between soil moisture and soil decomposition rates leading to respiration fluxes, as recently pointed out by Guenet et al., (2024). Additionally, our results point towards a stronger ENSO-driven temperature impact on carbon sink anomalies for the vast majority of ESMs, compared to the effects associated with deficits in water availability. Accordingly, the CMIP6 multi-model ensemble considered shows a robust and statistically significant increase in carbon sink sensitivity to ENSO-driven temperature anomalies under global warming in the region of the Amazon basin: as a consequence, climate change is likely to significantly diminish the Amazon ecosystem capacity to function as a carbon sink, further aggravating the atmospheric CO_2 burden. This outcome highlights the critical role that global warming induced changes in the dynamics of modes of interannual variability could have on the Amazon region, thus contributing to the expanding scientific literature on the topic (see for

example Le, 2023; Yan *et al.*, 2023). Overall, despite we were able to, at least partially, understand and quantify the contributions of different driving factors in affecting Amazon carbon cycle projections, important uncertainties still remain in the projections of Amazon response to global warming in CMIP6 generation of ESMs. On another note, we acknowledge some limitations affecting our study, particularly the application of a linear framework to describe interannual variability of carbon fluxes and ENSO-mediated impacts. A potential approach to overcome this limitation could be the adoption of machine-learning algorithms, able to detect non-linearities and describe the complex spatio-temporal features of the Earth system (Reichstein *et al.*, 2019). This, together with a more up-to-date and uniform representation of vegetation physiological and biogeochemical processes in the next generation of ESMs, will hopefully help generate more coherent and reliable projections of terrestrial carbon fluxes, helping to understand the faith of the Amazon basin under global warming scenarios.

Code and Data Availability

The code used to perform the analysis is publicly available at https://github.com/Matteo-Mastro/Amazon_CMIP6. CMIP6 data are freely available and accessible from the ESGF repository (https://aims2.llnl.gov/search). FLUXCOM energy and carbon fluxes data are accessible from the Data Portal of the Max Planck Institute for Biogeochemistry, previous registration (https://www.bgc-jena.mpg.de/geodb/projects/Home.php). HadISST dataset is freely accessible from the MetOffice website (https://www.metoffice.gov.uk/hadobs/hadisst/data/download.html). ERA5 and ERA5-Land data are freely accessible from the Copernicus Climate Data Store (https://cds.climate.copernicus.eu/#!/home). The Amazon shapefile used for computing the spatial mean statistics is freely available from the Amazon basin water resources observation service (https://hybam.obs-mip.fr/).

Annex

Table S9: Overview of ESMs considered in this study

ESM	Ref	Curvilinear Ocean Grid	Land carbon	N cycle	P cycle	Fires	Dynamic vegetation	ECS (°C)
IPSL-CM6A-LR	(Boucher *et al.*, 2020)	Yes	ORCHIDEE, br.2.0	No	No	No	No	4.70
CNRM-ESM2-1	(Séférian *et al.*, 2019)	Yes	ISBA-CTRIP	Implicit	No	Yes (natural)	No	4.79
CanESM5	(Swart *et al.*, 2019)	Yes	CLASS-CTEM	Implicit	No	No	dynamic wetlands	5.64
UKESM1-0-LL	(Sellar *et al.*, 2019)	No	JULES-ES-1.0	Yes	No	No	Yes	5.36
MIROC-ES2L	(Hajima *et al.*, 2020)	No	VISIT-e	Yes	No	No	No	2.66
ACCESS-ESM1-5	(Ziehn *et al.*, 2020)	No	CABLE	Yes	Yes	No	No	3.88
MPI-ESM1-2-LR	(Mauritsen *et al.*, 2019)	Yes	JSBACH3.2	Yes	No	No	Yes	3.03
NorESM2-LM	(Seland *et al.*, 2020)	No	CLM5	Yes	No	Yes	No	2.49
CMCC-ESM2	(Lovato *et al.*, 2022)	Yes	CLM-4.5	Yes	No	Yes (natural)	No	3.58
CESM2	(Danabasoglu *et al.*, 2020)	No	CLM5	Yes	No	Yes	dynamic wetlands	4.68
MRI-ESM2-0	(Yukimoto *et al.*, 2019)	No	HAL	No	No	No	No	3.14

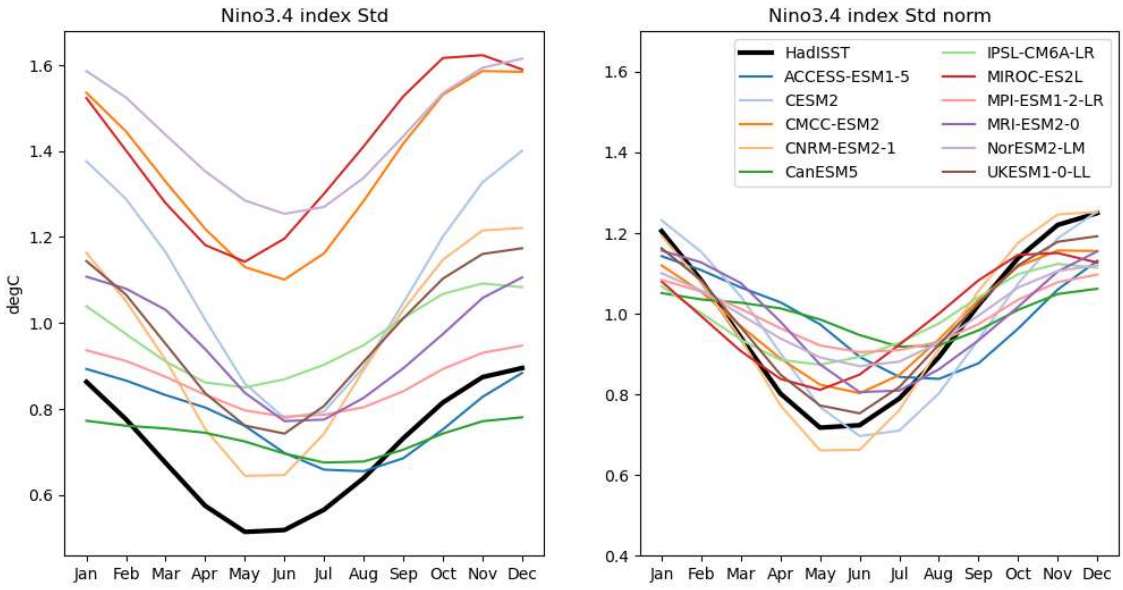


Figure S30: Model biases with respect to the HadISST dataset in ENSO seasonal variability, for the period 1979/2013. a) seasonality as expressed by the Nino3.4 index standard deviation, b) seasonality expressed by the normalized Nino3.4 standard deviation.

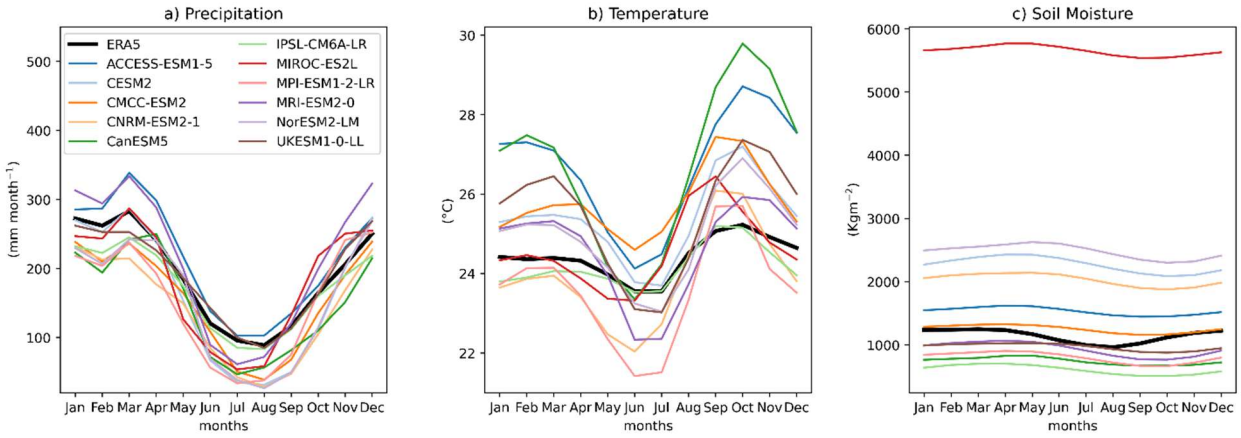


Figure S31: Model biases with respect to the ERA5 dataset in the climatological seasonal variability, for the period 1979/2013. Shown are the monthly zonal means within the Amazon basin for a) precipitation, b) temperature and c) soil moisture.

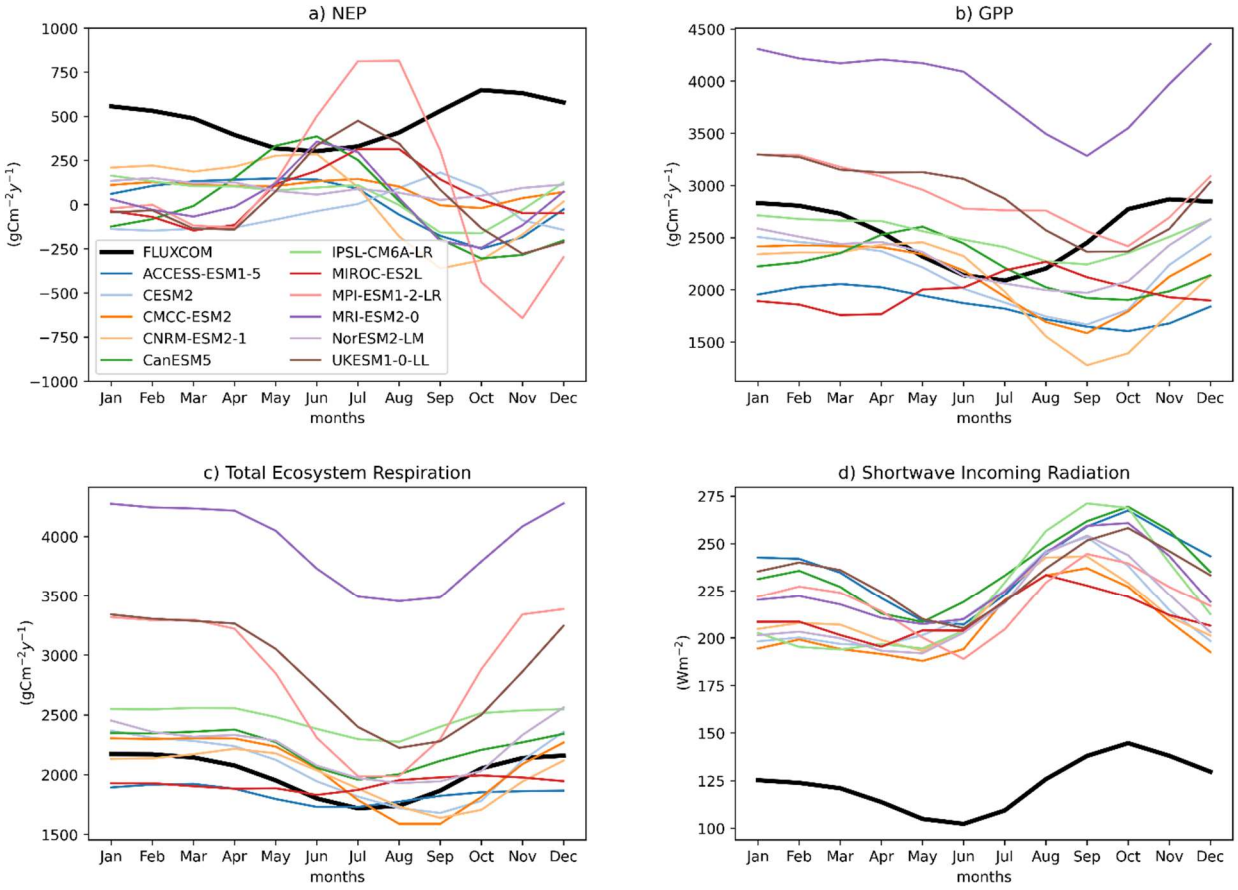


Figure S32: Model biases with respect to the FLUXCOM dataset in the seasonal variability, for the period 1979/2013. Shown are the monthly zonal means within the Amazon basin for a) NEP, b) GPP and c) TER and d) shortwave incoming radiation.

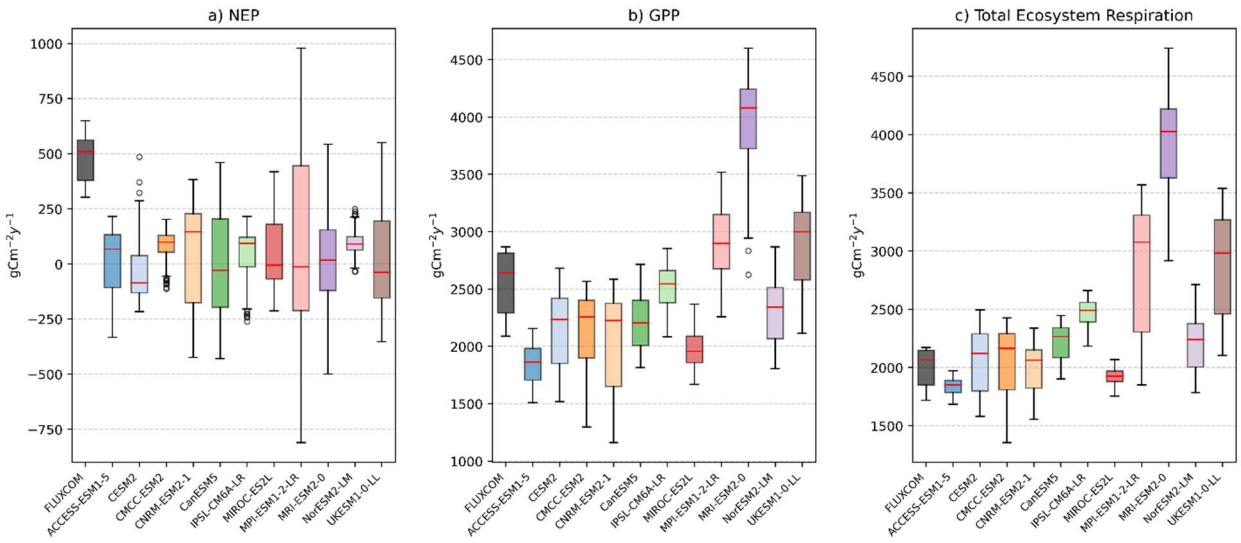


Figure S33: Model biases with respect to the FLUXCOM dataset in the distribution of carbon fluxes values, for the period 1979/2013. Shown are the yearly zonal values within the Amazon basin for a) NEP, b) GPP and c) total ecosystem respiration (TER, the sum of autotrophic and heterotrophic respirations for ESMs).

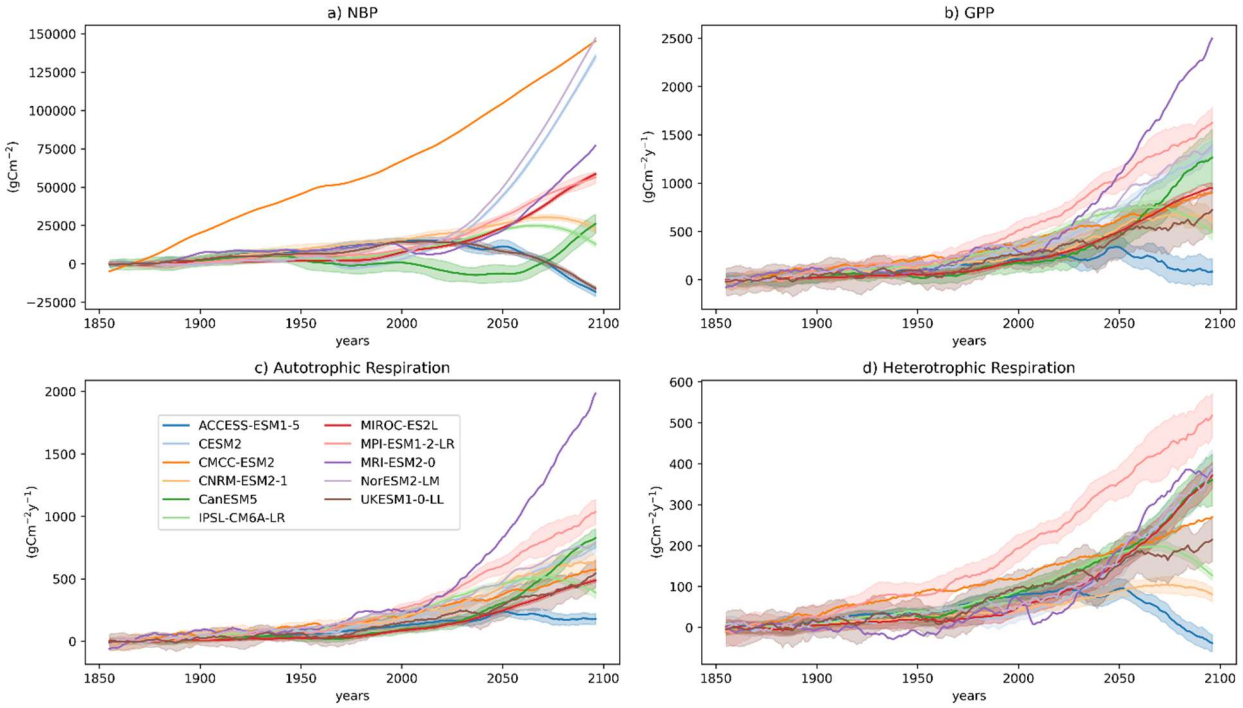


Figure S34: Simulated anomalies of (a) cumulative NBP, (b) GPP, (c) Ra and (d) Rh in the Amazon basin for the historical and ssp585 experiments. Trends are computed with respect to the 1850 mean and are visualized as a 10-years moving average for clarity. For the models with more than one realization, both the model-ensemble mean (line) and the spread (±1 standard deviation, shading) are shown.

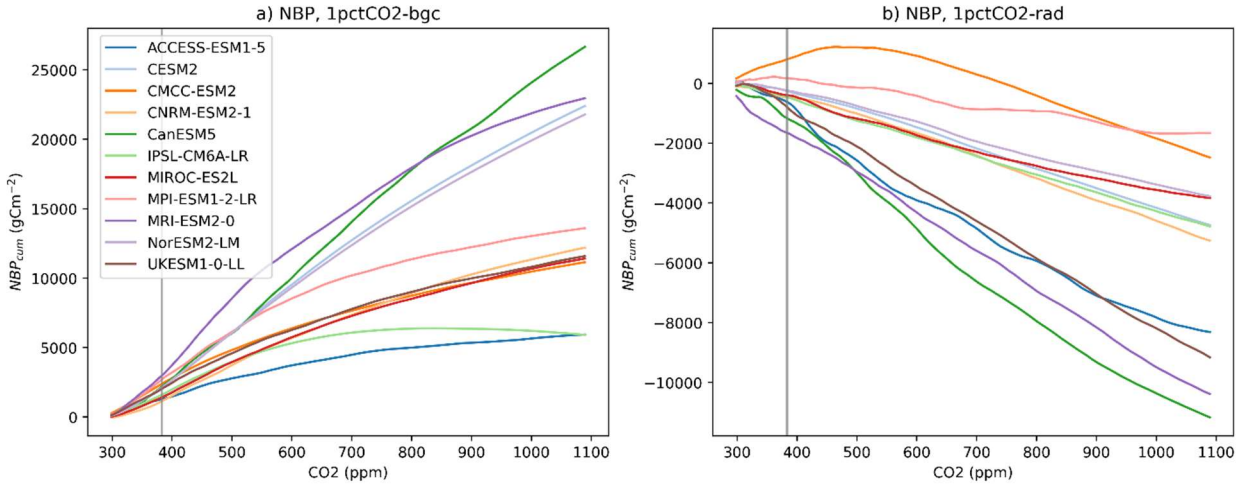


Figure S35: Cumulative NBP anomalies from a) 1pctCO_2-bgc and b) 1pctCO_2-rad simulations. Trends are computed with respect to the start of the simulation and are showed as 10-years moving averages for clarity.

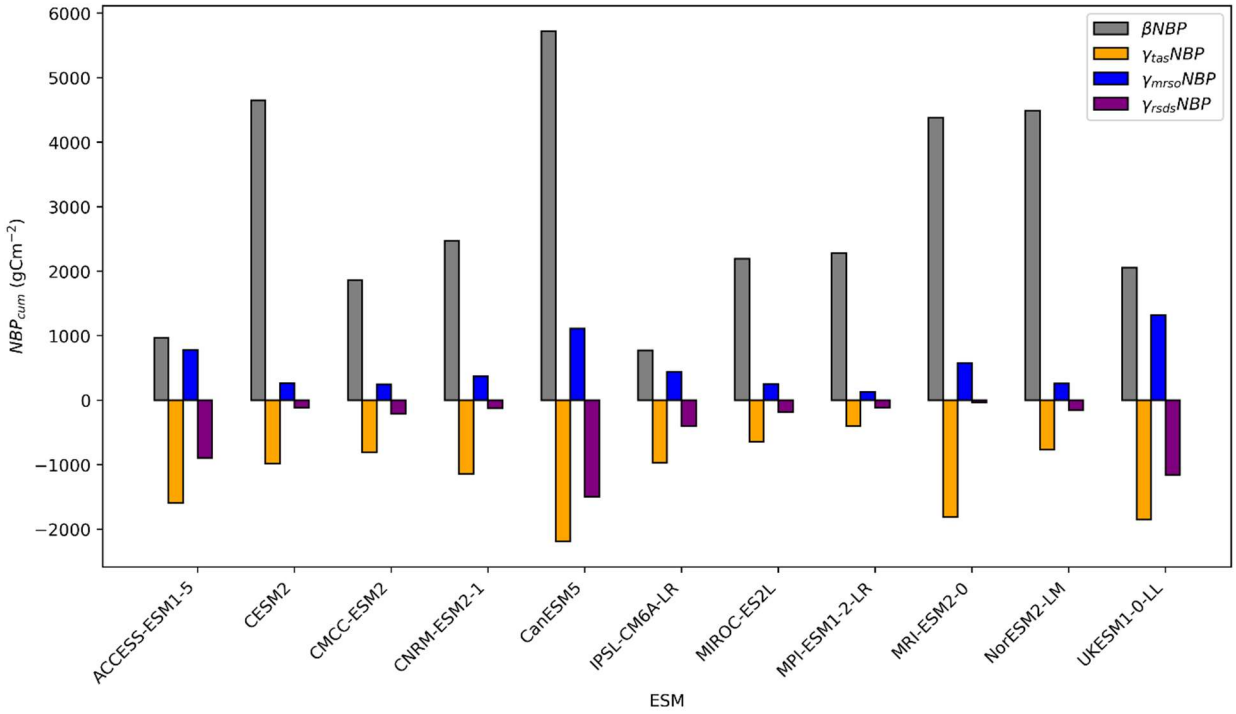


Figure S36: Standardized values of β and γ averaged over the Amazon basin, representing their contribution to cumulative NBP in the 1pctCO₂-bgc and 1pctCO₂-rad simulations respectively.

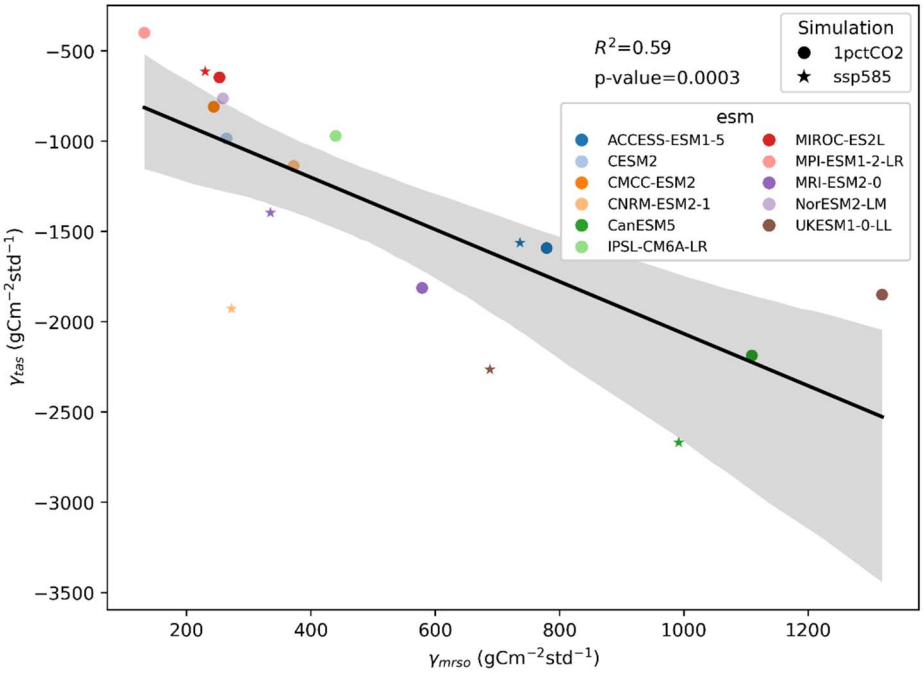


Figure S37: Inverse relationship between ESMs representation of temperature (γ_{tas}) and soil moisture (γ_{mrso}) impacts in 1pctCO₂-rad and ssp585-rad simulations.

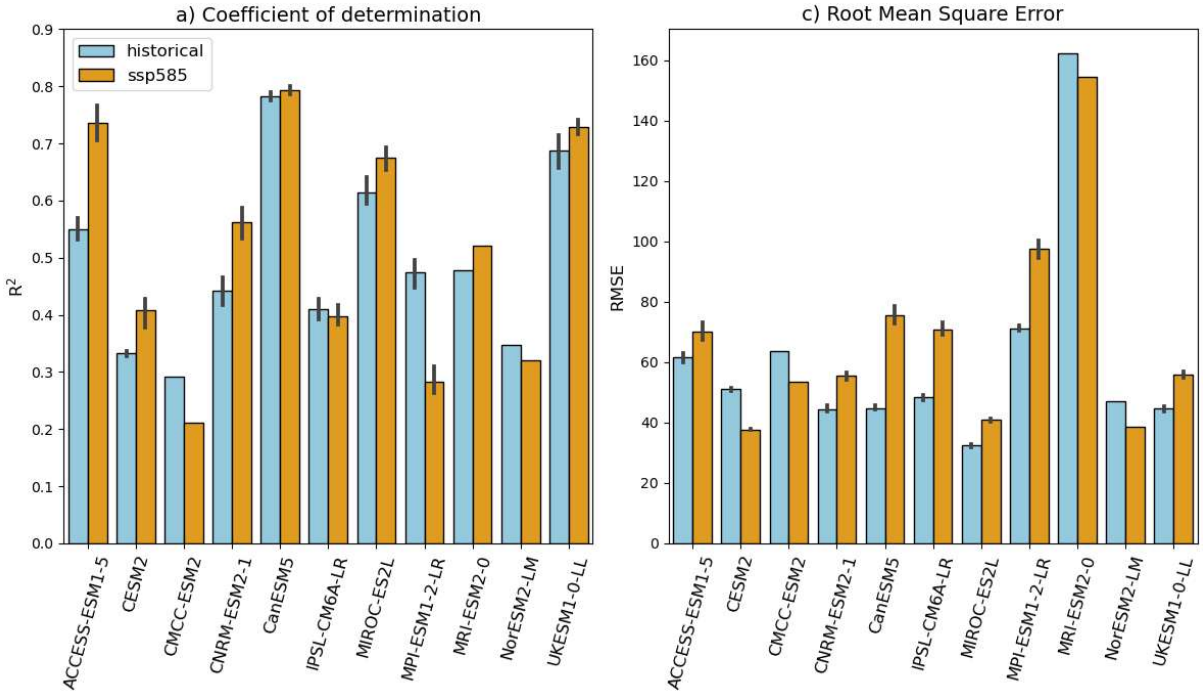


Figure S38: Predictive skills of the ridge regression model by adopting the 5-fold cross-validation procedure, for every ESM and for both the historical and the ssp585 scenario. In panel a) is reported R^2, in panel b) the RMSE..

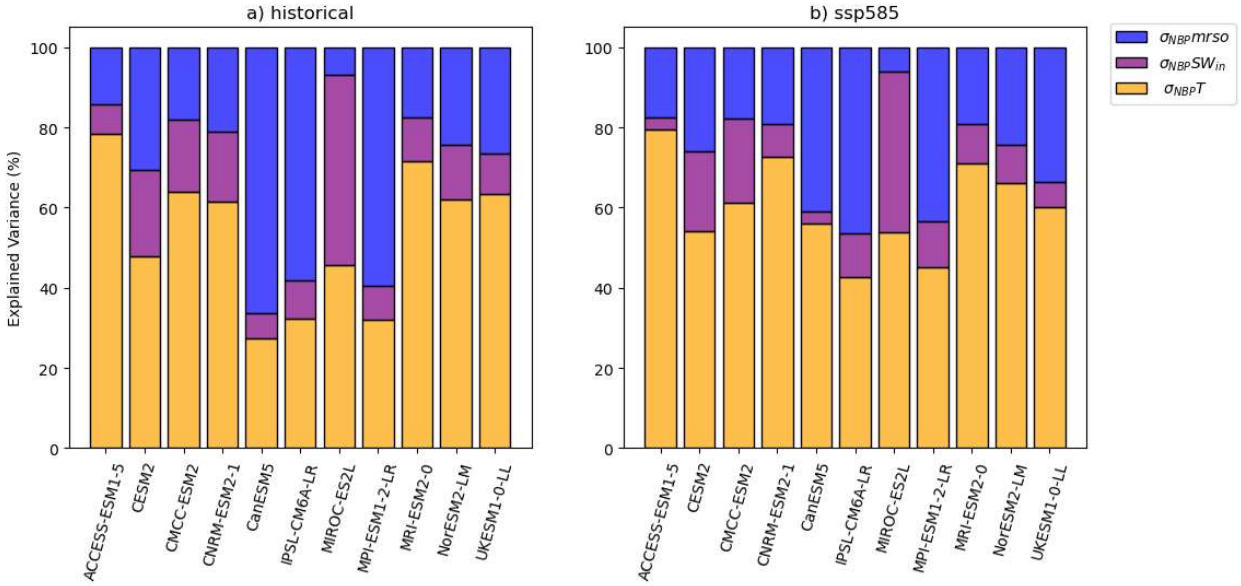


Figure S39: Share of interannual NBP explained variance (%), by means of temperature (yellow), soil-moisture (blue) and shortwave incoming radiation (purple) for every ESM for a) historical period and b) ssp585 scenario.

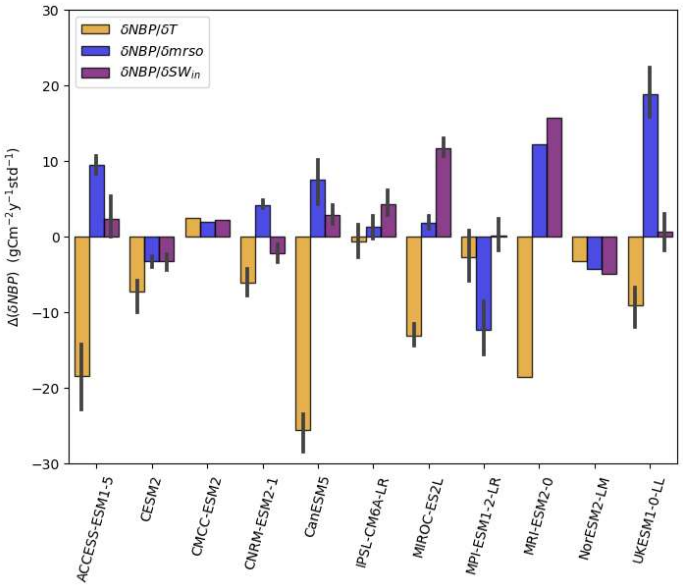


Figure S40: Changes in the coefficients of the 5-fold CV ridge regression model in the ssp585 scenario with respect to the historical period, for all the ESMs. Shown are the Amazon basin mean values of the regression coefficients.

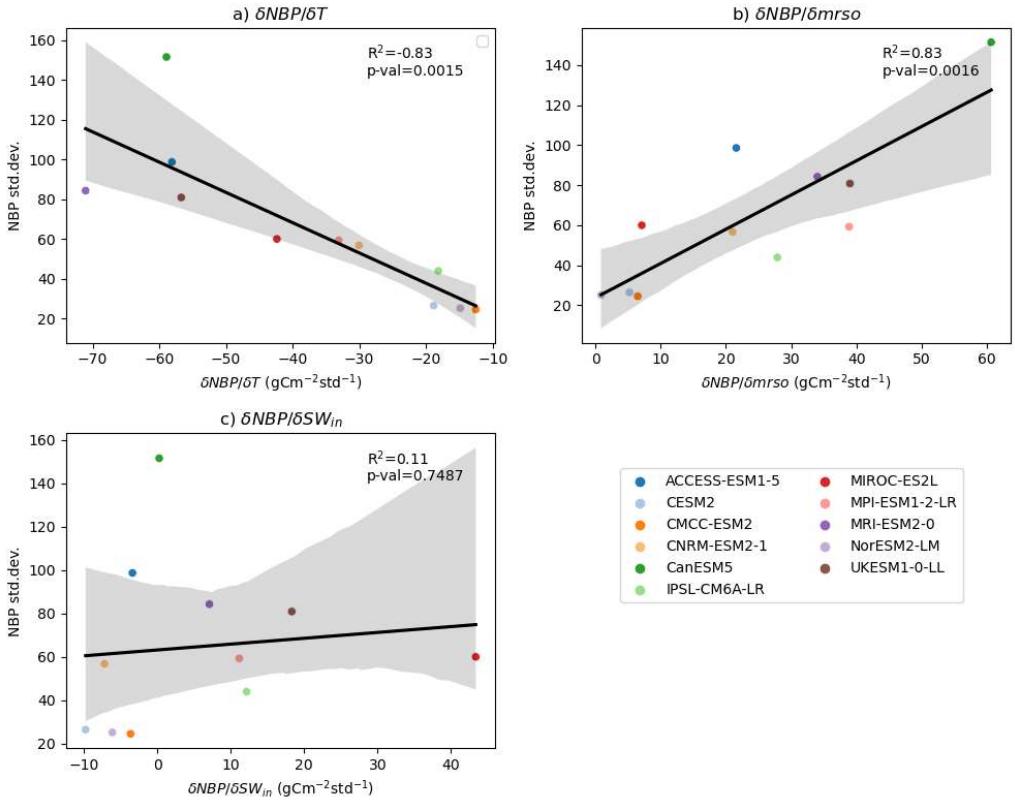


Figure S41: Intermodel uncertainty in interannual variability of NBP (y-axis) as explained by the 5-fold CV ridge regression coefficients with respect to: a) temperature, b) soil moisture and c) shortwave incoming radiation.

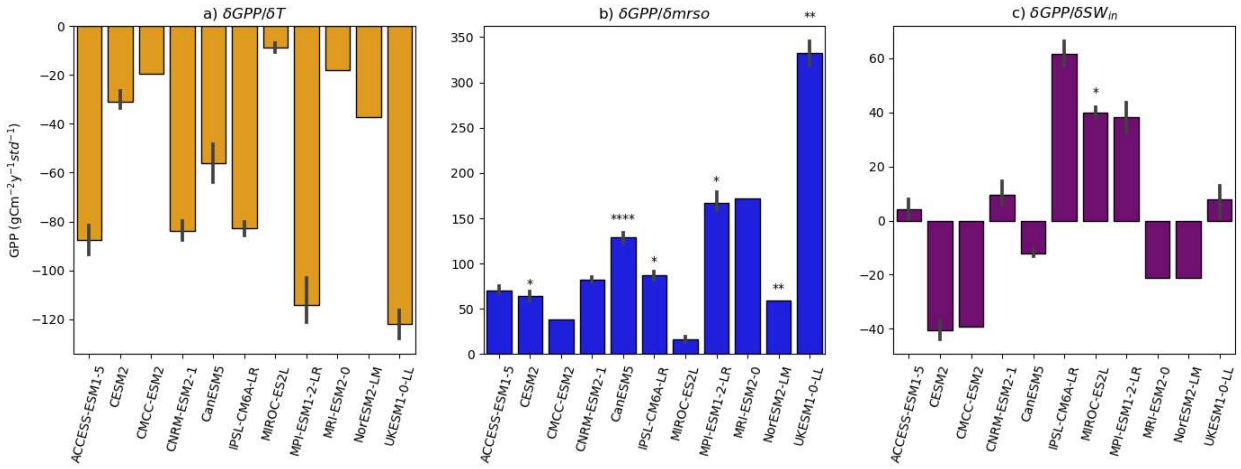


*Figure S42: Partial derivatives explaining the contribution of temperature (a), soil moisture (b) and shortwave incoming radiation (c) to interannual GPP, averaged across the Amazon basin. The black vertical bars represent the spread in the predictors coefficients for models with more than one realization available, whereas the stars indicate the level of significance (p-value), averaged over the Amazon basin, associated to every coefficient. Statistical significance refers to the following convention: *: 1.00e-02 < p <= 5.00e-02; **: 1.00e-03 < p <= 1.00e-02; ***: 1.00e-04 < p <= 1.00e-03; ****: p <= 1.00e-04*

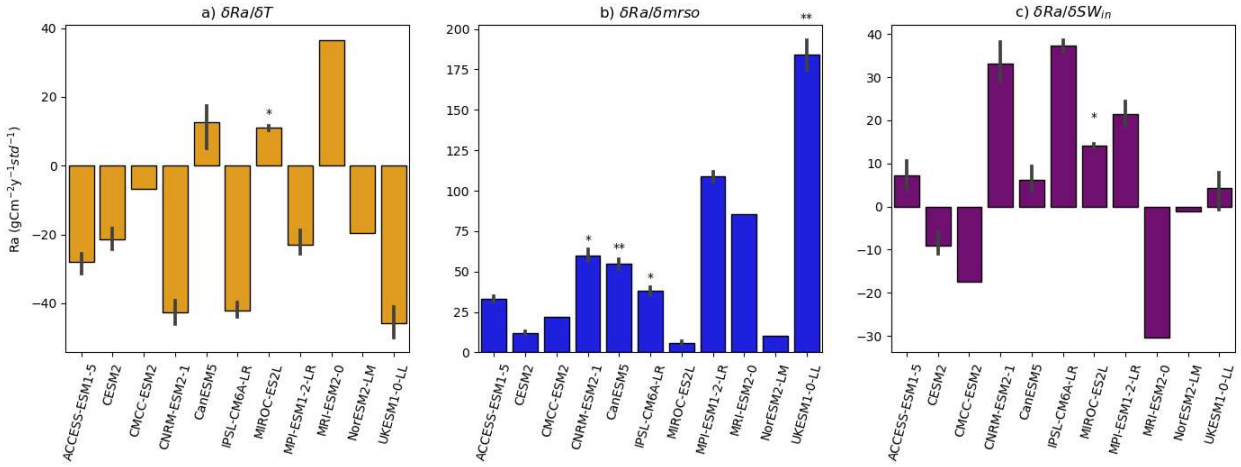


*Figure S43: Partial derivatives explaining the contribution of temperature (a), soil moisture (b) and shortwave incoming radiation (c) to interannual Ra, averaged across the Amazon basin. The black vertical bars represent the spread in the predictors coefficients for models with more than one realization available, whereas the stars indicate the level of significance (p-value), averaged over the Amazon basin, associated to every coefficient. Statistical significance refers to the following convention: *: 1.00e-02 < p <= 5.00e-02; **: 1.00e-03 < p <= 1.00e-02; ***: 1.00e-04 < p <= 1.00e-03; ****: p <= 1.00e-04*

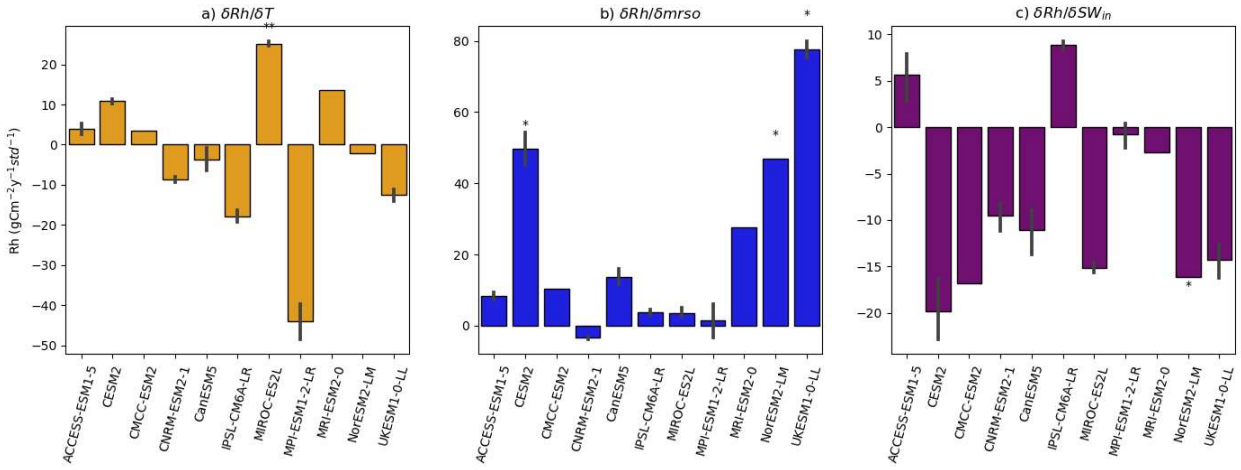


*Figure S44: Partial derivatives explaining the contribution of temperature (a), soil moisture (b) and shortwave incoming radiation (c) to interannual Rh, averaged across the Amazon basin. The black vertical bars represent the spread in the predictors coefficients for models with more than one realization available, whereas the stars indicate the level of significance (p-value), averaged over the Amazon basin, associated to every coefficient. Statistical significance refers to the following convention: *: 1.00e-02 < p <= 5.00e-02; **: 1.00e-03 < p <= 1.00e-02; ***: 1.00e-04 < p <= 1.00e-03; ****: p <= 1.00e-04*

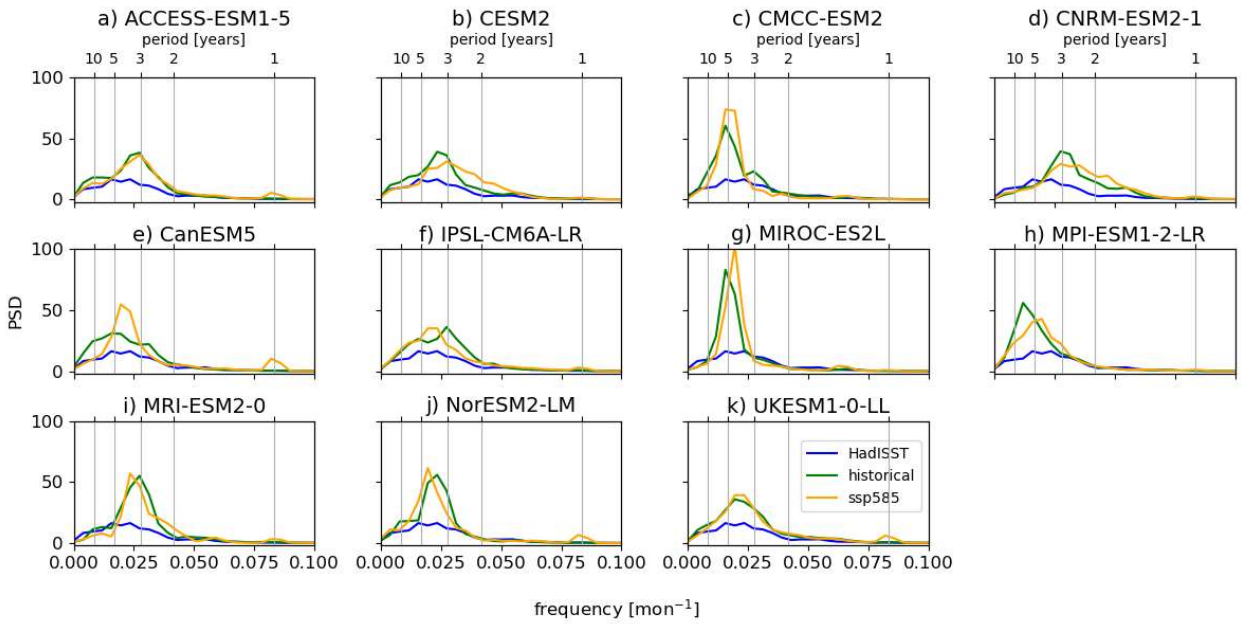


Figure S45: Power Spectrum Density (PSD) of the Nino3.4 signal in all the considered ESMs under the historical (green) and ssp585 (yellow) scenarios. The historical HadISST Nino3.4 frequency (blue line) is added as reference.

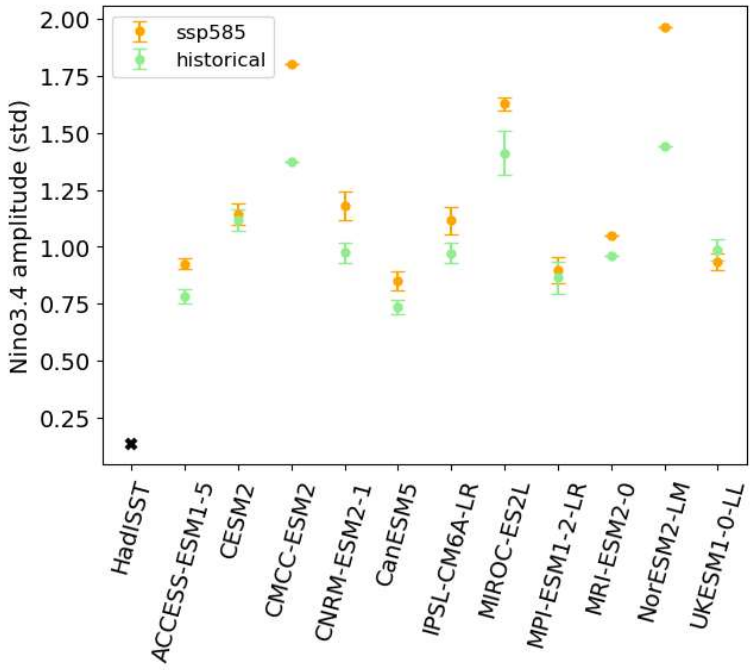


Figure S46: ENSO amplitude change as represented by the Nino3.4 signal standard deviation from the historical period (green crosses) to the future ssp585 scenario (orange dots). The black cross represents the value of Nino3.4 signal amplitude calculated from the HadISST dataset.

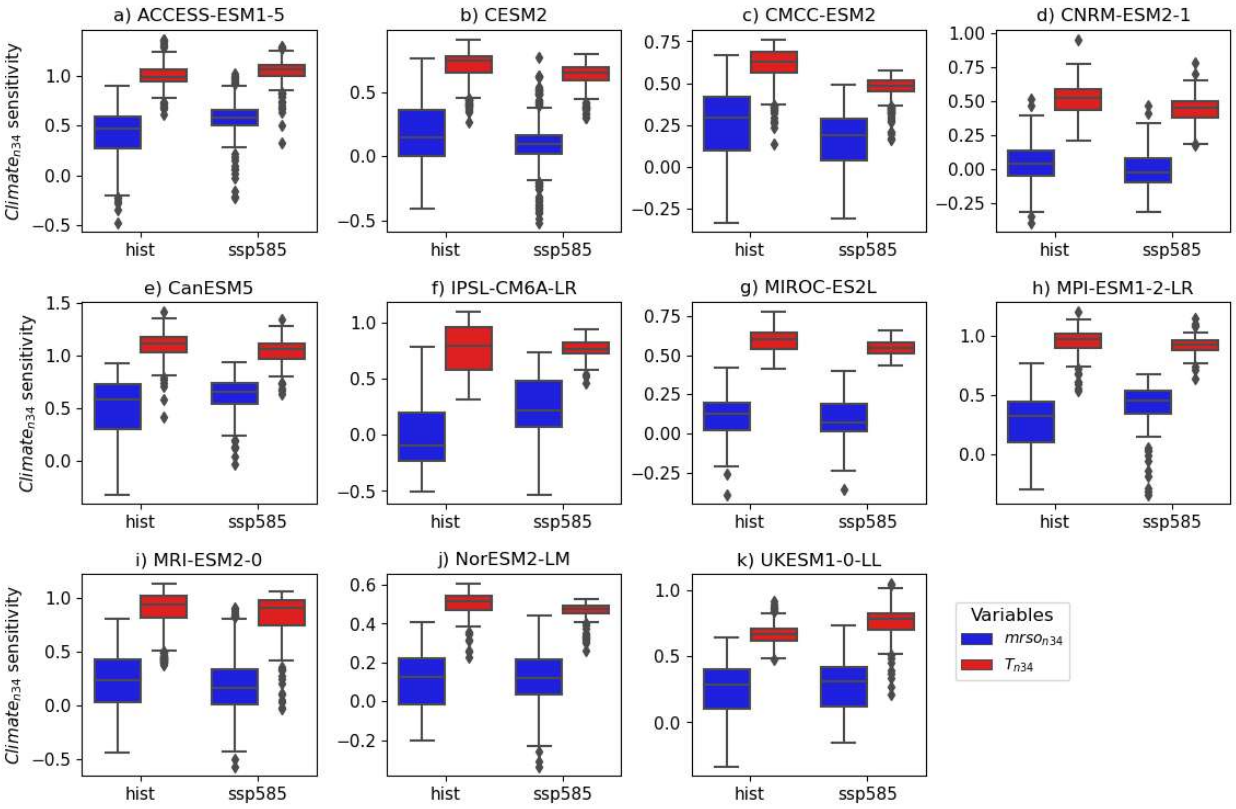


Figure S47: ENSO influence on interannual variability of soil moisture (blue) and temperature (red), for the ESMs considered. Reported are the distribution of univariate coefficients values, masked within the Amazon basin, for both the historical and ssp585 simulations (x-axis).

3 Chapter 3: Emerging trade-offs in the deployment of large-scale Afforestation in a high CO_2 climate

3.1 Abstract

Land-based mitigation is emerging as one of the most cost-effective Climate Dioxide Removal (CDR) solution, and is increasingly considered in the context of international climate agreements. However, biophysical implications are often neglected from the consideration of climatic effects of large-scale afforestation/reforestation (A/R) efforts. In this study, the temperature impacts of a large-scale adoption of A/R under a high radiative forcing future scenario is assessed in an ensemble of seven Earth System Models. A surface energy balance decomposition reveals the major role played by latent heat fluxes increase in determining a local surface temperature cooling driven by increased tree-cover. Specifically, this cooling benefit is particularly evident in land regions interested by a water-limited evapotranspiration regime, suggesting these ecosystems as the most suitable for the implementation of A/R solutions. However, results also point to a reduction of local water availability as a consequence of increased tree-cover, which, unless replenished, could pose a serious threat to local human activities and ecosystems persistence. Therefore, the decline in local groundwater resources ultimately determines an important trade-off between local adaptation potential and long-term sustainability of large-scale A/R projects.

3.2 Introduction

Land-Use and Land Cover Change (LULCC) is considered as one of the driver of climatic and environmental change globally, contributing approximately to 25% of annual anthropogenic emissions (11 $GtCO_2e$) (Hong *et al.*, 2021). The understanding of LULCC effects on both local and global climate is therefore critical for correctly assessing the underlying human impact on climate as well as the mitigation potential of land-based measures. In particular, large-scale afforestation represents one of the main solutions and the most cost-effective one for climate change mitigation, not only for the increased carbon sink capacity (Shukla *et al.*, 2019; Masson-Delmotte *et al.*, 2022). With this respect, the potential of land-based solutions is related on the one hand to a biogeochemical effect, by means of the exchange of greenhouse gases (GHG) and their precursors with the atmosphere. On the other hand, by means of a perturbation in physical properties of the land surface (e.g. albedo, roughness, evapotranspiration), LULCC exerts a change in the surface energy balance, influencing local and global temperature (biogeophysical effect) (Claussen *et al.*, 2001; Pongratz *et al.*, 2010; Winckler, Reick, Bright, *et al.*, 2019). Different studies have been conducted by means of both observation-based estimates and modelling approaches with the aim of estimating the biogeophysical climatic effects of LULCC. We remind to the work of Pongratz et al., (2021) for a comprehensive review of LULCC impacts on climate.

Given the substantial deforestation occurred in the last two centuries in temperate Eurasian and North American ecosystems and, in recent decades, in tropical regions, several research efforts have mainly assessed the climatic consequences of deforestation at both global and local scale (Pongratz *et al.*, 2010). Generally, deforestation leads to a net global cooling as a result of an increase in albedo, particularly relevant for northern high latitudes (Davin and Noblet-Ducoudré, 2010). However, the change of in-situ biogeophysical properties, namely an abrupt reduction in surface roughness and reduced evapotranspiration fluxes, promote an increase of local temperatures due to a reduced coupling and heat dissipation between land and the lower troposphere (Lejeune *et al.*, 2018; Winckler, Lejeune, *et al.*, 2019;

Winckler, Reick, Luyssaert, *et al.*, 2019). These effects have been confirmed by observationally-based studies, which also point to an asymmetrical stronger warming effect of tropical forest loss over forest gain due to a predominance of local non-radiative processes (Alkama and Cescatti, 2016; Bright *et al.*, 2017; Zhang *et al.*, 2024). Accordingly, idealized deforestation experiments reaffirmed the scale-dependent effects of deforestation, therefore a generalized cooling of global temperatures due to non-local biogeophysical effects, and additionally demonstrate the potential of LULCC in mitigating regional temperature and precipitation extremes (Boysen *et al.*, 2020; Chen and Dirmeyer, 2020; Hong *et al.*, 2022; Liu *et al.*, 2023). A general conclusion from these studies is that high latitude deforestation is associated with local cooling due to an increase in albedo (especially during the snow season), whereas tropical deforestation typically causes an evapotranspiration induced local warming and a reduction in local precipitation, with potential consequences on ecosystems tipping behavior to drier states (Lovejoy and Nobre, 2019; Pongratz *et al.*, 2021).

At the same time, the recognition of LULCC as a key climate mitigation solution has led to the exploration of its potential impacts in future and idealized scenarios by means of factorial ESMs experiments (Brovkin *et al.*, 2013; Boysen *et al.*, 2014; Davies-Barnard *et al.*, 2014). By simulating a strong afforestation scenario (RCP4.5) in a high emissions background climate (RCP8.5), the modelling study of Sonntag et al., (2016, 2018), showed both a global annual mean surface temperature cooling effects, as well as a potential reduction of extreme warm days in several areas of the mid-northern latitudes. On the other hand, De Hertog et al., (2022) explored local and non-local effects of several idealized land management scenarios, among which aggressive afforestation is undertaken in all non-forested land portions by following the checkerboard approach from Winckler et al., (2017). Their results, obtained by considering the output of three ESMs, show that tropical (boreal) afforestation causes local cooling (warming), opposite to cropland expansion, and generalized non-local warming, despite uncertainties in the underlying energy processes determining these temperature outcomes. Their conclusion, however, is in contrast with recent estimates reported by Loughran et al., (2023), which considered a single model ensemble to report a

positive correlation between surface air temperature and increase tree cover fraction in tropical regions, an effect mainly dominated by a decreased surface albedo. These and other studies relying on ESM simulations, such as those by Luo *et al.*, 2022, 2023 and Grant *et al.*, 2023), highlight ongoing inconsistencies in estimating the magnitude and extent of the biogeophysical effects of afforestation. This is particularly critical, considering the increasing relevance that large-scale afforestation policies and other nature-based solutions will have in order to meet national and international climate targets (Grassi *et al.*, 2017; Duveiller *et al.*, 2020).

Given these premises, this study aims to investigate the climatic effects of large-scale afforestation by means of factorial ESMs simulations from the Scenario Model Intercomparison project (ScenarioMIP) and the Land Use Model Intercomparison Project (LUMIP) (Lawrence *et al.*, 2016; O'Neill *et al.*, 2016). One of the purpose of LUMIP is to foster the understanding of the biogeophysical impact of LULCC by providing a common experimental protocol for multi-model simulations. In particular, we take advantage of ssp370-ssp126Lu experiments from different ESMs and compare them with the ssp370.
Therefore, the main goal of this work is to identify the biophysical effects of large-scale LULCC, most importantly afforestation, and its relevance in the context of climate change. A specific focus will be on the role that background climatic conditions play in modulating the biophysical effects and processes resulting from afforestation. A prominent study by Forzieri et al., (2020) has demonstrated that in recent decades the vegetation control on latent heat fluxes, and therefore its evapotranspiration cooling capacity, is dominated by regions characterized by a limited water supply, where changes in background climatic conditions have led to an increased ratio of transpiration to evaporation. We therefore emphasize the different role of water and energy limited climates and speculate that water supply-limited climatic conditions could be the most favorable for deploying large-scale afforestation, potentially reducing the uncertainty regarding the theoretical spatial allocation of large-scale LULCC policies. With this respect, implications for the hydrological cycle are

examined, to test whether a reduction of available water resources could be envisioned in water-supply limited regions as a consequence of increased tree cover (King *et al.*, 2024)

3.3 Data and Methods

3.3.1 Data

We took advantage of seven different ESMs that participated in both ScenarioMIP and LUMIP simulation, and for which all the variables required for the analysis are available. An overview of the ESMs considered for the analysis is reported below in Table 10. The land-use projections used as forcings by all CMIP6 models derive from a harmonized land-use database, LUH2 (Hurtt *et al.*, 2020), which collects the output data of future land transitions by Integrated Assessment Models (IAMs), that for the ssp370 and ssp126 are developed by AIM-CGE (Fujimori *et al.*, 2014) and IMAGE (Stehfest, 2014) respectively.
We consider the ScenarioMIP ssp370 simulation (O'Neill *et al.*, 2016) as the reference one to estimate the effect of an afforestation scenario. The ssp370 scenario represents a future high emissions pathway, which leads to a 7.0 Wm^{-2} radiative imbalance by the end of the 21^{st} century as a consequence of low international climate cooperation, high fossil fuel emissions and very low land-use change regulations, with strong forest-cover reductions worldwide. The afforestation scenario is represented by the LUMIP ssp370-ssp126Lu simulation (Lawrence *et al.*, 2016), which is characterized by an incoherent coupling of socioeconomic developments from the ssp370 with high atmospheric CO_2 concentrations and radiative forcing, and a land-use scenario derived from the ssp126. The latter, assumes a sustainable development with low population growth, high agricultural productivity and reduced animal-share diets which results in a reduction of the land-use allocated to agriculture globally. As a consequence, natural vegetation and forests are allowed to expand (Figure S53b). On the opposite, the ssp370 scenario is characterized by substantial deforestation rates in the tropics by the end of the century with respect to 2015, most

prominently in central Africa, western Amazonia and some parts of North-America, with other regions, like south-eastern China, interested by reforestation (Figure S53a). It is important to mention that, despite not relevant from the biophysical point of view of this paper, the strong differences in forest cover as a result of the comparison between the two scenarios (represented in Figure S54 for all the ESMs) are mainly due to avoided deforestation, rather than afforestation or reforestation. However, we will refer to it as A/R through the manuscript, for simplicity.

Land-use states from the LUH2 dataset are translated into fractional coverages of several Plant Functional Types (PFTs), whose number differs for every model, as reported in Table 10. Depending on the different setups of ESMs land modules and the spatial implementation of common land-use states and transitions, the tree-cover extent widely varies across the ESMs for both the ssp126 and ssp370 scenarios (Figure S54 and Figure S55, respectively).

Those models with a dynamic vegetation scheme, MPI-ESM1-2-LR and UKESM1-0-LL, are also able to simulate plant competition and plant spatial allocation, and result in a widespread northward expansion of forest for both the scenarios considered (Figure S54 and Figure S55), as global climate warms during the 21st century.

Table 10:ESMs to be used in the analysis

ESM	Institution	Dynamic Vegetation	PFTs	Resolution (lat x lon)	Reference
ACCESS-ESM1-5	CSIRO	No	10	1.8758 × 1.258°	(Swart *et al.*, 2019)
CMCC-ESM2	CMCC	No	15	0.9° × 1.25°	(Lovato *et al.*, 2022)
CESM2	NCAR	No	14	0.9° × 1.25°	(Danabasoglu *et al.*, 2020)
CanESM5	CCCma	No	9	2.8 × 2.8°	(Ziehn *et al.*, 2020)
IPSL-CM6A-LR	IPSL	No	15	1.27° x 2.5°	(Boucher *et al.*, 2020)
MPI-ESM1-2-LR	MPI-M	Yes	12	1.8° × 1.8°	(Mauritsen *et al.*, 2019)
UKESM1-0-LL	MOHC	Yes	12	1.25 × 1.875°	(Sellar *et al.*, 2019)

Finally, the climatic effects of afforestation are estimated by considering the differences, for every variable analyzed, between the ssp370-ssp126Lu and the ssp370 simulations. By doing this, it is possible can isolate the net effect of LULCC, and therefore provide an estimate of the biophysical potential of large-scale afforestation as a land-based climate policy, in this case also accounting for future avoided deforestation.

3.3.2 Surface Energy Balance (SEB) decomposition

A Surface Energy Balance (SEB) decomposition approach is adopted to disentangle the processes underneath the local biogeophysical effects (Juang *et al.*, 2007; Luyssaert *et al.*, 2014; Winckler *et al.*, 2017; De Hertog *et al.*, 2022). The SEB decomposition equation is derived from the energy balance equation by taking its first derivative in order to obtain the changes in surface temperature, thus allowing to unravel the biophysical mechanisms contributing to local temperature changes derived from large-scale afforestation:

$$\Delta T_s = \frac{1}{4}\sigma T_s^3(-SW_{in}\Delta\alpha + (1-\alpha)\Delta SW_{in} + \Delta LW_{in} - \Delta LE - \Delta H) \quad (11)$$

Here, T_s represents temperature at surface, α is the albedo (calculated as *SWout/SWin*), SW_{in} and LW_{in} are incoming short- and longwave radiation, whereas LE and H are respectively latent and sensible heat fluxes. Temperature variations as a result of ground heat fluxes have been excluded due to their very low magnitude at the global scale.

3.3.3 Intrinsic Biophysical Mechanism (IBPM) decomposition

Another method that allows to disentangle different processes related to the changes in physical properties of the land surface and surface energy balance is the Intrinsic Biophysical Mechanism (IBPM)(Lee *et al.*, 2011; Chen and Dirmeyer, 2016; Chen *et al.*, 2020; Liu *et al.*, 2023). The IBPM allows for a more direct estimation of vegetation physiological control over the atmospheric boundary layer by the estimation of a surface roughness term. Taking the SEB equation as a reference, we could approximate surface temperature changes as:

$$\Delta T_s = \frac{\lambda_0}{1+f}(\Delta R_n - \Delta G) + \frac{-\lambda_0}{(1+f)^2} \times \frac{1}{2}(R_n - G)\Delta f_1 + \frac{-\lambda_0}{(1+f)^2} \times \frac{1}{4}(R_n - G)\Delta f_2 + \Delta T_a \qquad (12)$$

Where the four additive terms represent changes in radiative forcing, surface roughness (or aerodynamic resistance), Bowen ratio, and atmospheric feedback (representing advection by surface air temperature). Δf is the change in the energy redistribution factor, attributable to changes in surface roughness (Δf_1) and Bowen ratio (Δf_2) respectively.

3.3.4 Sensitivity of turbulent fluxes to changes in LAI

Lastly, a multilinear regression framework was used to quantify the influence of afforestation, specifically the consequent increased vegetation greening in terms of Leaf Area Index (LAI), on the surface energy partitioning. Similar to the approach of Forzieri et al., (2020), the relationship between LE, afforestation and other climatic predictors is modeled as follows:

$$\Delta LE = \frac{\delta LE}{\delta LAI}\Delta LAI + \frac{\delta LE}{\delta T_s}\Delta T_s + \frac{\delta LE}{\delta p_r}\Delta p_r + \frac{\delta LE}{\delta SW_{in}}\Delta SW_{in} + \epsilon \qquad (13)$$

Here, LAI is Leaf Area Index, *pr* represents precipitation, T_s is temperature at surface, SW_{in} is incoming shortwave radiation. The coefficient $\frac{\delta LE}{\delta LAI}$ is the partial contribution of afforestation, taking LAI as a proxy of land-use change, in partitioning the surface available

energy into evaporative fluxes, therefore representing its indirect contribution to surface temperature. Finally, the effect of LAI on surface temperatures, modulated by latent heat, is considered as the product of $\frac{\delta LE}{\delta LAI}$ with the univariate estimate of $\frac{dT_s}{dLE}$.

Finally, the contribution of afforestation in partitioning available energy across ecosystems climatic regimes, is investigated by differentiating between water-limited and energy-limited ones. To do so, the correlation of latent heat and precipitation as $\rho(LE, pr)$, and surface temperature as $\rho(LE, ts)$ have been considered. Water-limited regions are those where $\rho(LE, pr) > \rho(LE, ts)$, meaning that the correlation between latent heat and precipitation is stronger than the correlation between latent heat and surface temperature, whereas the opposite condition defines energy-limited regimes.

3.4 Results and Discussion

3.4.1 SEB and IBPM decomposition

Every ESM have a different representation of LUC transitions, despite the shared land use forcing of the LUH2 dataset, which originates from the translation of land use into fractional coverages of a different number of PFTs. As a consequence, the tree fraction coverage from the ssp370 and ssp126 scenarios differs for every model, and the resulting difference representing the idealized adoption of large-scale afforestation widely varies in magnitude and extent, despite having some common spatial features, as observed in Figure S56. Particularly, CanESM5 stands out for its almost net-zero gain of afforested area in central Africa, due to a lack of deforestation in the ssp370 scenario compared to the other ESMs. The reason for this mismatch is to be found in the specific vegetation modelling scheme of CanESM5, lacking this model an explicit representation of rangelands and shrubs, which are by contrast allocated to forest areas (Swart *et al.*, 2019). As a consequence, deforestation that implies a conversion from trees to shrubs or rangelands is not represented as a reduction of tree-cover within the same area.

To isolate a stronger LULCC biophysical signal for the investigation of the local climatic effect, the focus is on the land area interested by at least a 10% increase in tree fraction coverage change in the 30 years period between 2070 and 2100, which varies from a minimum of 8.9 Mkm^2 for CanESM5 to a maximum of 15.6 Mkm^2 for MPI-ESM1-2-LR.

Table 11: Area affected by a 10% increase in tree cover fraction, its local surface temperature response and percentage with significant temperature difference for every ESM

ESM	**Area of ΔtreeFrac > 10% (Mkm^2)**	**Temperature (K)**	**Afforested land with significant Ts signal**
ACCESS-ESM1-5	9.8	-0.14	23 %
CMCC-ESM2	19.5	-0.09	34 %
CESM2	19.3	-0.75	45 %
CanESM5	8.9	-0.31	16 %
IPSL-CM6A-LR	14.1	-0.55	37 %
MPI-ESM1-2-LR	15.6	-0.83	49 %
UKESM1-0-LL	9.6	0.17	6 %

The mean surface temperature for those regions interested by afforestation are reported in Table 11, whereas the spatially explicit values are in Figure S57. Six out of seven models show a statistically robust net cooling signal (tested with a non-parametric Man-Whitney U-test, considering a 90% confidence interval), with the noticeable exception of UKESM1-0-LL, for which a small temperature increase is projected (Table 11). CESM2 and MPI-ESM1-2-LR depict the strongest cooling, with the land portion with a significative surface temperature difference slightly below 50% of the total afforested land for these two models,

whereas this is less than 25% for the other ESMs, indicating that the magnitude of LUC applied in these simulations is not strong enough to derive a widespread significant local temperature change. The surface temperature effect reported above is confirmed by the correlation by Ts and treeFrac, which is negative for all the models but UKESM1-0-LL, both globally as well as in Africa, while opposite results are obtained for MPI-ESM-LR and UKESM1-0-LL for South America (Figure 48).

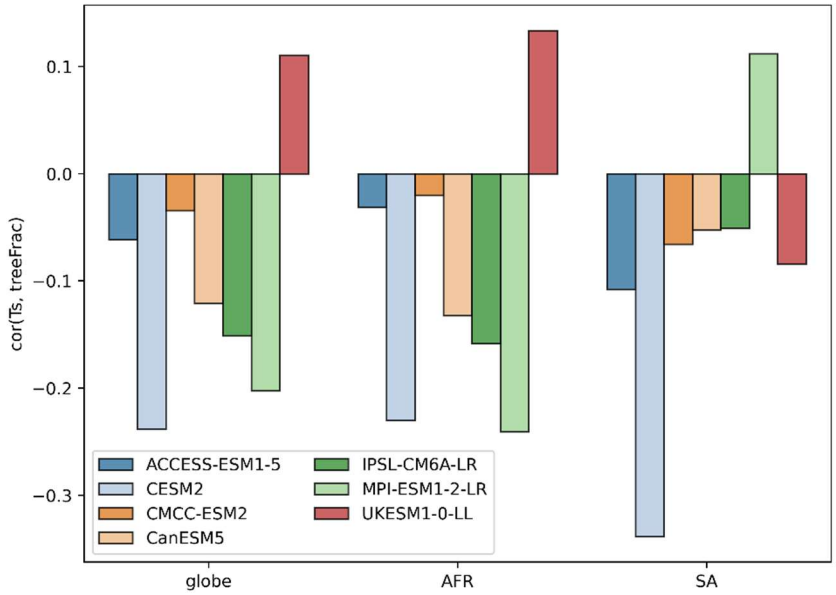


Figure 48: Correlation coefficient between surface temperature and tree cover fraction for different geographical domains (global, Africa and South America) and ESM.

Delving into the surface temperature signal decomposition by means of the SEB equation, its application is justified by the close resemblance of surface temperature estimated by summing the SEB components with the original difference between the two factorial simulations (Figure S58). From Figure 49, it is evident the prominent contribution of variations in albedo and in turbulent heat fluxes (Latent Heat and Sensible Heat) to the overall surface temperature effect. Specifically, the temperature increase associated with albedo is related to its decrease as a consequence of the lower amount of shortwave upwelling

radiation reflected by the darker tree canopies in afforested regions. This physical process has been demonstrated to be well captured by ESMs (Davin and Noblet-Ducoudré, 2010), thus the observed total agreement among the ensemble of model considered, despite the differences in magnitude, having UKESM1-0-LL (0.6 K) a response which is four to five times compared to CESM2 and CanESM5 (0.15 K circa). Latent heat fluxes emerges as another major source of surface temperature variability, contributing with a cooling effect for CESM2, IPSL-CM6A-LR, MPI-ESM1-2-LR and UKESM1-0-LL as a consequence of increased heat dissipation by evaporative cooling, whereas the opposite effect is shown by ACCESS-ESM1-5 ì, CMCC-ESM2 and CanESM5.

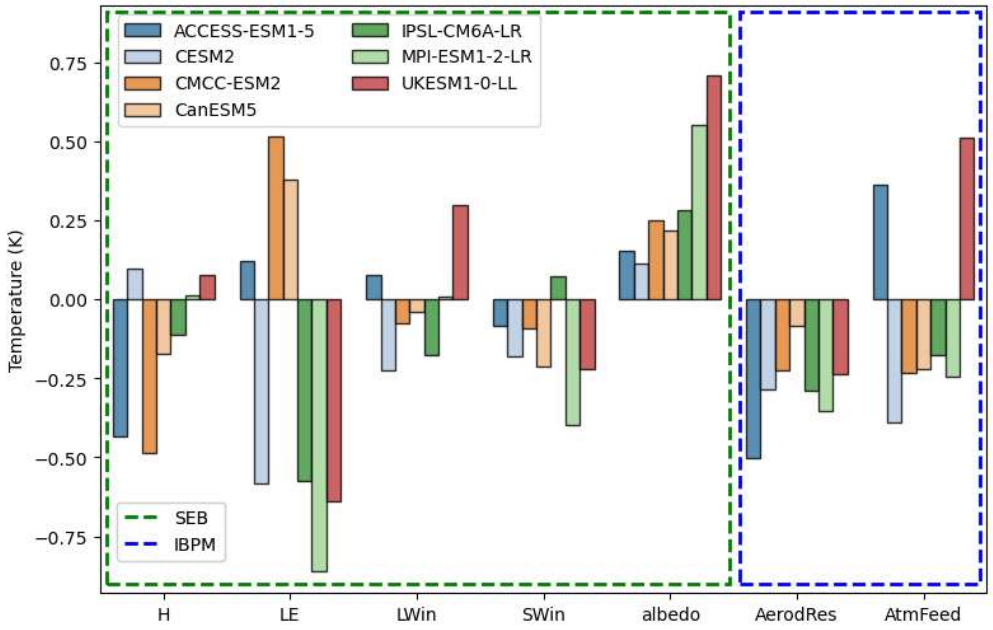


Figure 49: Temperature contribution of the variables resulting from the SEB decomposition (green patch) and from the IBPM (blue patch).

Similarly, we took advantage of the Intrinsic Biophysical Mechanism (IBPM) decomposition that, similarly to the SEB decomposition, is able to resemble the surface temperature effect directly retrieved from the ESMs (Figure S59), to assess the surface temperature contribution of aerodynamic resistance, which is tightly coupled with the local change in

roughness resulting from the land surface alteration. Consequently to the replacement of grasses with tree cover in the ssp370-ssp126Lu simulation, roughness length (representing the theoretical height at which wind speed is equal to zero) is increased, favoring the turbulence of the atmospheric boundary layer and thus decreasing the aerodynamic resistance, as shown in Figure 49. Furthermore, the cooling effect of afforestation as a consequence of variation in roughness and thus aerodynamic resistance appears to be stronger for low levels of initial tree cover, indicating that the marginal efficacy is inversely proportional to the abundance of tree cover, scaling quasi-logarithmically for IPSL-CM6A-LR, MPI-ESM1-2-LR and UKESM1-0-LL, whereas this relationship is completely missing for both CanESM5 and ACCESS-ESM1-5, as reported in the figure below.

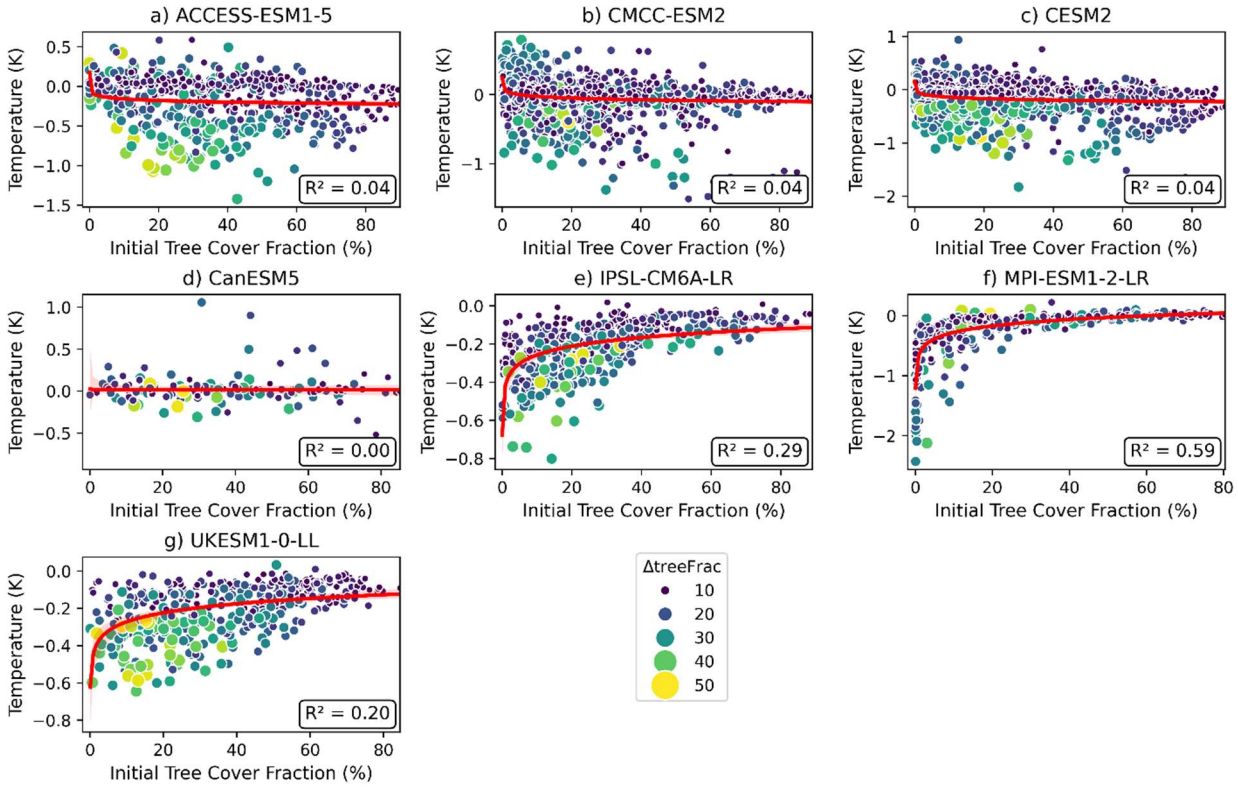


Figure 50: Mean surface temperature effect of afforestation for the period 2070-2100, derived from the change in aerodynamic resistance, as a function of initial tree cover fraction. Only those grid cells with at least 10% increase in tree fraction coverage are plotted as markers. The red line is a logarithmic fit, whereas the colored legend (ΔtreeFrac) represents the intensity of afforestation in terms of tree cover fraction changes.

3.4.2 Cooling mechanisms and hydrological implications

Afforested regions trigger a sharp and consistent increase of LAI, which affects the water and energy fluxes at the land-atmosphere intersection. Given the strong cooling signal originating from variations in latent heat fluxes, we estimated its sensitivity to LAI, whose increase we considered a proxy of increased tree cover, and differentiate the results for dry (water-limited) and humid (energy-limited) regions. Estimates of the partial derivative for latent heat fluxes sensitivity to LAI at interannual timescales show a positive effect for all the ESMs, meaning that an increase in LAI (driven by increased tree cover) enhances evapotranspiration. Furthermore, this effect emerges to be stronger for drier water-limited regions with respect to the energy-limited ones, as a consequence of the increase in evaporative surface in these regions, and statistically significant (p-value <0.001) for all the ESMs by considering a Mann-Whitney non-parametric test with a Bonferroni correction. Being latent heat and sensible heat competitive pathways for the dissipation of energy from the land surface, specular results of Figure 51 are found when applying equation 11 for estimating the sensible heat sensitivity to the predictors of interest (Figure S61).

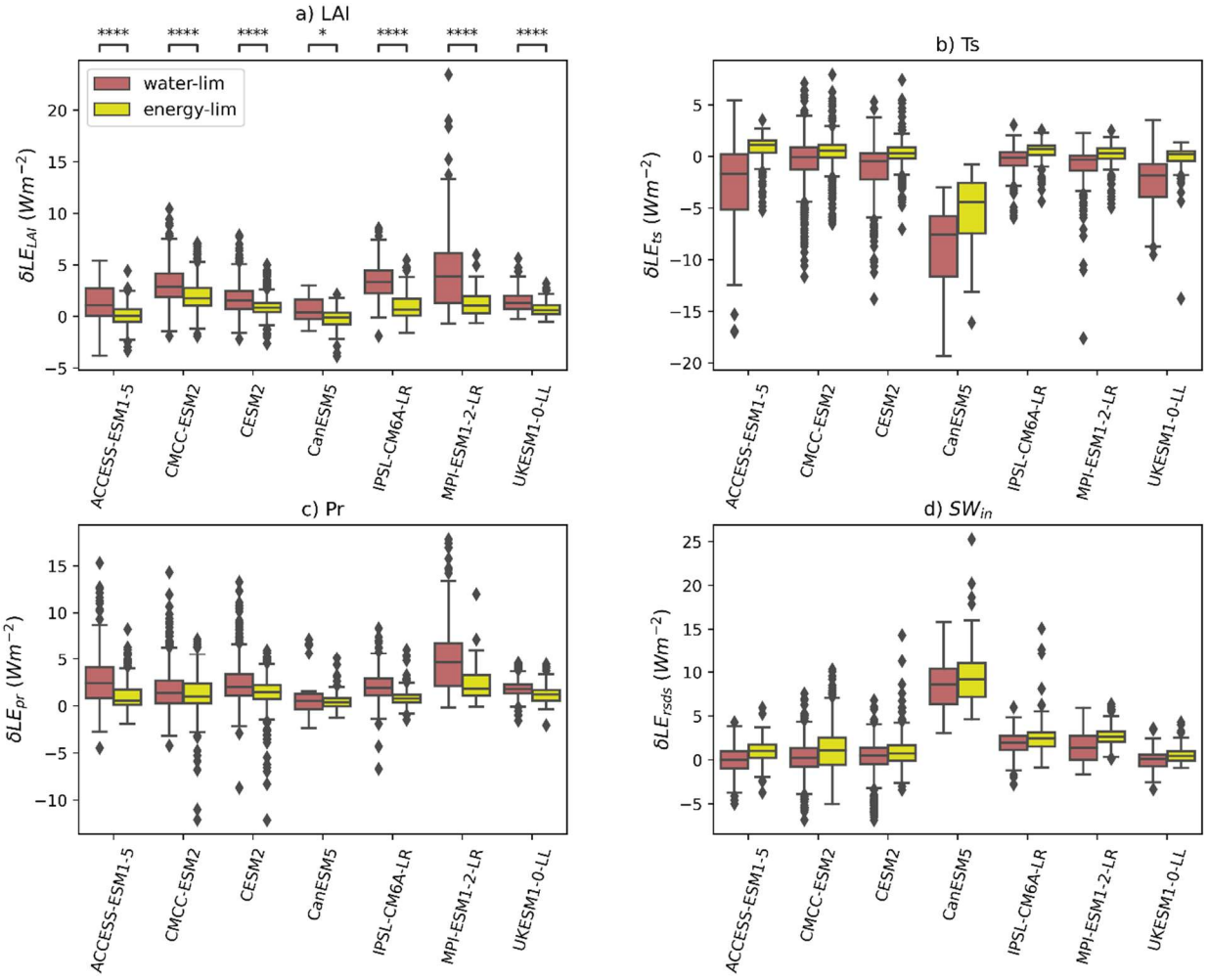


*Figure 51: Coefficients distribution of the partial derivatives representing the sensitivity of latent heat to respectively LAI, surface temperature, precipitation and shortwave incoming radiation, for water (red) and energy limited (yellow) areas interested by afforestation in every ESMs. Statistical significance, tested by means of a Mann-Whitney U-test, is reported in the stars above the plot of panel a), and refers to the following convention: *: 1.00e-02 < p <= 5.00e-02; **: 1.00e-03 < p <= 1.00e-02; ***: 1.00e-04 < p <= 1.00e-03; ****: p <= 1.00e-04.*

The effects of increased LAI on surface temperature, mediated by the effects of latent heat, are derived by multiplying the latent heat sensitivity to LAI (panel a) in Figure 51) by the surface temperature sensitivity to latent heat. The results show that the increase of LAI occurring as a consequence of afforestation lead to a net reduction of surface temperature for all the ESMs, with a multi-model mean value of -0.073 ± 0.054 K/m^2m^{-2}. As for latent heat sensitivity to LAI, we found this effect to be more pronounced for regions with a water-limited regime (Figure 52), and the difference with respect to energy-limited ecosystems to

be statistically significant for all models but ACCESS-ESM1-5, with consistent cooling for five ESM: CMCC-ESM2 (–0.155 ± 0.148K/m^{2}m^{-2}), CESM2 (-0.119 ± 0.132 K/m^{2}m^{-2}) IPSL-CM6A-LR (-0.138 ± 0.153 K/m^{2}m^{-2}), MPI-ESM1-2-LR (-0.246 ± 0.202 K/m^{2}m^{-2}) and UKESM1-0-LL (-0.129 ± 0.11 K/m^{2}m^{-2}). An indication of those regions classified as water- or energy-limited can be found, for all the ESMs considered, in Figure S60.

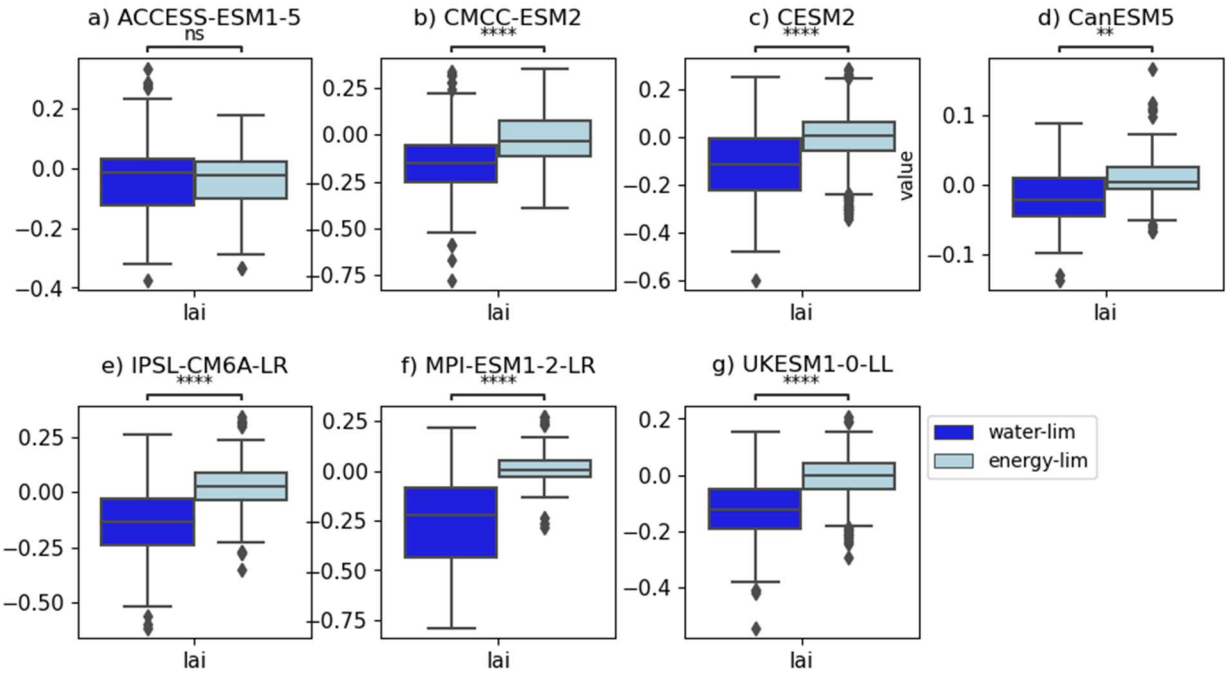


*Figure 52: Coefficients distribution of the partial derivatives representing the sensitivity of surface temperature LAI, for water (blue) and energy limited (lightblue) areas interested by afforestation in every ESMs. Statistical significance, tested by means of a Mann-Whitney U-test, is reported in the stars above the plot, and refers to the following convention: *: 1.00e-02 < p <= 5.00e-02; **: 1.00e-03 < p <= 1.00e-02; ***: 1.00e-04 < p <= 1.00e-03; ****: p <= 1.00e-04.*

These results emphasize the role that environmental conditions, specifically the physical regime that controls evapotranspiration dynamics, play in driving surface temperature responses to A/R efforts at interannual timescales. All of the ESMs used (but ACCESS-ESM1-5, in Figure 52a) show that an intensification of forest cover could effectively dampen the climate change driven increase in local temperatures by the end of the 21st century by means of evaporative cooling, and that this mechanism is particularly effective in water-

scarce regions (blue box-plots in Figure 52). However, this potential benefit does not comes without risks, as vegetation greening has been demonstrated to potentially lead to a depletion of local water resources (Chen *et al.*, 2023; King *et al.*, 2024). With this respect, the recent study of King and colleagues adopted the CESM2 ESM to explore the hydrological implications of A/R, showing a reduced availability of groundwater resources in those regions as a consequence of the higher water demand of forests compared to grasslands and shrublands. Here, this hypothesis is tested for seven ESM by analyzing the cumulative soil water content (over the entire soil column) for the regions interested by A/R compared to the ones where no LUC occurs. A/R regions experience a statistically relevant (tested with a Mann-Whitney U-test) decrease in total soil water content for five out of seven models, respectively CMCC-ESM2, CESM2, CanESM5, IPSL-CM6A-LR and MPI-ESM1-2-LR, whereas an opposite effect is found for UKESM1-0-LL (i.e. wetter soils for A/R regions) and no difference is presented by ACCESS-ESM1-5 (Table 12). Results therefore confirm, for five different ESMs, that a hypothetical forest expansion in a high CO_2 future scenario poses serious concerns regarding its long-term biophysical cooling opportunities due to the potential depletion of local water resources, confirming what recently reported by King et al., (2024) and Peng et al., (2024). Additionally, the reduction of water resources availability that comes from the higher water demand of forests compared to shrublands and grasslands overcomes the increase in water use efficiency (WUE) that occurs as a consequence of plants' partial stomatal closure, a result of the high atmospheric CO_2 concentrations of the ssp370 scenario.

Table 12: Effect of A/R on total soil water content (expressed in kgm^{-2}) and its statistical significance compared to non-afforested regions

ESM	A/R Soil Water Content (kgm^{-2}) 25^{th}, mean, 75^{th}	No A/R Soil Water Content (kgm^{-2}) 25^{th}, mean, 75^{th}	Mann-Whitney U-test p-value
ACCESS-ESM1-5	[-12.76, -4.97, 8.73]	-1.39	0.55
CMCC-ESM2	[-6.35, -2.85, 9.71]	-0.29	****<0.0000
CESM2	[-49.13, -33.33, 5.26]	-1.27	****<0.0000
CanESM5	[-9.56, -3.86, 2.82]	0.11	****<0.0000
IPSL-CM6A-LR	[-15.27, -8.0, -0.09]	-0.65	****<0.0000
MPI-ESM1-2-LR	[-24.5, -11.69, 4.27]	0.84	****<0.0000
UKESM1-0-LL	[-6.53, 6.65, 17.26]	-0.76	****<0.0000

3.5 Conclusions

This chapter investigated the biophysical climatic consequences of large-scale afforestation/reforestation under a future high CO_2 climate using seven available ESMs from the LUMIP project. The comparison of an afforestation scenario (ssp370-ssp126Lu) with a high-CO_2 baseline (ssp370), allows to assess the impacts on surface energy partitioning, surface temperature, and the hydrological cycle. All the ESMs display a local decrease in surface temperatures as a consequence of increased tree-cover, with CMCC-ESM2 and MPI-ESM1-2-LR showing a significant cooling, whereas UKESM1-0-LL is the only model that represents a clear local warming signal. Albedo changes and latent heat fluxes emerged as the main physical mechanisms which modulate surface temperatures. Due to the predominance of tropical A/R, changes in albedo lead to a surface warming, an effect clearly represented by all the ESMs, while surface cooling is the result of increases in evapotranspiration. Another effect of increase tree-covered area is the increase in roughness length compared to lower vegetation types, which favors the instability of the atmospheric boundary layer and the heat dissipation due to stronger turbulent mixing, an effect that

contributes to local temperature decrease. Still, the predominant heat-dissipation mechanism remains evaporative cooling, which appears to be more pronounced and effective for ecosystems whose productivity is limited by local water availability (water-limited), rather then incoming solar radiation (energy-limited). Despite increased tree-cover in these water-limited ecosystems leads to a stronger evaporation-driven cooling for all the ESMs (with the exception of ACCESS-ESM1-5), with important implications for the geographical effectiveness and allocation of LUC policies, considerable concerns could arise with respect to local water resources. Higher local water availability is required for the sustainment of forests ecosystems compared to grass and shrub-lands, and all the ESMs considered (except for ACCESS-ESM1-5) agree in showing a significant decrease of soil water content in A/R regions compared to those not interested by large-scale afforestation. If water resources depletion is not replenished by precipitation inflow in A/R areas, this mechanism could pose a serious threat to the long-term sustainability of large scale land-based climate solutions. These results therefore emphasize on the one hand the regional and local mitigation benefits that could arise from the adoption of large-scale land CDR policies implemented in the context of a sustained future warming scenario. The consideration of biophysical effects of LUC, however, should also account for the negative implications that could arise from the depletion of local water resources due to increased water demand from forest expansion, suggesting a trade-off between long-term biophysical (and biogeochemical) benefits and water resources availability.

Code and Data Availability

The code used to process the data, obtain the results and generate the figures is publicly available at https://github.com/Matteo-Mastro/Afforestation_LUMIP_biophys. CMIP6 and LUMIP data are freely available and accessible from one of the ESGF repository (e.g. https://aims2.llnl.gov/search).

Annex

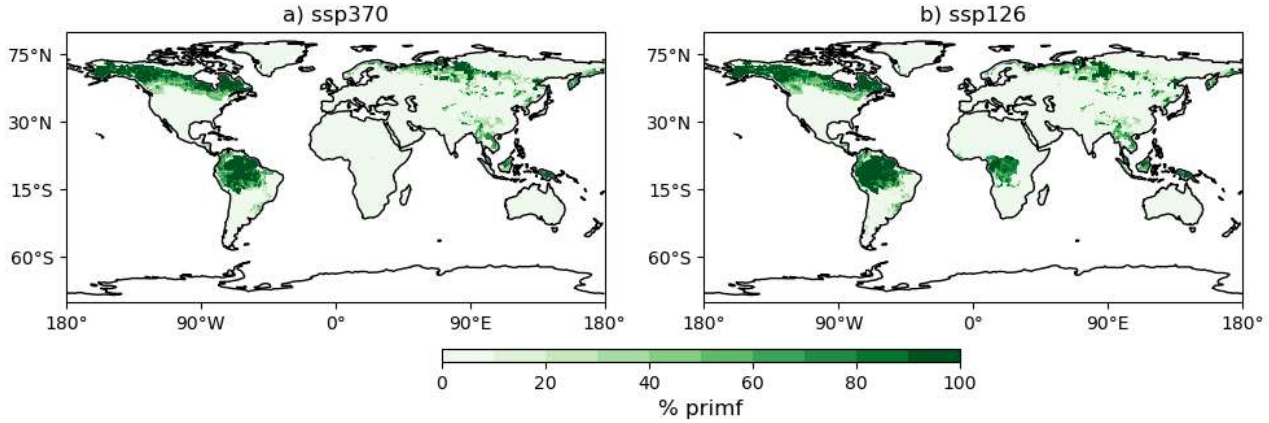


Figure S53. Extension of primary forests as percentage of the grid cell area for the year 2100 in the a) ssp370 and b) ssp126 scenario, as represented in the LUH2 dataset.

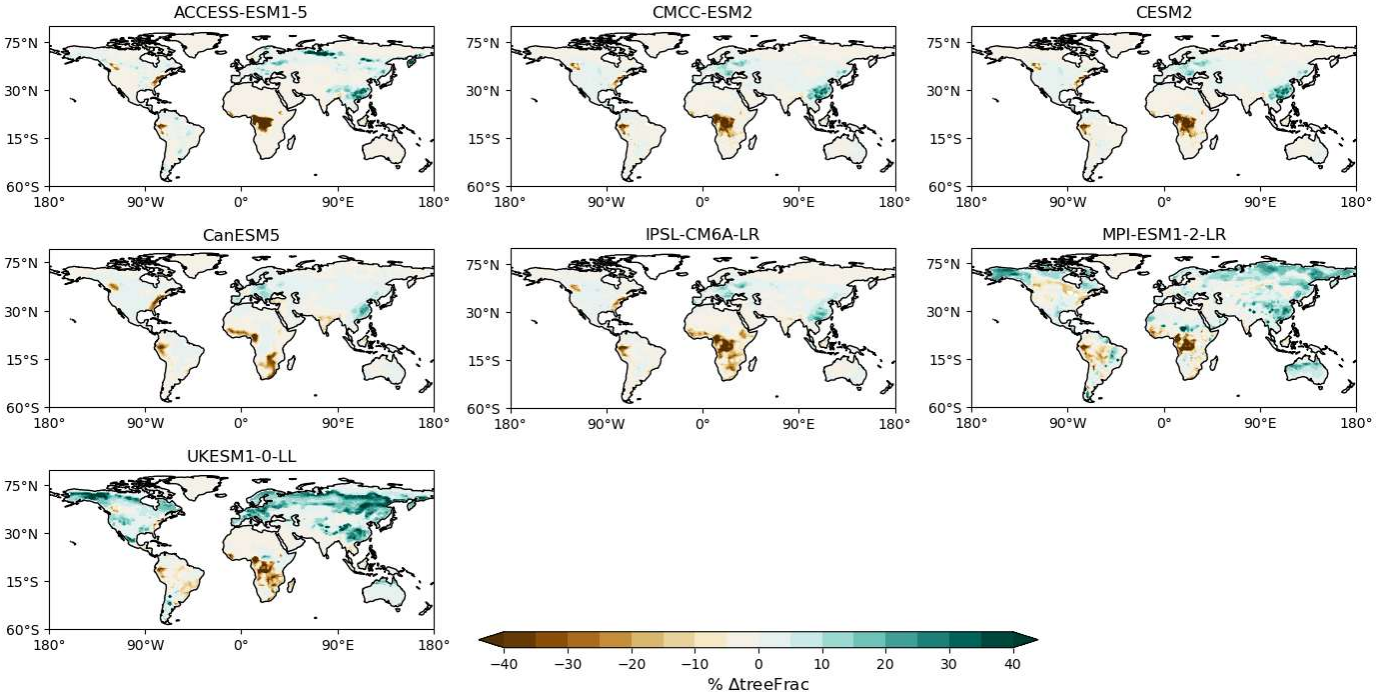


Figure S54. Tree cover fraction extent for the scenario ssp370, at the year 2100, expressed as the difference compared to the year 2015.

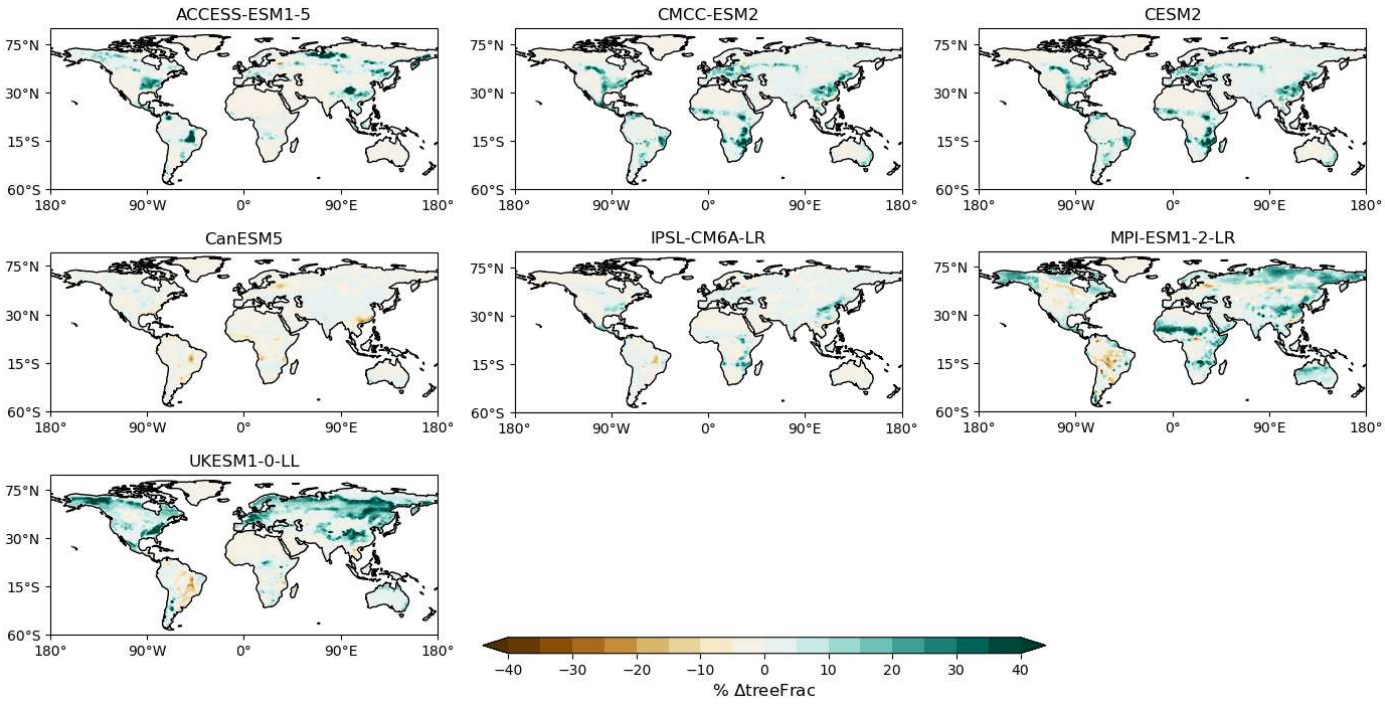


Figure S55. Tree cover fraction extent for the scenario ssp126, at the year 2100, expressed as the difference compared to the year 2015.

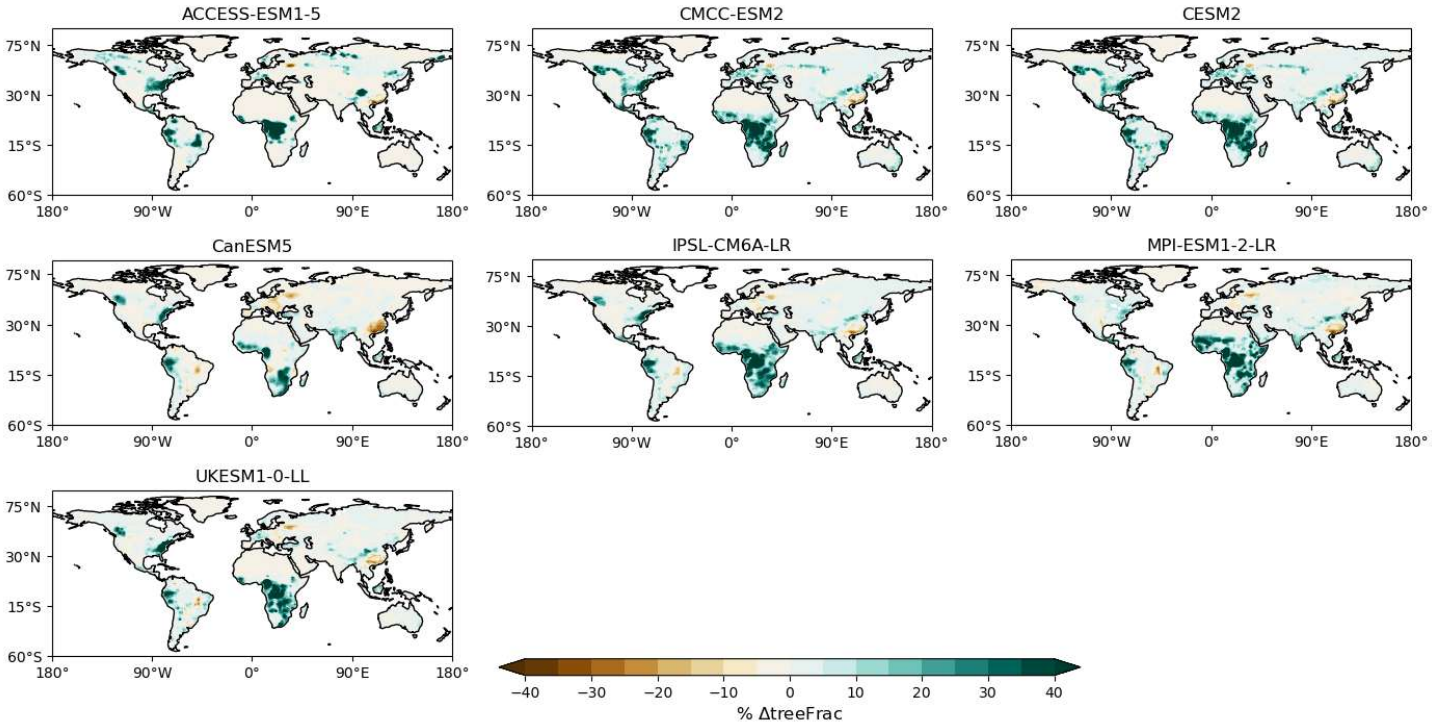


Figure S56. Difference in tree cover fraction between ssp370-ssp126Lu and ssp370, at the year 2100.

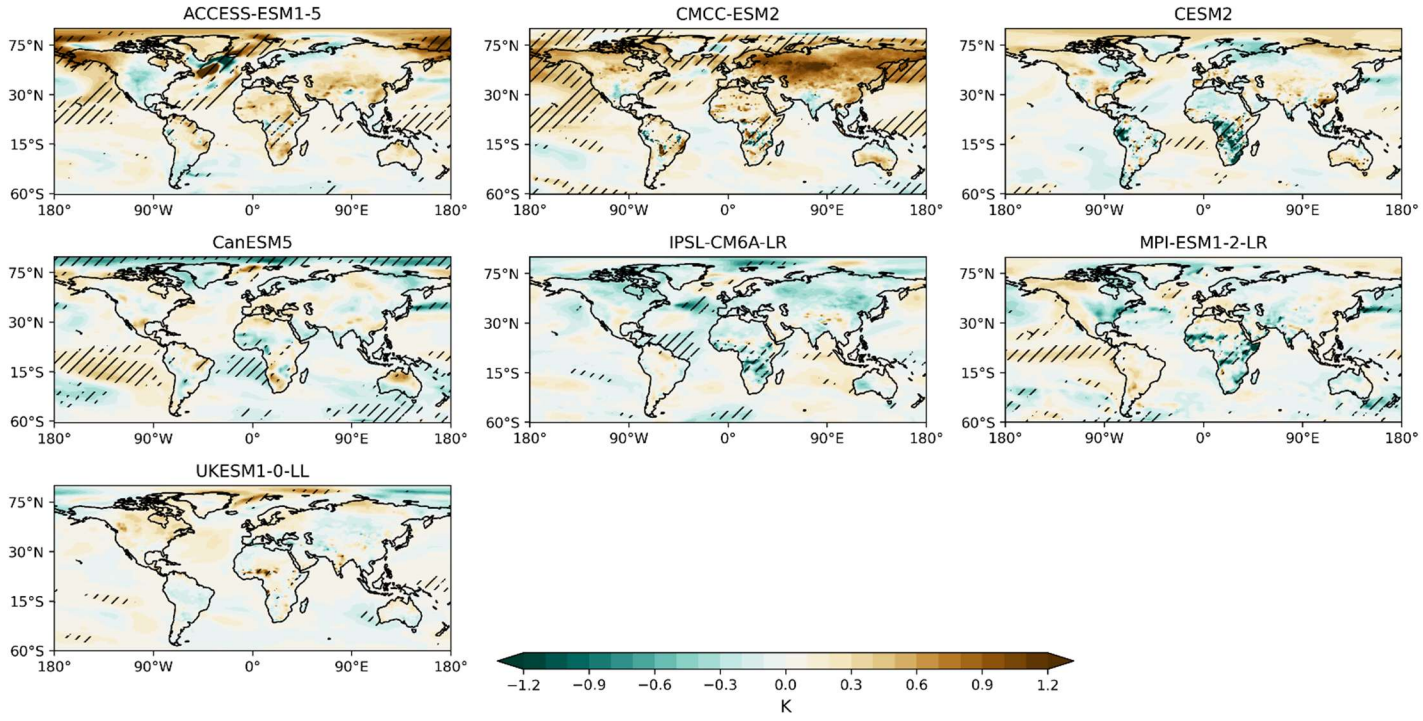


Figure S57. Mean surface temperature effect of afforestation for the period 2070-2100. Hatches represent grid-cells with a 95% confidence interval significance level.

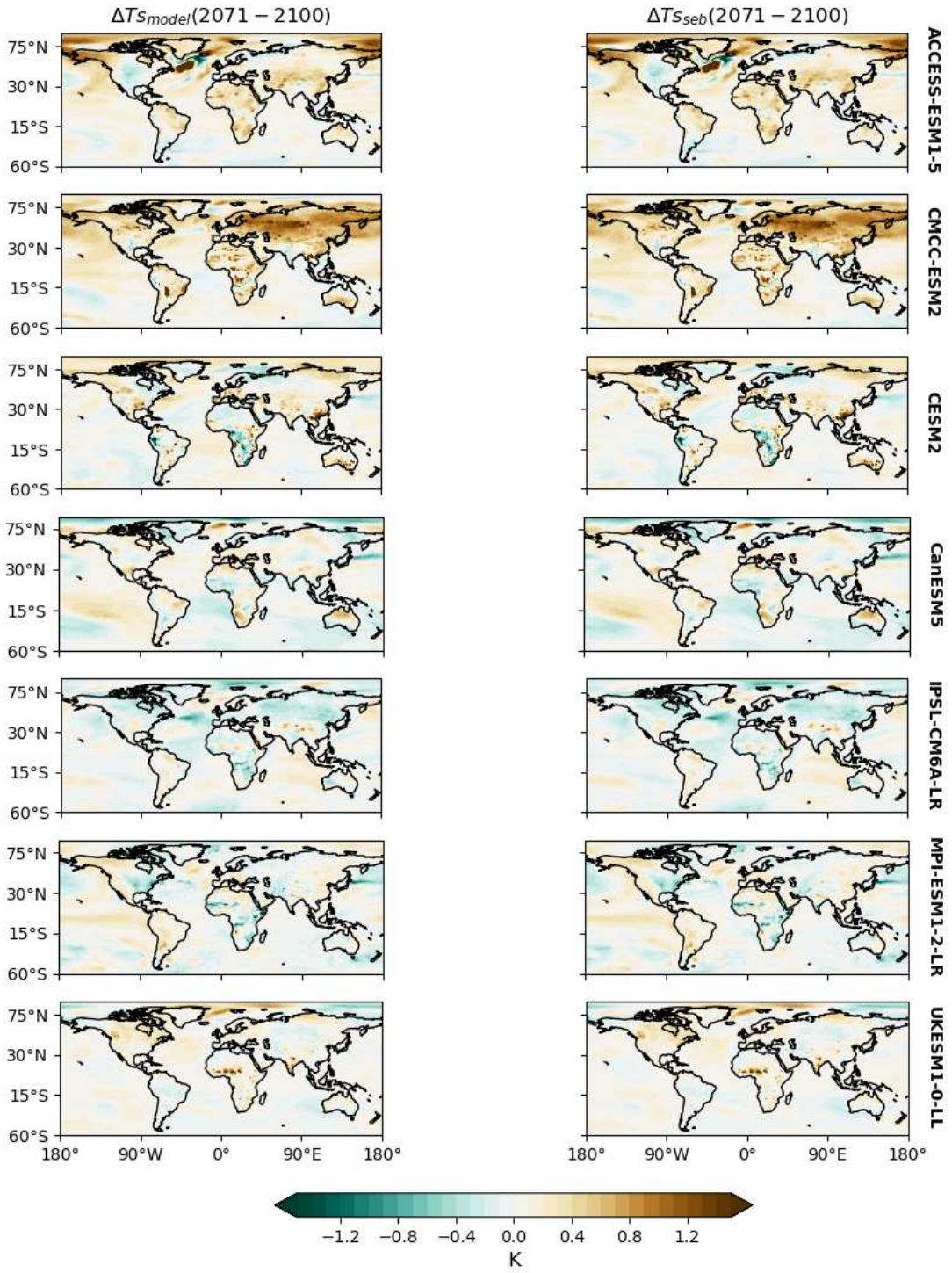


Figure S58. Mean surface temperature effect of afforestation for the period 2070-2100, as retrieved directly from the factorial simulations (ΔTsmodel, left column), and estimated from the SEB decomposition (ΔTsseb, right column).

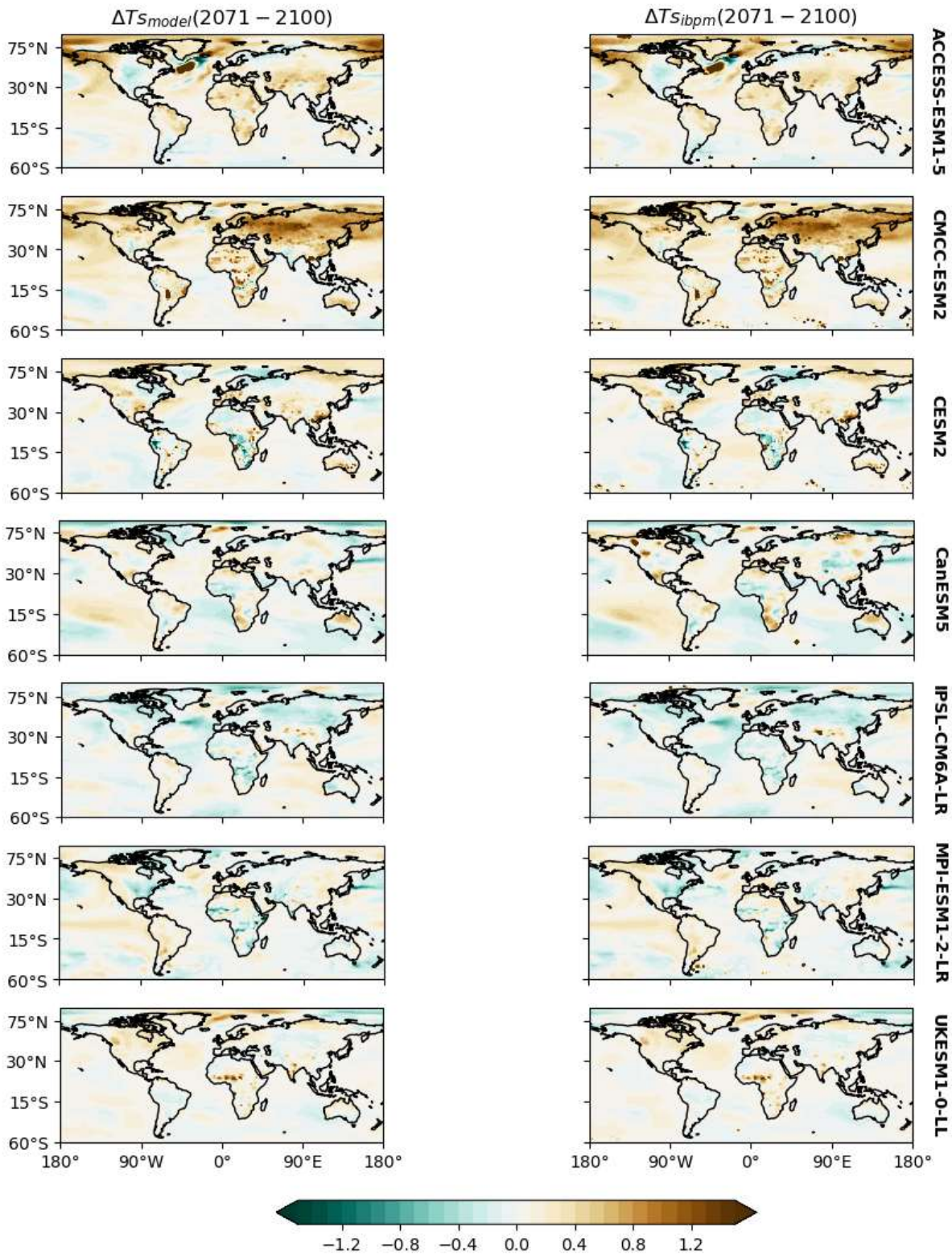


Figure S59. Mean surface temperature effect of afforestation for the period 2070-2100, as retrieved directly from the factorial simulations (ΔTsmodel, left column), and estimated from the IBPM decomposition (ΔTsibpm, right column).

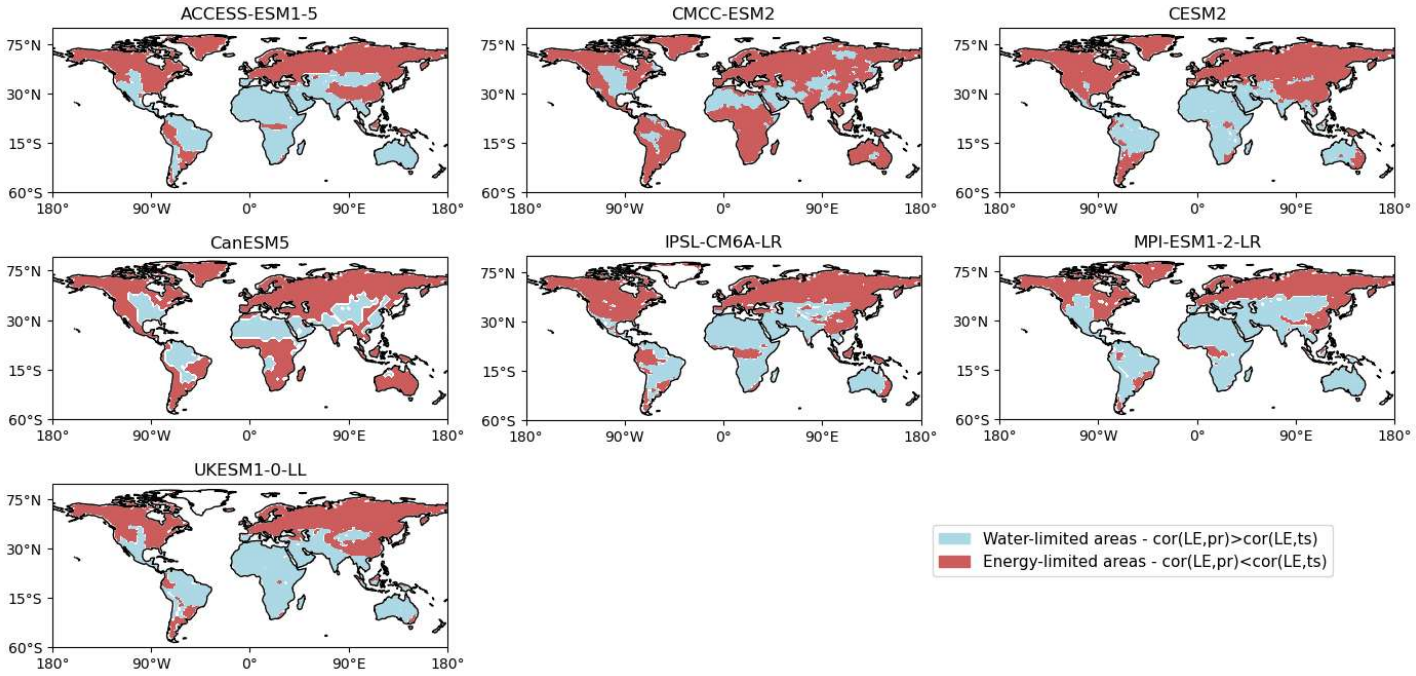


Figure S60. Water and Energy limited regions, as defined in the main text, for every ESM.

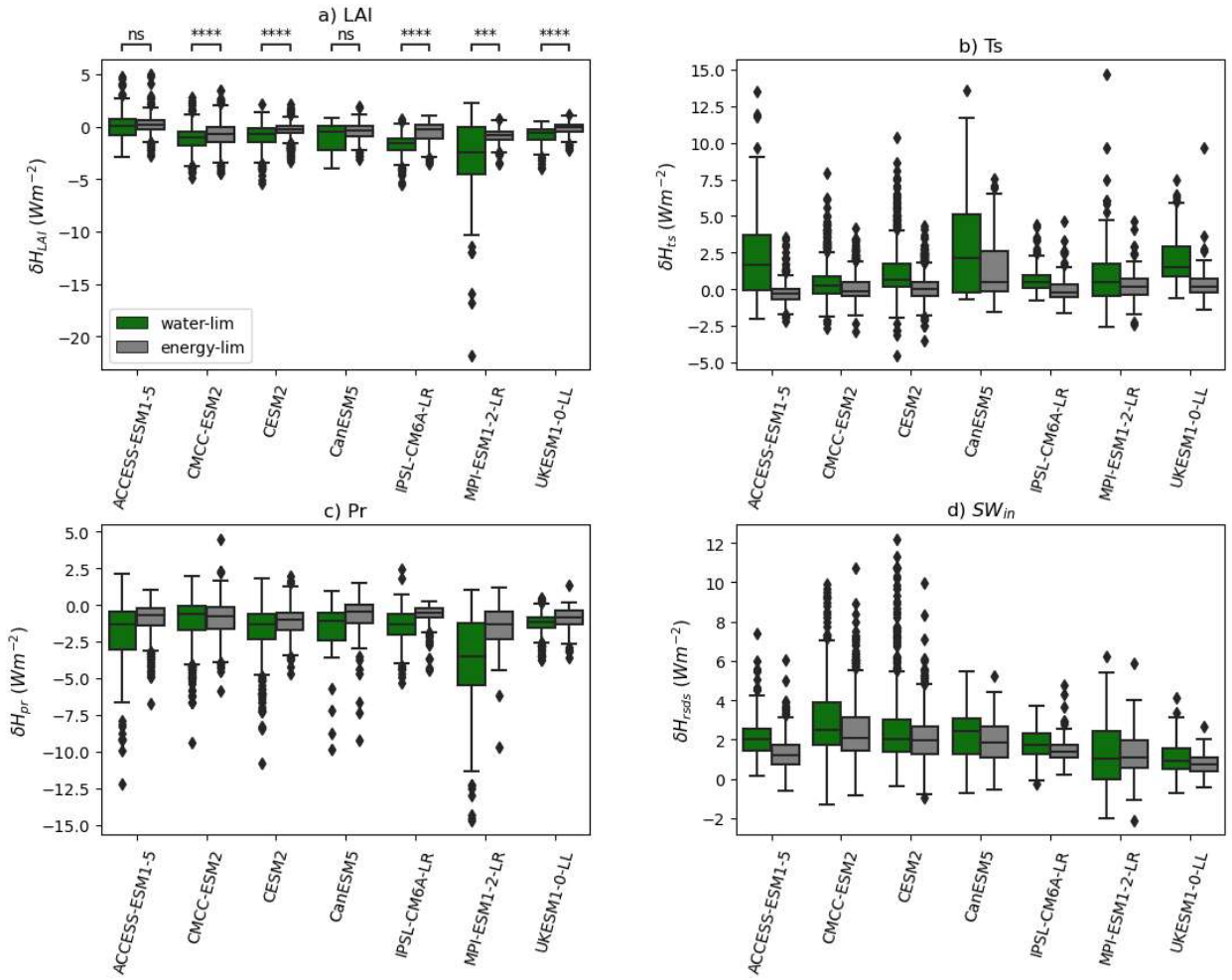


*Figure S61: Coefficients distribution of the partial derivatives representing the sensitivity of sensible heat to respectively LAI, surface temperature, precipitation and shortwave incoming radiation, for water (green) and energy limited (grey) areas interested by afforestation in every ESMs. Statistical significance, tested by means of a Mann-Whitney U-test, is reported in the stars above the plot of panel a), and refers to the following convention: *: 1.00e-02 < p <= 5.00e-02; **: 1.00e-03 < p <= 1.00e-02; ***: 1.00e-04 < p <= 1.00e-03; ****: p <= 1.00e-04.*

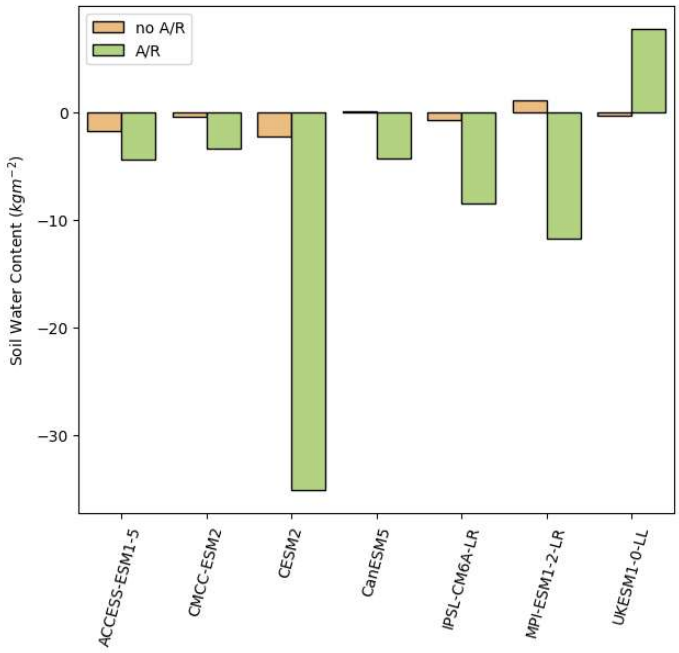


Figure S62: Mean soil water content (expressed here is the 2070-2100 mean difference between ssp370-ssp126Lu and ssp370) within regions interested by A/R (green) and not affected by increased tree cover (orange). The 25th and 75th percentiles and the means of the distributions, together with the statistical significance of the differences, are reported in Table 11.

Thesis Conclusion

One of the most important and globally recognized goals of climate policies is the need to keep global mean surface temperatures well below 2 °C, and possibly avoid surpassing the 1.5 °C threshold, which represents the ambition as stated in the Paris Agreement in 2015. The possibility to keep temperatures below these two values are substantially determined by the so-called remaining Carbon Budget, which quantifies the amount of cumulative carbon that can still be emitted in the atmosphere before reaching a specific temperature target. In this dissertation, three critical aspects that affect the uncertainty surrounding the remaining Carbon Budget, potentially undermining its reliability and consistency, have been examined and assessed in the three chapters, namely the role of non-CO_2 climate forcers, carbon-climate feedbacks and LUC scenarios uncertainty. In the first chapter, the role of non-CO_2 forcers, in particular Methane (CH_4) in influencing the remaining Carbon Budget has been investigated. Specifically, it was demonstrated that the usage of a newly developed metric, denominated GWP-star (GWP*), if adopted for converting Methane emissions to CO_2-equivalents in the context of overshoot scenarios, may lead to a misleading temperature representation in the case of sharp CH_4 emissions (thus temperature) declines, and for long-term scenarios beyond 2100. The main relevance of this study emerges from shedding lights on the limitations of using the GWP* metric for including the contribution of short-lived climate forcers into the global carbon budget, a scientific topic which is still currently debated.

On another note, the second chapter have tackled the role that land carbon feedbacks play in the global carbon cycle. The focus of this research is the Amazon basin, a tropical ecosystem whose role as a positive carbon sink under climate change scenarios is at risk, therefore threatening the stability and assumptions of the remaining carbon budget. By using a multi-model approach, this work assessed the different environmental variables influencing the long-term cumulative carbon sink and its variability at interannual time-

scales. With this respect, an important consideration that must be stressed is the divergence in the carbon fluxes projections of different ESMs from the CMIP6 generation. The work, as at the moment of writing this manuscript, has not included the contribution of natural and anthropogenic disturbances (fire, Land Use Change) in the projections of the carbon sink, which can further contribute to the uncertainty and spread in the models projections. Nevertheless, the results calls for a strong need to improve the representation of land carbon and vegetation dynamics in ESMs in order to provide better estimates of carbon fluxes and carbon feedbacks for future scenarios.

Lastly, the third chapter assessed the biophysical impact of anthropogenic LUC, specifically afforestation and reforestation (A/R), on climate and surface temperatures. This large-scale land-based policies have important implications for the remaining carbon budget as they can potentially lower global mean temperatures, while exerting a biogeochemical effect. By taking advantage of factorial simulations, the chapter therefore explored the implications of A/R adopted in a high radiative forcing scenario using seven ESMs, showing a good intermodel agreement in the physical processes driving surface temperature decrease at interannual timescales, namely latent heat fluxes. The research demonstrates on the one hand the stronger cooling associated with A/R adoption in water-limited ecosystems, because of the higher induced evapotranspiration as a consequence of the background water-scarce environment. On the other hand, however, it reveals potential trade-offs associated with an increase of tree-coverage, as the higher latent heat fluxes, conveying moisture from the soils to the lower troposphere, drive a substantial and significant reduction of local water resources. This, as a consequence, can potentially threaten and undermine the long-term sustainability of A/R practices, at least in the context of a high radiative forcing scenario.

The works that constitute this dissertation have tried to clarify the uncertainties surrounding three aspect of the carbon cycle and carbon budget„ with substantial implications from a policy perspective. Nevertheless, improvements can be made in future works. The role of non-CO_2 forcers in overshoot scenarios could be assessed by using more complex models (e.g.

ESMs) able to better represent the atmospheric chemistry and the interactions with other components of the Earth system (Melnikova *et al.*, 2025), as a first example. The research question covered by the second chapter could be further expanded by considering non-linear methods (e.g. Machine Learning algorithms) for estimating the contributions of environmental factors and modes of climate variability (e.g. ENSO, Tropical Atlantic modes) driving carbon fluxes variability, not only for the Amazon basin, but for several tropical wet- and dryland ecosystems as well. Lastly, A/R studies employing ESMs currently suffer from huge uncertainties regarding the different implementations of LUC scenarios and dynamics. Additionally, coarse-resolution models may not be completely realistic in their representation of land-atmosphere interactions due to the necessity of adopting sub-grid parameterizations. With this respect, the usage of high-resolution models, as for example the non-hydrostatic model ICON could enable a better estimation of LUC effects and of the carbon-water coupling (Lee and Hohenegger, 2024).

4 Bibliography

Ackerman, F., DeCanio, S.J., Howarth, R.B. and Sheeran, K. (2009) 'Limitations of integrated assessment models of climate change', *Climatic change*, 95(3), pp. 297–315.

Ahlström, A., Schurgers, G., Arneth, A. and Smith, B. (2012) 'Robustness and uncertainty in terrestrial ecosystem carbon response to CMIP5 climate change projections', *Environmental Research Letters*, 7(4), p. 044008. Available at: https://doi.org/10.1088/1748-9326/7/4/044008.

Alkama, R. and Cescatti, A. (2016) 'Biophysical climate impacts of recent changes in global forest cover', *Science*, 351(6273), pp. 600–604. Available at: https://doi.org/10.1126/science.aac8083.

Allen, M., Tanaka, K., Macey, A., Cain, M., Jenkins, S., Lynch, J. and Smith, M. (2021) 'Ensuring that offsets and other internationally transferred mitigation outcomes contribute effectively to limiting global warming', *Environmental Research Letters*, 16(7), pp. 074009–074009. Available at: https://doi.org/10.1088/1748-9326/ABFCF9.

Allen, M.R., Frame, D.J., Huntingford, C., Jones, C.D., Lowe, J.A., Meinshausen, M. and Meinshausen, N. (2009) 'Warming caused by cumulative carbon emissions towards the trillionth tonne', *Nature*, 458(7242), pp. 1163–1166. Available at: https://doi.org/10.1038/nature08019.

Allen, M.R., Fuglestvedt, J.S., Shine, K.P., Reisinger, A., Pierrehumbert, R.T. and Forster, P.M. (2016) 'New use of global warming potentials to compare cumulative and short-lived climate pollutants', *Nature Climate Change 2016 6:8*, 6(8), pp. 773–776. Available at: https://doi.org/10.1038/nclimate2998.

Allen, M.R., Peters, G.P., Shine, K.P., Azar, C., Balcombe, P., Boucher, O., Cain, M., Ciais, P., Collins, W., Forster, P.M., Frame, D.J., Friedlingstein, P., Fyson, C., Gasser, T., Hare, B., Jenkins, S., Hamburg, S.P., Johansson, D.J.A., Lynch, J., Macey, A., Morfeldt, J., Nauels, A., Ocko, I., Oppenheimer, M., Pacala, S.W., Pierrehumbert, R., Rogelj, J., Schaeffer, M., Schleussner, C.F., Shindell, D., Skeie, R.B., Smith, S.M. and Tanaka, K. (2022) 'Indicate separate contributions of long-lived and short-lived greenhouse gases in emission targets', *npj Climate and*

Atmospheric Science 2022 5:1, 5(1), pp. 1–4. Available at: https://doi.org/10.1038/s41612-021-00226-2.

Allen, M.R., Shine, K.P., Fuglestvedt, J.S., Millar, R.J., Cain, M., Frame, D.J. and Macey, A.H. (2018) 'A solution to the misrepresentations of CO2-equivalent emissions of short-lived climate pollutants under ambitious mitigation', *npj Climate and Atmospheric Science 2018 1:1*, 1(1), pp. 1–8. Available at: https://doi.org/10.1038/s41612-018-0026-8.

Archer, D., Eby, M., Brovkin, V., Ridgwell, A., Cao, L., Mikolajewicz, U., Caldeira, K., Matsumoto, K., Munhoven, G., Montenegro, A. and Tokos, K. (2009) 'Atmospheric Lifetime of Fossil Fuel Carbon Dioxide', *Annual Review of Earth and Planetary Sciences*, 37(1), pp. 117–134. Available at: https://doi.org/10.1146/annurev.earth.031208.100206.

Baker, J.C.A., Garcia-Carreras, L., Gloor, M., Marsham, J.H., Buermann, W., da Rocha, H.R., Nobre, A.D., de Araujo, A.C. and Spracklen, D.V. (2021) 'Evapotranspiration in the Amazon: spatial patterns, seasonality, and recent trends in observations, reanalysis, and climate models', *Hydrology and Earth System Sciences*, 25(4), pp. 2279–2300. Available at: https://doi.org/10.5194/hess-25-2279-2021.

Ballantyne, A.P., Alden, C.B., Miller, J.B., Tans, P.P. and White, J.W.C. (2012) 'Increase in observed net carbon dioxide uptake by land and oceans during the past 50 years', *Nature*, 488(7409), pp. 70–72. Available at: https://doi.org/10.1038/nature11299.

Bastos, A., Friedlingstein, P., Sitch, S., Chen, C., Mialon, A., Wigneron, J.P., Arora, V.K., Briggs, P.R., Canadell, J.G., Ciais, P., Chevallier, F., Cheng, L., Delire, C., Haverd, V., Jain, A.K., Joos, F., Kato, E., Lienert, S., Lombardozzi, D., Melton, J.R., Myneni, R., Nabel, J.E.M.S., Pongratz, J., Poulter, B., Rödenbeck, C., Séférian, R., Tian, H., Van Eck, C., Viovy, N., Vuichard, N., Walker, A.P., Wiltshire, A., Yang, J., Zaehle, S., Zeng, N. and Zhu, D. (2018) 'Impact of the 2015/2016 El Niño on the terrestrial carbon cycle constrained by bottom-up and top-down approaches', *Philosophical Transactions of the Royal Society B: Biological Sciences*, 373(1760). Available at: https://doi.org/10.1098/RSTB.2017.0304.

Beobide-Arsuaga, G., Bayr, T., Reintges, A. and Latif, · Mojib (2021) 'Uncertainty of ENSO-amplitude projections in CMIP5 and CMIP6 models', *Climate Dynamics*, 56, pp. 3875–3888. Available at: https://doi.org/10.1007/s00382-021-05673-4.

Berner, J., Christensen, H.M. and Sardeshmukh, P.D. (2020) 'Does ENSO Regularity Increase in a Warming Climate?', *Journal of Climate*, 33(4), pp. 1247–1259. Available at: https://doi.org/10.1175/JCLI-D-19-0545.1.

Betts, R.A., Burton, C.A., Feely, R.A., Collins, M., Jones, C.D. and Wiltshire, A.J. (2020) 'ENSO and the Carbon Cycle', in *El Niño Southern Oscillation in a Changing Climate*. American Geophysical Union (AGU), pp. 453–470. Available at: https://doi.org/10.1002/9781119548164.ch20.

Boer, G.J. and Arora, V. (2009) 'Temperature and concentration feedbacks in the carbon cycle', *Geophysical Research Letters*, 36(2).

Bossy, T., Gasser, T., Tanaka, K. and Ciais, P. (2024) 'On the chances of staying below the 1.5°C warming target', *Cell Reports Sustainability*, 0(0). Available at: https://doi.org/10.1016/j.crsus.2024.100127.

Boucher, O., Servonnat, J., Albright, A.L., Aumont, O., Balkanski, Y., Bastrikov, V., Bekki, S., Bonnet, R., Bony, S. and Bopp, L. (2020) 'Presentation and evaluation of the IPSL-CM6A-LR climate model', *Journal of Advances in Modeling Earth Systems*, 12(7), p. e2019MS002010.

Boysen, L.R., Brovkin, V., Arora, V.K., Cadule, P., de Noblet-Ducoudré, N., Kato, E., Pongratz, J. and Gayler, V. (2014) 'Global and regional effects of land-use change on climate in 21st century simulations with interactive carbon cycle', *Earth System Dynamics*, 5(2), pp. 309–319.

Boysen, L.R., Brovkin, V., Pongratz, J., Lawrence, D.M., Lawrence, P., Vuichard, N., Peylin, P., Liddicoat, S., Hajima, T., Zhang, Y., Rocher, M., Delire, C., Séférian, R., Arora, V.K., Nieradzik, L., Anthoni, P., Thiery, W., Laguë, M.M., Lawrence, D. and Lo, M.H. (2020) 'Global climate response to idealized deforestation in CMIP6 models', *Biogeosciences*, 17(22), pp. 5615–5638. Available at: https://doi.org/10.5194/BG-17-5615-2020.

Brienen, R.J.W., Phillips, O.L., Feldpausch, T.R., Gloor, E., Baker, T.R., Lloyd, J., Lopez-Gonzalez, G., Monteagudo-Mendoza, A., Malhi, Y., Lewis, S.L., Vásquez Martinez, R., Alexiades, M., Álvarez Dávila, E., Alvarez-Loayza, P., Andrade, A.,

Aragaõ, L.E.O.C., Araujo-Murakami, A., Arets, E.J.M.M., Arroyo, L., Aymard C., G.A., Bánki, O.S., Baraloto, C., Barroso, J., Bonal, D., Boot, R.G.A., Camargo, J.L.C., Castilho, C.V., Chama, V., Chao, K.J., Chave, J., Comiskey, J.A., Cornejo Valverde, F., Da Costa, L., De Oliveira, E.A., Di Fiore, A., Erwin, T.L., Fauset, S., Forsthofer, M., Galbraith, D.R., Grahame, E.S., Groot, N., Hérault, B., Higuchi, N., Honorio Coronado, E.N., Keeling, H., Killeen, T.J., Laurance, W.F., Laurance, S., Licona, J., Magnussen, W.E., Marimon, B.S., Marimon-Junior, B.H., Mendoza, C., Neill, D.A., Nogueira, E.M., Núñez, P., Pallqui Camacho, N.C., Parada, A., Pardo-Molina, G., Peacock, J., Penã-Claros, M., Pickavance, G.C., Pitman, N.C.A., Poorter, L., Prieto, A., Quesada, C.A., Ramírez, F., Ramírez-Angulo, H., Restrepo, Z., Roopsind, A., Rudas, A., Salomaõ, R.P., Schwarz, M., Silva, N., Silva-Espejo, J.E., Silveira, M., Stropp, J., Talbot, J., Ter Steege, H., Teran-Aguilar, J., Terborgh, J., Thomas-Caesar, R., Toledo, M., Torello-Raventos, M., Umetsu, R.K., Van Der Heijden, G.M.F., Van Der Hout, P., Guimarães Vieira, I.C., Vieira, S.A., Vilanova, E., Vos, V.A. and Zagt, R.J. (2015) 'Long-term decline of the Amazon carbon sink', *Nature 2015 519:7543*, 519(7543), pp. 344–348. Available at: https://doi.org/10.1038/nature14283.

Bright, R.M., Davin, E., O'Halloran, T., Pongratz, J., Zhao, K. and Cescatti, A. (2017) 'Local temperature response to land cover and management change driven by non-radiative processes', *Nature Climate Change*, 7(4), pp. 296–302. Available at: https://doi.org/10.1038/nclimate3250.

Brovkin, V., Boysen, L., Arora, V.K., Boisier, J.P., Cadule, P., Chini, L., Claussen, M., Friedlingstein, P., Gayler, V. and Van Den Hurk, B. (2013) 'Effect of anthropogenic land-use and land-cover changes on climate and land carbon storage in CMIP5 projections for the twenty-first century', *Journal of Climate*, 26(18), pp. 6859–6881.

Brown, J.R., Brierley, C.M., An, S.I., Guarino, M.V., Stevenson, S., Williams, C.J.R., Zhang, Q., Zhao, A., Abe-Ouchi, A., Braconnot, P., Brady, E.C., Chandan, D., D'Agostino, R., Guo, C., Legrande, A.N., Lohmann, G., Morozova, P.A., Ohgaito, R., O'Ishi, R., Otto-Bliesner, B.L., Richard Peltier, W., Shi, X., Sime, L., Volodin, E.M., Zhang, Z. and Zheng, W. (2020) 'Comparison of past and future simulations of ENSO in CMIP5/PMIP3 and CMIP6/PMIP4 models', *Climate of the Past*, 16(5), pp. 1777–1805. Available at: https://doi.org/10.5194/CP-16-1777-2020.

Cai, W., Borlace, S., Lengaigne, M., Van Rensch, P., Collins, M., Vecchi, G., Timmermann, A., Santoso, A., Mcphaden, M.J., Wu, L., England, M.H., Wang, G.,

Guilyardi, E. and Jin, F.F. (2014) 'Increasing frequency of extreme El Niño events due to greenhouse warming', *Nature Climate Change 2014 4:2*, 4(2), pp. 111–116. Available at: https://doi.org/10.1038/nclimate2100.

Cai, W., McPhaden, M.J., Grimm, A.M., Rodrigues, R.R., Taschetto, A.S., Garreaud, R.D., Dewitte, B., Poveda, G., Ham, Y.G., Santoso, A., Ng, B., Anderson, W., Wang, G., Geng, T., Jo, H.S., Marengo, J.A., Alves, L.M., Osman, M., Li, S., Wu, L., Karamperidou, C., Takahashi, K. and Vera, C. (2020) 'Climate impacts of the El Niño–Southern Oscillation on South America', *Nature Reviews Earth and Environment*, 1(4), pp. 215–231. Available at: https://doi.org/10.1038/s43017-020-0040-3.

Cai, W., Ng, B., Wang, G., Santoso, A., Wu, L. and Yang, K. (2022) 'Increased ENSO sea surface temperature variability under four IPCC emission scenarios', *Nature Climate Change 2022 12:3*, 12(3), pp. 228–231. Available at: https://doi.org/10.1038/s41558-022-01282-z.

Cai, W., Santoso, A., Collins, M., Dewitte, B., Karamperidou, C., Kug, J.S., Lengaigne, M., McPhaden, M.J., Stuecker, M.F., Taschetto, A.S., Timmermann, A., Wu, L., Yeh, S.W., Wang, G., Ng, B., Jia, F., Yang, Y., Ying, J., Zheng, X.T., Bayr, T., Brown, J.R., Capotondi, A., Cobb, K.M., Gan, B., Geng, T., Ham, Y.G., Jin, F.F., Jo, H.S., Li, X., Lin, X., McGregor, S., Park, J.H., Stein, K., Yang, K., Zhang, L. and Zhong, W. (2021) 'Changing El Niño–Southern Oscillation in a warming climate', *Nature Reviews Earth and Environment*, 2(9), pp. 628–644. Available at: https://doi.org/10.1038/s43017-021-00199-z.

Cai, W., Wang, G., Santoso, A., Mcphaden, M.J., Wu, L., Jin, F.-F., Timmermann, A., Vecchi, G., Lengaigne, M., England, M.H., Dommenget, D., Takahashi, K. and Guilyardi, E. (2015) 'Increased frequency of extreme La Niña events under greenhouse warming', pp. 26–26. Available at: https://doi.org/10.1038/NCLIMATE2492.

Cain, M., Lynch, J., Allen, M.R., Fuglestvedt, J.S., Frame, D.J. and Macey, A.H. (2019) 'Improved calculation of warming-equivalent emissions for short-lived climate pollutants', *npj Climate and Atmospheric Science 2019 2:1*, 2(1), pp. 1–7. Available at: https://doi.org/10.1038/s41612-019-0086-4.

Canadell, J.G., Monteiro, P.M., Costa, M.H., Da Cunha, L.C., Cox, P.M., Alexey, V., Henson, S., Ishii, M., Jaccard, S. and Koven, C. (2021) 'Global carbon and other

biogeochemical cycles and feedbacks', in *Climate Change 2021: The Physical Science Basis. Contribution of Working Group I to the Sixth Assessment Report of the Intergovernmental Panel on Climate Change*. Cambridge, United Kingdom and New York, NY, USA: Cambridge University Press, pp. 673–816.

Canadell, J.G., Monteiro, P.M.S., Costa, M.H., Cunha, L.C.D., Cox, P.M., Eliseev, A.V., Henson, S., Ishii, M., Jaccard, S., Koven, C., Lohila, A., Patra, P.K., Piao, S., Syampungani, S., Zaehle, S., Zickfeld, K., Alexandrov, G.A., Bala, G., Bopp, L., Boysen, L., Cao, L., Chandra, N., Ciais, P., Denisov, S.N., Dentener, F.J., Douville, H., Fay, A., Forster, P., Fox-Kemper, B., Friedlingstein, P., Fu, W., Fuss, S., Garçon, V., Gier, B., Gillett, N.P., Gregor, L., Haustein, K., Haverd, V., He, J., Hewitt, H.T., Hoffman, F.M., Ilyina, T., Jackson, R., Jones, C., Keller, D.P., Kwiatkowski, L., Lamboll, R.D., Lan, X., Laufkötter, C., Quéré, C.L., Lenton, A., Lewis, J., Liddicoat, S., Lorenzoni, L., Lovenduski, N., Macdougall, A.H., Mathesius, S., Matthews, D.H., Meinshausen, M., Mokhov, I.I., Naik, V., Nicholls, Z.R.J., Nurhati, I.S., O'sullivan, M., Peters, G., Pongratz, J., Poulter, B., Sallée, J.-B., Saunois, M., Schuur, E.A.G., Seneviratne, S.I., Stavert, A., Suntharalingam, P., Tachiiri, K., Terhaar, J., Thompson, R., Tian, H., Turnbull, J., Vicente-Serrano, S.M., Wang, X., Wanninkhof, R.H., Williamson, P., Brovkin, V., Feely, R.A. and Lebehot, A.D. (2022) 'Global Carbon and other Biogeochemical Cycles and Feedbacks'.

Chen, C., Li, D., Li, Y., Piao, S., Wang, X., Huang, M., Gentine, P., Nemani, R.R. and Myneni, R.B. (2020) 'Biophysical impacts of Earth greening largely controlled by aerodynamic resistance', *Science Advances*, 6(47), p. eabb1981. Available at: https://doi.org/10.1126/sciadv.abb1981.

Chen, L. and Dirmeyer, P.A. (2016) 'Adapting observationally based metrics of biogeophysical feedbacks from land cover/land use change to climate modeling', *Environmental Research Letters*, 11(3), p. 034002. Available at: https://doi.org/10.1088/1748-9326/11/3/034002.

Chen, L. and Dirmeyer, P.A. (2020) 'Reconciling the disagreement between observed and simulated temperature responses to deforestation', *Nature Communications*, 11(1), p. 202. Available at: https://doi.org/10.1038/s41467-019-14017-0.

Chen, L., Li, T., Yu, Y. and Behera, S.K. (2017) 'A possible explanation for the divergent projection of ENSO amplitude change under global warming', *Climate*

Dynamics 2017 49:11, 49(11), pp. 3799–3811. Available at: https://doi.org/10.1007/S00382-017-3544-X.

Chen, Z., Wang, W., Cescatti, A. and Forzieri, G. (2023) 'Climate-driven vegetation greening further reduces water availability in drylands', *Global Change Biology*, 29(6), pp. 1628–1647. Available at: https://doi.org/10.1111/gcb.16561.

Cherubini, F., Fuglestvedt, J., Gasser, T., Reisinger, A., Cavalett, O., Huijbregts, M.A., Johansson, D.J., Jørgensen, S.V., Raugei, M. and Schivley, G. (2016) 'Bridging the gap between impact assessment methods and climate science', *Environmental Science & Policy*, 64, pp. 129–140.

Claussen, M., Brovkin, V. and Ganopolski, A. (2001) 'Biogeophysical versus biogeochemical feedbacks of large-scale land cover change', *Geophysical research letters*, 28(6), pp. 1011–1014.

Copernicus Climate Change Service (C3S) (2017) 'ERA5: Fifth generation of ECMWF atmospheric reanalyses of the global climate'. https://cds.climate.copernicus.eu/cdsapp#!/home: Copernicus Climate Change Service Climate Data Store (CDS).

Damon Matthews, H., Tokarska, K.B., Rogelj, J., Smith, C.J., MacDougall, A.H., Haustein, K., Mengis, N., Sippel, S., Forster, P.M. and Knutti, R. (2021) 'An integrated approach to quantifying uncertainties in the remaining carbon budget', *Communications Earth & Environment*, 2(1). Available at: https://doi.org/10.1038/s43247-020-00064-9.

Danabasoglu, G., Lamarque, J.-F., Bacmeister, J., Bailey, D.A., DuVivier, A.K., Edwards, J., Emmons, L.K., Fasullo, J., Garcia, R. and Gettelman, A. (2020) 'The community earth system model version 2 (CESM2)', *Journal of Advances in Modeling Earth Systems*, 12(2), p. e2019MS001916.

Davidson, E.A., de Araújo, A.C., Artaxo, P., Balch, J.K., Brown, I.F., C. Bustamante, M.M., Coe, M.T., DeFries, R.S., Keller, M., Longo, M., Munger, J.W., Schroeder, W., Soares-Filho, B.S., Souza, C.M. and Wofsy, S.C. (2012) 'The Amazon basin in transition', *Nature*, 481(7381), pp. 321–328. Available at: https://doi.org/10.1038/nature10717.

Davies-Barnard, T., Valdes, P.J., Singarayer, J.S., Pacifico, F.M. and Jones, C.D. (2014) 'Full effects of land use change in the representative concentration pathways', *Environmental Research Letters*, 9(11), p. 114014.

Davin, E.L. and Noblet-Ducoudré, N. de (2010) 'Climatic Impact of Global-Scale Deforestation: Radiative versus Nonradiative Processes', *Journal of Climate*, 23(1), pp. 97–112. Available at: https://doi.org/10.1175/2009JCLI3102.1.

De Hertog, S.J., Havermann, F., Vanderkelen, I., Guo, S., Luo, F., Manola, I., Coumou, D., Davin, E.L., Duveiller, G. and Lejeune, Q. (2022) 'The biogeophysical effects of idealized land cover and land management changes in Earth system models', *Earth system dynamics*, 13(3), pp. 1305–1350.

Dhakal, S., Minx, J.C., Toth, F.L., Abdel-Aziz, A., Figueroa, M.J., Hubacek, K., Jonckheere, I.G., Yong-gun, K., Nemet, G. and Pachauri, S. (2022) 'Emissions Trends and Drivers', in *Climate Change 2022: Mitigation of Climate Change*. IPCC: Intergovernmental Panel on Climate Change.

Duveiller, G., Caporaso, L., Abad-Viñas, R., Perugini, L., Grassi, G., Arneth, A. and Cescatti, A. (2020) 'Local biophysical effects of land use and land cover change: towards an assessment tool for policy makers', *Land Use Policy*, 91, p. 104382.

Eby, M., Zickfeld, K., Montenegro, A., Archer, D., Meissner, K.J. and Weaver, A.J. (2009) 'Lifetime of Anthropogenic Climate Change: Millennial Time Scales of Potential CO2 and Surface Temperature Perturbations', *Journal of Climate*, 22(10), pp. 2501–2511. Available at: https://doi.org/10.1175/2008JCLI2554.1.

Emmerling, J., Drouet, L., Wijst, K.-I. van der, Vuuren, D. van, Bosetti, V. and Tavoni, M. (2019) 'The role of the discount rate for emission pathways and negative emissions', *Environmental Research Letters*, 14(10), p. 104008. Available at: https://doi.org/10.1088/1748-9326/ab3cc9.

Erb, K.-H., Luyssaert, S., Meyfroidt, P., Pongratz, J., Don, A., Kloster, S., Kuemmerle, T., Fetzel, T., Fuchs, R., Herold, M., Haberl, H., Jones, C.D., Marín-Spiotta, E., McCallum, I., Robertson, E., Seufert, V., Fritz, S., Valade, A., Wiltshire, A. and Dolman, A.J. (2017) 'Land management: data availability and process understanding for global change studies', *Global Change Biology*, 23(2), pp. 512–533. Available at: https://doi.org/10.1111/gcb.13443.

Eyring, V., Bony, S., Meehl, G.A., Senior, C.A., Stevens, B., Stouffer, R.J. and Taylor, K.E. (2016) 'Overview of the Coupled Model Intercomparison Project Phase 6 (CMIP6) experimental design and organization', *Geosci. Model Dev.*, 9(5), pp. 1937–1958. Available at: https://doi.org/10.5194/gmd-9-1937-2016.

Fleischer, K., Rammig, A., De Kauwe, M.G., Walker, A.P., Domingues, T.F., Fuchslueger, L., Garcia, S., Goll, D.S., Grandis, A. and Jiang, M. (2019) 'Amazon forest response to CO2 fertilization dependent on plant phosphorus acquisition', *Nature Geoscience*, 12(9), pp. 736–741.

Forster, P., Storelvmo, T., Armour, K., Collins, W., Dufresne, J.-L., Frame, D., Lunt, D., Mauritsen, T., Palmer, M. and Watanabe, M. (2021) 'The Earth's energy budget, climate feedbacks, and climate sensitivity', in *Climate Change 2021: The Physical Science Basis. Contribution of Working Group I to the Sixth Assessment Report of the Intergovernmental Panel on Climate Change*. Cambridge, United Kingdom and New York, NY, USA: Cambridge University Press, pp. 923–1054.

Forzieri, G., Miralles, D.G., Ciais, P., Alkama, R., Ryu, Y., Duveiller, G., Zhang, K., Robertson, E., Kautz, M., Martens, B., Jiang, C., Arneth, A., Georgievski, G., Li, W., Ceccherini, G., Anthoni, P., Lawrence, P., Wiltshire, A., Pongratz, J., Piao, S., Sitch, S., Goll, D.S., Arora, V.K., Lienert, S., Lombardozzi, D., Kato, E., Nabel, J.E.M.S., Tian, H., Friedlingstein, P. and Cescatti, A. (2020) 'Increased control of vegetation on global terrestrial energy fluxes', *Nature Climate Change*, 10(4), pp. 356–362. Available at: https://doi.org/10.1038/s41558-020-0717-0.

Fredriksen, H.B., Berner, J., Subramanian, A.C. and Capotondi, A. (2020) 'How Does El Niño–Southern Oscillation Change Under Global Warming—A First Look at CMIP6', *Geophysical Research Letters*, 47(22), p. e2020GL090640-e2020GL090640. Available at: https://doi.org/10.1029/2020GL090640.

Friedlingstein, P., Cox, P., Betts, R., Bopp, L., von Bloh, W., Brovkin, V., Cadule, P., Doney, S., Eby, M. and Fung, I. (2006) 'Climate–carbon cycle feedback analysis: results from the C4MIP model intercomparison', *Journal of climate*, 19(14), pp. 3337–3353.

Friedlingstein, P., Jones, M.W., O'Sullivan, M., Andrew, R.M., Bakker, D.C.E., Hauck, J., Le Quéré, C., Peters, G.P., Peters, W., Pongratz, J., Sitch, S., Canadell, J.G., Ciais, P., Jackson, R.B., Alin, S.R., Anthoni, P., Bates, N.R., Becker, M., Bellouin, N., Bopp, L., Chau, T.T.T., Chevallier, F., Chini, L.P., Cronin, M., Currie,

K.I., Decharme, B., Djeutchouang, L.M., Dou, X., Evans, W., Feely, R.A., Feng, L., Gasser, T., Gilfillan, D., Gkritzalis, T., Grassi, G., Gregor, L., Gruber, N., Gürses, Ö., Harris, I., Houghton, R.A., Hurtt, G.C., Iida, Y., Ilyina, T., Luijkx, I.T., Jain, A., Jones, S.D., Kato, E., Kennedy, D., Klein Goldewijk, K., Knauer, J., Korsbakken, J.I., Körtzinger, A., Landschützer, P., Lauvset, S.K., Lefèvre, N., Lienert, S., Liu, J., Marland, G., McGuire, P.C., Melton, J.R., Munro, D.R., Nabel, J.E.M.S., Nakaoka, S.-I., Niwa, Y., Ono, T., Pierrot, D., Poulter, B., Rehder, G., Resplandy, L., Robertson, E., Rödenbeck, C., Rosan, T.M., Schwinger, J., Schwingshackl, C., Séférian, R., Sutton, A.J., Sweeney, C., Tanhua, T., Tans, P.P., Tian, H., Tilbrook, B., Tubiello, F., van der Werf, G.R., Vuichard, N., Wada, C., Wanninkhof, R., Watson, A.J., Willis, D., Wiltshire, A.J., Yuan, W., Yue, C., Yue, X., Zaehle, S. and Zeng, J. (2021) 'Global Carbon Budget 2021', *Earth System Science Data*, 14(4), pp. 1917–2005. Available at: https://doi.org/10.5194/ESSD-14-1917-2022.

Friedlingstein, P., O'Sullivan, M., Jones, M.W., Andrew, R.M., Bakker, D.C.E., Hauck, J., Landschützer, P., Le Quéré, C., Luijkx, I.T., Peters, G.P., Peters, W., Pongratz, J., Schwingshackl, C., Sitch, S., Canadell, J.G., Ciais, P., Jackson, R.B., Alin, S.R., Anthoni, P., Barbero, L., Bates, N.R., Becker, M., Bellouin, N., Decharme, B., Bopp, L., Brasika, I.B.M., Cadule, P., Chamberlain, M.A., Chandra, N., Chau, T.-T.-T., Chevallier, F., Chini, L.P., Cronin, M., Dou, X., Enyo, K., Evans, W., Falk, S., Feely, R.A., Feng, L., Ford, D.J., Gasser, T., Ghattas, J., Gkritzalis, T., Grassi, G., Gregor, L., Gruber, N., Gürses, Ö., Harris, I., Hefner, M., Heinke, J., Houghton, R.A., Hurtt, G.C., Iida, Y., Ilyina, T., Jacobson, A.R., Jain, A., Jarníková, T., Jersild, A., Jiang, F., Jin, Z., Joos, F., Kato, E., Keeling, R.F., Kennedy, D., Klein Goldewijk, K., Knauer, J., Korsbakken, J.I., Körtzinger, A., Lan, X., Lefèvre, N., Li, H., Liu, J., Liu, Z., Ma, L., Marland, G., Mayot, N., McGuire, P.C., McKinley, G.A., Meyer, G., Morgan, E.J., Munro, D.R., Nakaoka, S.-I., Niwa, Y., O'Brien, K.M., Olsen, A., Omar, A.M., Ono, T., Paulsen, M., Pierrot, D., Pocock, K., Poulter, B., Powis, C.M., Rehder, G., Resplandy, L., Robertson, E., Rödenbeck, C., Rosan, T.M., Schwinger, J., Séférian, R., Smallman, T.L., Smith, S.M., Sospedra-Alfonso, R., Sun, Q., Sutton, A.J., Sweeney, C., Takao, S., Tans, P.P., Tian, H., Tilbrook, B., Tsujino, H., Tubiello, F., van der Werf, G.R., van Ooijen, E., Wanninkhof, R., Watanabe, M., Wimart-Rousseau, C., Yang, D., Yang, X., Yuan, W., Yue, X., Zaehle, S., Zeng, J. and Zheng, B. (2023) 'Global Carbon Budget 2023', *Earth System Science Data*, 15(12), pp. 5301–5369. Available at: https://doi.org/10.5194/essd-15-5301-2023.

Fuglestvedt, J.S., Berntsen, T.K., Godal, O., Sausen, R., Shine, K.P. and Skodvin, T. (2003) 'Metrics of Climate Change: Assessing Radiative Forcing and Emission Indices', *Climatic Change*, 58(3), pp. 267–331. Available at: https://doi.org/10.1023/A:1023905326842.

Fujimori, S., Hasegawa, T., Masui, T. and Takahashi, K. (2014) 'Land use representation in a global CGE model for long-term simulation: CET vs. logit functions', *Food Security*, 6(5), pp. 685–699. Available at: https://doi.org/10.1007/s12571-014-0375-z.

Gao, Q., Wang, G., Xue, K., Yang, Y., Xie, J., Yu, H., Bai, S., Liu, F., He, Z. and Ning, D. (2020) 'Stimulation of soil respiration by elevated CO2 is enhanced under nitrogen limitation in a decade-long grassland study', *Proceedings of the National Academy of Sciences*, 117(52), pp. 33317–33324.

Gentine, P., Green, J.K., Guérin, M., Humphrey, V., Seneviratne, S.I., Zhang, Y. and Zhou, S. (2019) 'Coupling between the terrestrial carbon and water cycles—a review', *Environmental Research Letters*, 14(8), pp. 083003–083003. Available at: https://doi.org/10.1088/1748-9326/AB22D6.

Grant, L., Gudmundsson, L., Davin, E.L., Lawrence, D.M., Vuichard, N., Robertson, E., Séférian, R., Ribes, A., Hirsch, A.L. and Thiery, W. (2023) 'Biogeophysical Effects of Land-Use and Land-Cover Change Not Detectable in Warmest Month', *Journal of Climate*, 36(6), pp. 1845–1861. Available at: https://doi.org/10.1175/JCLI-D-22-0391.1.

Grassi, G., House, J., Dentener, F., Federici, S., den Elzen, M. and Penman, J. (2017) 'The key role of forests in meeting climate targets requires science for credible mitigation', *Nature Climate Change*, 7(3), pp. 220–226. Available at: https://doi.org/10.1038/nclimate3227.

Green, J.K., Seneviratne, S.I., Berg, A.M., Findell, K.L., Hagemann, S., Lawrence, D.M. and Gentine, P. (2019) 'Large influence of soil moisture on long-term terrestrial carbon uptake', *Nature 2019 565:7740*, 565(7740), pp. 476–479. Available at: https://doi.org/10.1038/s41586-018-0848-x.

Gregory, J.M., Jones, C.D., Cadule, P. and Friedlingstein, P. (2009) 'Quantifying carbon cycle feedbacks', *Journal of Climate*, 22(19), pp. 5232–5250.

Guenet, B., Orliac, J., Cécillon, L., Torres, O., Sereni, L., Martin, P.A., Barré, P. and Bopp, L. (2024) 'Spatial biases reduce the ability of Earth system models to simulate soil heterotrophic respiration fluxes', *Biogeosciences*, 21(2), pp. 657–669. Available at: https://doi.org/10.5194/bg-21-657-2024.

Hajima, T., Watanabe, M., Yamamoto, A., Tatebe, H., Noguchi, M.A., Abe, M., Ohgaito, R., Ito, A., Yamazaki, D. and Okajima, H. (2020) 'Development of the MIROC-ES2L Earth system model and the evaluation of biogeochemical processes and feedbacks', *Geoscientific Model Development*, 13(5), pp. 2197–2244.

Hersbach, H., Bell, B., Berrisford, P., Hirahara, S., Horányi, A., Muñoz-Sabater, J., Nicolas, J., Peubey, C., Radu, R. and Schepers, D. (2020) 'The ERA5 global reanalysis', *Quarterly Journal of the Royal Meteorological Society*, 146(730), pp. 1999–2049.

Hong, C., Burney, J.A., Pongratz, J., Nabel, J.E., Mueller, N.D., Jackson, R.B. and Davis, S.J. (2021) 'Global and regional drivers of land-use emissions in 1961–2017', *Nature*, 589(7843), pp. 554–561.

Hong, T., Wu, J., Kang, X., Yuan, M. and Duan, L. (2022) 'Impacts of Different Land Use Scenarios on Future Global and Regional Climate Extremes', *Atmosphere*, 13(6), p. 995.

Hubau, W., Lewis, S.L., Phillips, O.L., Affum-Baffoe, K., Beeckman, H., Cuní-Sanchez, A., Daniels, A.K., Ewango, C.E., Fauset, S. and Mukinzi, J.M. (2020) 'Asynchronous carbon sink saturation in African and Amazonian tropical forests', *Nature*, 579(7797), pp. 80–87.

Huete, A.R., Didan, K., Shimabukuro, Y.E., Ratana, P., Saleska, S.R., Hutyra, L.R., Yang, W., Nemani, R.R. and Myneni, R. (2006) 'Amazon rainforests green-up with sunlight in dry season', *Geophysical Research Letters*, 33(6). Available at: https://doi.org/10.1029/2005GL025583.

Humphrey, V., Zscheischler, J., Ciais, P., Gudmundsson, L., Sitch, S. and Seneviratne, S.I. (2018) 'Sensitivity of atmospheric CO2 growth rate to observed changes in terrestrial water storage', *Nature*, 560(7720), pp. 628–631.

Huntingford, C., Zelazowski, P., Galbraith, D., Mercado, L.M., Sitch, S., Fisher, R., Lomas, M., Walker, A.P., Jones, C.D. and Booth, B.B. (2013) 'Simulated resilience

of tropical rainforests to CO2-induced climate change', *Nature Geoscience*, 6(4), pp. 268–273.

Huntzinger, D.N., Michalak, A.M., Schwalm, C., Ciais, P., King, A.W., Fang, Y., Schaefer, K., Wei, Y., Cook, R.B., Fisher, J.B., Hayes, D., Huang, M., Ito, A., Jain, A.K., Lei, H., Lu, C., Maignan, F., Mao, J., Parazoo, N., Peng, S., Poulter, B., Ricciuto, D., Shi, X., Tian, H., Wang, W., Zeng, N. and Zhao, F. (2017) 'Uncertainty in the response of terrestrial carbon sink to environmental drivers undermines carbon-climate feedback predictions', *Scientific Reports*, 7(1), p. 4765. Available at: https://doi.org/10.1038/s41598-017-03818-2.

Hurtt, G.C., Chini, L., Sahajpal, R., Frolking, S., Bodirsky, B.L., Calvin, K., Doelman, J.C., Fisk, J., Fujimori, S., Klein Goldewijk, K., Hasegawa, T., Havlik, P., Heinimann, A., Humpenöder, F., Jungclaus, J., Kaplan, J.O., Kennedy, J., Krisztin, T., Lawrence, D., Lawrence, P., Ma, L., Mertz, O., Pongratz, J., Popp, A., Poulter, B., Riahi, K., Shevliakova, E., Stehfest, E., Thornton, P., Tubiello, F.N., van Vuuren, D.P. and Zhang, X. (2020) 'Harmonization of global land use change and management for the period 850–2100 (LUH2) for CMIP6', *Geoscientific Model Development*, 13(11), pp. 5425–5464. Available at: https://doi.org/10.5194/gmd-13-5425-2020.

INPE, N.I.F.S.RESEARCH.E.O.G.C. (2019) 'MONITORING PROGRAM OF THE AMAZON AND OTHER BIOMES.' Available at: http://terrabrasilis.dpi.inpe.br/downloads/. (Accessed: 5 January 2019).

Jenkins, S., Cain, M., Friedlingstein, P., Gillett, N., Walsh, T. and Allen, M.R. (2021) 'Quantifying non-CO2 contributions to remaining carbon budgets', *npj Climate and Atmospheric Science*, 4(1). Available at: https://doi.org/10.1038/s41612-021-00203-9.

Jenkins, S., Millar, R.J., Leach, N. and Allen, M.R. (2018) 'Framing Climate Goals in Terms of Cumulative CO2-Forcing-Equivalent Emissions', *Geophysical Research Letters*, 45(6), pp. 2795–2804. Available at: https://doi.org/10.1002/2017GL076173.

Jenkins, S., Sanderson, B., Peters, G., Frölicher, T.L., Friedlingstein, P. and Allen, M. (2022) 'The Multi-Decadal Response to Net Zero CO2 Emissions and Implications for Emissions Policy', *Geophysical Research Letters*, 49(23), p. e2022GL101047. Available at: https://doi.org/10.1029/2022GL101047.

Jia, G., Shevliakova, E., Artaxo, P., De-Docoudré, N., Houghton, R., House, J., Kitajima, K., Lennard, C., Popp, A., Sirin, A., Sukumar, R., Verchot, L. and Sporre, M. (2019) 'Land–Climate interactions', in *Special Report on Climate Change and Land*. IPCC, pp. 133–206.

Jiménez-Muñoz, J.C., Mattar, C., Barichivich, J., Santamaría-Artigas, A., Takahashi, K., Malhi, Y., Sobrino, J.A. and Schrier, G.V.D. (2016) 'Record-breaking warming and extreme drought in the Amazon rainforest during the course of El Niño 2015–2016', *Scientific Reports 2016 6:1*, 6(1), pp. 1–7. Available at: https://doi.org/10.1038/srep33130.

Johansson, D.J.A. (2021) 'The question of overshoot', *Nature Climate Change*, 11(12), pp. 1021–1022. Available at: https://doi.org/10.1038/s41558-021-01229-w.

Jones, C.D., Arora, V., Friedlingstein, P., Bopp, L., Brovkin, V., Dunne, J., Graven, H., Hoffman, F., Ilyina, T., John, J.G., Jung, M., Kawamiya, M., Koven, C., Pongratz, J., Raddatz, T., Randerson, J.T. and Zaehle, S. (2016) 'C4MIP-The Coupled Climate-Carbon Cycle Model Intercomparison Project: experimental protocol for CMIP6', *Geosci. Model Dev*, 9, pp. 2853–2880. Available at: https://doi.org/10.5194/gmd-9-2853-2016.

Jones, C.D., Collins, M., Cox, P.M. and Spall, S.A. (2001) 'The carbon cycle response to ENSO: A coupled climate–carbon cycle model study', *Journal of Climate*, 14(21), pp. 4113–4129.

Jones, C.D., Frölicher, T.L., Koven, C., MacDougall, A.H., Matthews, H.D., Zickfeld, K., Rogelj, J., Tokarska, K.B., Gillett, N.P., Ilyina, T., Meinshausen, M., Mengis, N., Séférian, R., Eby, M. and Burger, F.A. (2019) 'The Zero Emissions Commitment Model Intercomparison Project (ZECMIP) contribution to C4MIP: quantifying committed climate changes following zero carbon emissions', *Geoscientific Model Development*, 12(10), pp. 4375–4385. Available at: https://doi.org/10.5194/gmd-12-4375-2019.

Joos, F., Roth, R., Fuglestvedt, J.S., Peters, G.P., Enting, I.G., Von Bloh, W., Brovkin, V., Burke, E.J., Eby, M., Edwards, N.R., Friedrich, T., Frölicher, T.L., Frölicher, F., Halloran, P.R., Holden, P.B., Jones, C., Kleinen, T., Mackenzie, F., Matsumoto, K., Meinshausen, M., Plattner, G.-K., Reisinger, A., Segschneider, J., Shaffer, G., Steinacher, M., Strassmann, K., Tanaka, K., Timmermann, A. and Weaver, A.J. (2013) 'CO 2 and climate impulse response functions for metric

computation Atmospheric Chemistry and Physics Discussions Carbon dioxide and climate impulse response functions for the computation of greenhouse gas metrics: a multi-model analysis', *Atmos. Chem. Phys. Discuss*, 12. Available at: https://doi.org/10.5194/acpd-12-19799-2012.

Juang, J.-Y., Katul, G., Siqueira, M., Stoy, P. and Novick, K. (2007) 'Separating the effects of albedo from eco-physiological changes on surface temperature along a successional chronosequence in the southeastern United States', *Geophysical Research Letters*, 34(21).

Jung, M., Koirala, S., Weber, U., Ichii, K., Gans, F., Camps-Valls, G., Papale, D., Schwalm, C., Tramontana, G. and Reichstein, M. (2019) 'The FLUXCOM ensemble of global land-atmosphere energy fluxes', *Scientific data*, 6(1), pp. 1–14.

Jung, M., Reichstein, M., Schwalm, C.R., Huntingford, C., Sitch, S., Ahlström, A., Arneth, A., Camps-Valls, G., Ciais, P., Friedlingstein, P., Gans, F., Ichii, K., Jain, A.K., Kato, E., Papale, D., Poulter, B., Raduly, B., Rödenbeck, C., Tramontana, G., Viovy, N., Wang, Y.-P., Weber, U., Zaehle, S. and Zeng, N. (2017) 'Compensatory water effects link yearly global land CO2 sink changes to temperature', *Nature*, 541(7638), pp. 516–520. Available at: https://doi.org/10.1038/nature20780.

Jung, M., Schwalm, C., Migliavacca, M., Walther, S., Camps-Valls, G., Koirala, S., Anthoni, P., Besnard, S., Bodesheim, P., Carvalhais, N., Chevallier, F., Gans, F., Goll, D.S., Haverd, V., Köhler, P., Ichii, K., Jain, A.K., Liu, J., Lombardozzi, D., Nabel, J.E.M.S., Nelson, J.A., O'sullivan, M., Pallandt, M., Papale, D., Peters, W., Pongratz, J., Rödenbeck, C., Sitch, S., Tramontana, G., Walker, A., Weber, U. and Reichstein, M. (2020) 'Scaling carbon fluxes from eddy covariance sites to globe: synthesis and evaluation of the FLUXCOM approach', *Biogeosciences*, 17, pp. 1343–1365. Available at: https://doi.org/10.5194/bg-17-1343-2020.

K. Arora, V., Katavouta, A., Williams, R.G., Jones, C.D., Brovkin, V., Friedlingstein, P., Schwinger, J., Bopp, L., Boucher, O., Cadule, P., Chamberlain, M.A., Christian, J.R., Delire, C., Fisher, A.R.A., Hajima, T., Ilyina, T., Joetzjer, E., Kawamiya, M., Koven, C.D., Krasting, J.P., Law, R.M., Lawrence, D.M., Lenton, A., Lindsay, K., Pongratz, J., Raddatz, T., Séférian, R., Tachiiri, K., Tjiputra, J.F., Wiltshire, A., Wu, T. and Ziehn, T. (2020) 'Carbon-concentration and carbon-climate feedbacks in CMIP6 models and their comparison to CMIP5 models',

Biogeosciences, 17(16), pp. 4173–4222. Available at: https://doi.org/10.5194/BG-17-4173-2020.

Keeling, C.D., Piper, S.C., Bacastow, R.B., Wahlen, M., Whorf, T.P., Heimann, M. and Meijer, H.A. (2001) 'Exchanges of Atmospheric CO2 and 13CO2 with the Terrestrial Biosphere and Oceans from 1978 to 2000. I. Global Aspects'. Available at: https://escholarship.org/uc/item/09v319r9 (Accessed: 17 July 2024).

Keller, D.P., Lenton, A., Scott, V., Vaughan, N.E., Bauer, N., Ji, D., Jones, C.D., Kravitz, B., Muri, H. and Zickfeld, K. (2018) 'The Carbon Dioxide Removal Model Intercomparison Project (CDRMIP): Rationale and experimental protocol for CMIP6', *Geoscientific Model Development*, 11(3), pp. 1133–1160. Available at: https://doi.org/10.5194/GMD-11-1133-2018.

Kim, J.-S., Kug, J.-S. and Jeong, S.-J. (2017) 'Intensification of terrestrial carbon cycle related to El Niño–Southern Oscillation under greenhouse warming', *Nature Communications 2017 8:1*, 8(1), pp. 1–8. Available at: https://doi.org/10.1038/s41467-017-01831-7.

Kim, J.-S., Kug, J.-S., Yoon, J.-H. and Jeong, S.-J. (2016) 'Increased Atmospheric CO2 Growth Rate during El Niño Driven by Reduced Terrestrial Productivity in the CMIP5 ESMs', *Journal of Climate*, 29(24), pp. 8783–8805. Available at: https://doi.org/10.1175/JCLI-D-14-00672.1.

King, J.A., Weber, J., Lawrence, P., Roe, S., Swann, A.L.S. and Val Martin, M. (2024) 'Global and regional hydrological impacts of global forest expansion', *Biogeosciences*, 21(17), pp. 3883–3902. Available at: https://doi.org/10.5194/bg-21-3883-2024.

Koch, A., Brierley, C. and L. Lewis, S. (2021) 'Effects of Earth system feedbacks on the potential mitigation of large-scale tropical forest restoration', *Biogeosciences*, 18(8), pp. 2627–2647. Available at: https://doi.org/10.5194/BG-18-2627-2021.

Koch, A., Hubau, W. and Lewis, S.L. (2021) 'Earth system models are not capturing present-day tropical forest carbon dynamics', *Earth's Future*, 9(5), p. e2020EF001874.

Kooperman, G.J., Chen, Y., Hoffman, F.M., Koven, C.D., Lindsay, K., Pritchard, M.S., Swann, A.L.S. and Randerson, J.T. (2018) 'Forest response to rising CO2 drives zonally asymmetric rainfall change over tropical land', *Nature Climate*

Change, 8(5), pp. 434–440. Available at: https://doi.org/10.1038/s41558-018-0144-7.

Koren, G., van Schaik, E., Araújo, A.C., Boersma, K.F., Gärtner, A., Killaars, L., Kooreman, M.L., Kruijt, B., van der Laan-Luijkx, I.T., von Randow, C., Smith, N.E. and Peters, W. (2018) 'Widespread reduction in sun-induced fluorescence from the Amazon during the 2015/2016 El Niño', *Philosophical Transactions of the Royal Society B: Biological Sciences*, 373(1760), p. 20170408. Available at: https://doi.org/10.1098/rstb.2017.0408.

Langenbrunner, B., Pritchard, M.S., Kooperman, G.J. and Randerson, J.T. (2019) 'Why Does Amazon Precipitation Decrease When Tropical Forests Respond to Increasing CO2?', *Earth's Future*, 7(4), pp. 450–468. Available at: https://doi.org/10.1029/2018EF001026.

Lashof, D.A. and Ahuja, D.R. (1990) 'Relative contributions of greenhouse gas emissions to global warming', *Nature*, 344(6266), pp. 529–531. Available at: https://doi.org/10.1038/344529a0.

Lawrence, D.M., Hurtt, G.C., Arneth, A., Brovkin, V., Calvin, K.V., Jones, A.D., Jones, C.D., Lawrence, P.J., Noblet-Ducoudré, N.D., Pongratz, J., Seneviratne, S.I. and Shevliakova, E. (2016) 'The Land Use Model Intercomparison Project (LUMIP) contribution to CMIP6: Rationale and experimental design', *Geoscientific Model Development*, 9(9), pp. 2973–2998. Available at: https://doi.org/10.5194/gmd-9-2973-2016.

Le, T. (2023) 'Increased impact of the El Niño–Southern Oscillation on global vegetation under future warming environment', *Scientific Reports*, 13(1), p. 14459. Available at: https://doi.org/10.1038/s41598-023-41590-8.

Le, T., Ha, K.J. and Bae, D.H. (2021) 'Increasing Causal Effects of El Niño–Southern Oscillation on the Future Carbon Cycle of Terrestrial Ecosystems', *Geophysical Research Letters*, 48(24), p. e2021GL095804-e2021GL095804. Available at: https://doi.org/10.1029/2021GL095804.

Lee, J. and Hohenegger, C. (2024) 'Weaker land–atmosphere coupling in global storm-resolving simulation', *Proceedings of the National Academy of Sciences*, 121(12), p. e2314265121. Available at: https://doi.org/10.1073/pnas.2314265121.

Lee, X., Goulden, M.L., Hollinger, D.Y., Barr, A., Black, T.A., Bohrer, G., Bracho, R., Drake, B., Goldstein, A., Gu, L., Katul, G., Kolb, T., Law, B.E., Margolis, H., Meyers, T., Monson, R., Munger, W., Oren, R., Paw U, K.T., Richardson, A.D., Schmid, H.P., Staebler, R., Wofsy, S. and Zhao, L. (2011) 'Observed increase in local cooling effect of deforestation at higher latitudes', *Nature*, 479(7373), pp. 384–387. Available at: https://doi.org/10.1038/nature10588.

Lejeune, Q., Davin, E.L., Gudmundsson, L., Winckler, J. and Seneviratne, S.I. (2018) 'Historical deforestation locally increased the intensity of hot days in northern mid-latitudes', *Nature Climate Change*, 8(5), pp. 386–390.

Levasseur, A., Cavalett, O., Fuglestvedt, J.S., Gasser, T. and Johansson, D. (2016) 'JA, Jørgensen, SV,… Cherubini, F.(2016). Enhancing life cycle impact assessment from climate science: Review of recent findings and recommendations for application to LCA', *Ecological Indicators*, 71, pp. 163–174.

Lin, S., Hu, Z., Wang, Y., Chen, X., He, B., Song, Z., Sun, S., Wu, C., Zheng, Y., Xia, X., Liu, L., Tang, J., Sun, Q., Joos, F. and Yuan, W. (2023) 'Underestimated Interannual Variability of Terrestrial Vegetation Production by Terrestrial Ecosystem Models', *Global Biogeochemical Cycles*, 37(4), p. e2023GB007696. Available at: https://doi.org/10.1029/2023GB007696.

Liu, J., Bowman, K.W., Schimel, D.S., Parazoo, N.C., Jiang, Z., Lee, M., Bloom, A.A., Wunch, D., Frankenberg, C., Sun, Y., O'Dell, C.W., Gurney, K.R., Menemenlis, D., Gierach, M., Crisp, D. and Eldering, A. (2017) 'Contrasting carbon cycle responses of the tropical continents to the 2015–2016 El Niño', *Science*, 358(6360). Available at: https://doi.org/10.1126/science.aam5690.

Liu, L., Gudmundsson, L., Hauser, M., Qin, D., Li, S. and Seneviratne, S.I. (2020) 'Soil moisture dominates dryness stress on ecosystem production globally', *Nature communications*, 11(1), p. 4892.

Liu, S., Hua, W., Zhou, L., Chen, H., Yu, M., Li, X. and Cui, Y. (2023) 'Local and Non-Local Biophysical Impacts of Deforestation on Global Temperature During Boreal Summer: CMIP6-LUMIP Multimodel Analysis', *Journal of Geophysical Research: Atmospheres*, 128(11), p. e2022JD038229. Available at: https://doi.org/10.1029/2022JD038229.

Loughran, T.F., Ziehn, T., Law, R., Canadell, J.G., Pongratz, J., Liddicoat, S., Hajima, T., Ito, A., Lawrence, D.M. and Arora, V.K. (2023) 'Limited Mitigation

Potential of Forestation Under a High Emissions Scenario: Results From Multi-Model and Single Model Ensembles', *Journal of Geophysical Research: Biogeosciences*, 128(12), p. e2023JG007605. Available at: https://doi.org/10.1029/2023JG007605.

Lovato, T., Peano, D., Butenschön, M., Materia, S., Iovino, D., Scoccimarro, E., Fogli, P.G., Cherchi, A., Bellucci, A. and Gualdi, S. (2022) 'CMIP6 Simulations With the CMCC Earth System Model (CMCC-ESM2)', *Journal of Advances in Modeling Earth Systems*, 14(3), p. e2021MS002814.

Lovejoy, T.E. and Nobre, C. (2019) *Amazon tipping point: Last chance for action*, *Science Advances*. American Association for the Advancement of Science, p. eaba2949.

Luo, X., Ge, J., Guo, W., Cao, Y., Liu, Y., Chen, C. and Yang, L. (2023) 'An Evaluation of CMIP6 Models in Representing the Biophysical Effects of Deforestation With Satellite-Based Observations', *Journal of Geophysical Research: Atmospheres*, 128(12), p. e2022JD038198. Available at: https://doi.org/10.1029/2022JD038198.

Luo, X., Ge, J., Guo, W., Fan, L., Chen, C., Liu, Y. and Yang, L. (2022) 'The Biophysical Impacts of Deforestation on Precipitation: Results from the CMIP6 Model Intercomparison', *Journal of Climate*, 35(11), pp. 3293–3311. Available at: https://doi.org/10.1175/JCLI-D-21-0689.1.

Luyssaert, S., Jammet, M., Stoy, P.C., Estel, S., Pongratz, J., Ceschia, E., Churkina, G., Don, A., Erb, K. and Ferlicoq, M. (2014) 'Land management and land-cover change have impacts of similar magnitude on surface temperature', *Nature Climate Change*, 4(5), pp. 389–393.

Lynch, J., Cain, M., Frame, D. and Pierrehumbert, R. (2021) 'Agriculture's Contribution to Climate Change and Role in Mitigation Is Distinct From Predominantly Fossil CO2-Emitting Sectors', *Frontiers in Sustainable Food Systems*, 4, pp. 300–300. Available at: https://doi.org/10.3389/FSUFS.2020.518039/BIBTEX.

Lynch, J., Cain, M., Pierrehumbert, R. and Allen, M. (2020) 'Demonstrating GWP: A means of reporting warming-equivalent emissions that captures the contrasting impacts of short- A nd long-lived climate pollutants', *Environmental Research Letters*, 15(4). Available at: https://doi.org/10.1088/1748-9326/ab6d7e.

Ma, Y., Yue, X., Zhou, H., Gong, C., Lei, Y., Tian, C. and Cao, Y. (2021) 'Identifying the dominant climate-driven uncertainties in modeling gross primary productivity', *Science of The Total Environment*, 800, p. 149518. Available at: https://doi.org/10.1016/j.scitotenv.2021.149518.

MacDougall, A.H., Frölicher, T.L., Jones, C.D., Rogelj, J., Matthews, H.D., Zickfeld, K., Arora, V.K., Barrett, N.J., Brovkin, V., Burger, F.A., Eby, M., Eliseev, A.V., Hajima, T., Holden, P.B., Jeltsch-Thömmes, A., Koven, C., Mengis, N., Menviel, L., Michou, M., Mokhov, I.I., Oka, A., Schwinger, J., Séférian, R., Shaffer, G., Sokolov, A., Tachiiri, K., Tjiputra, J., Wiltshire, A. and Ziehn, T. (2020) 'Is there warming in the pipeline? A multi-model analysis of the Zero Emissions Commitment from CO_2', *Biogeosciences*, 17(11), pp. 2987–3016. Available at: https://doi.org/10.5194/bg-17-2987-2020.

Mackenzie, F.T. and Lerman, A. (2006) *Carbon in the Geobiosphere:-Earth's Outer Shell*. Springer Science & Business Media.

Manne, A.S. and Richels, R.G. (2001) 'An alternative approach to establishing trade-offs among greenhouse gases', *Nature*, 410(6829), pp. 675–677. Available at: https://doi.org/10.1038/35070541.

Masson-Delmotte, V., Zhai, P., Pörtner, H.-O., Roberts, D., Skea, J. and Shukla, P.R. (2022) *Global Warming of 1.5° C: IPCC Special Report on Impacts of Global Warming of 1.5° C above Pre-industrial Levels in Context of Strengthening Response to Climate Change, Sustainable Development, and Efforts to Eradicate Poverty*. Cambridge University Press.

Matthews, H.D., Gillett, N.P., Stott, P.A. and Zickfeld, K. (2009) 'The proportionality of global warming to cumulative carbon emissions', *Nature*, 459(7248), pp. 829–832. Available at: https://doi.org/10.1038/nature08047.

Matthews, H.D., Tokarska, K.B., Nicholls, Z.R., Rogelj, J., Canadell, J.G., Friedlingstein, P., Frölicher, T.L., Forster, P.M., Gillett, N.P. and Ilyina, T. (2020) 'Opportunities and challenges in using remaining carbon budgets to guide climate policy', *Nature geoscience*, 13(12), pp. 769–779.

Mauritsen, T., Bader, J., Becker, T., Behrens, J., Bittner, M., Brokopf, R., Brovkin, V., Claussen, M., Crueger, T. and Esch, M. (2019) 'Developments in the MPI-M Earth System Model version 1.2 (MPI-ESM1. 2) and its response to increasing CO2', *Journal of Advances in Modeling Earth Systems*, 11(4), pp. 998–1038.

McGregor, S., Cassou, C., Kosaka, Y. and Phillips, A.S. (2022) 'Projected ENSO Teleconnection Changes in CMIP6', *Geophysical Research Letters*, 49(11), p. e2021GL097511-e2021GL097511. Available at: https://doi.org/10.1029/2021GL097511.

Mcphaden, M.J., Santoso, A. and Cai, W. (2021a) *ENSO and the Carbon Cycle*.

Mcphaden, M.J., Santoso, A. and Cai, W. (2021b) *ENSO Teleconnections*.

Melnikova, I., Boucher, O., Cadule, P., Ciais, P., Gasser, T., Quilcaille, Y., Shiogama, H., Tachiiri, K., Yokohata, T. and Tanaka, K. (2021) 'Carbon cycle response to temperature overshoot beyond 2 C: An analysis of CMIP6 models', *Earth's Future*, 9(5).

Melnikova, I., Ciais, P., Boucher, O. and Tanaka, K. (2023) 'Assessing carbon cycle projections from complex and simple models under SSP scenarios', *Climatic Change*, 176(12), p. 168. Available at: https://doi.org/10.1007/s10584-023-03639-5.

Melnikova, I., Ciais, P., Tanaka, K., Shiogama, H., Tachiiri, K., Yokohata, T. and Boucher, O. (2025) 'Carbon cycle and climate feedbacks under CO_2 and non-CO_2 overshoot pathways', *Earth System Dynamics*, 16(1), pp. 257–273. Available at: https://doi.org/10.5194/esd-16-257-2025.

Mengis, N. and Matthews, H.D. (2020) 'Non-CO2 forcing changes will likely decrease the remaining carbon budget for 1.5 °C', *npj Climate and Atmospheric Science*, 3(1), pp. 1–7. Available at: https://doi.org/10.1038/s41612-020-0123-3.

Millar, R.J., Nicholls, Z.R., Friedlingstein, P. and Allen, M.R. (2017) 'A modified impulse-response representation of the global near-surface air temperature and atmospheric concentration response to carbon dioxide emissions', *Atmospheric Chemistry and Physics*, 17(11), pp. 7213–7228. Available at: https://doi.org/10.5194/acp-17-7213-2017.

Muñoz-Sabater, J., Dutra, E., Agustí-Panareda, A., Albergel, C., Arduini, G., Balsamo, G., Boussetta, S., Choulga, M., Harrigan, S. and Hersbach, H. (2021) 'ERA5-Land: A state-of-the-art global reanalysis dataset for land applications', *Earth System Science Data*, 13(9), pp. 4349–4383.

Myhre, G., Shindell, D., Bréon, F.-M., Collins, W., Fuglestvedt, J., Huang, J., Koch, D., Lamarque, J.-F., Lee, D., Mendoza, B., Nakajima, T., Robock, A., Stephens, G.,

Zhang, H., Aamaas, B., Boucher, O., Dalsøren, S.B., Daniel, J.S., Forster, P., Granier, C., Haigh, J., Hodnebrog, Ø., Kaplan, J.O., Marston, G., Nielsen, C.J., O'Neill, B.C., Peters, G.P., Pongratz, J., Ramaswamy, V., Roth, R., Rotstayn, L., Smith, S.J., Stevenson, D., Vernier, J.-P., Wild, O., Young, P., Jacob, D., Ravishankara, A.R. and Shine, K. (2013) 'Anthropogenic and Natural Radiative Forcing', in *Climate Change 2013: The Physical Science Basis. Contribution of Working Group I to the Fifth Assessment Report of the Intergovernmental Panel on Climate Change*. Cambridge, United Kingdom and New York, NY, USA: Cambridge University Press.

Net Zero Tracker / NewClimate Institute (no date). Available at: https://newclimate.org/what-we-do/projects/net-zero-tracker (Accessed: 19 July 2024).

Nicholls, Z., Meinshausen, M., Lewis, J., Gieseke, R., Dommenget, D., Dorheim, K., Fan5, C.S., Fuglestvedt, J.S., Gasser, T., Goluke, U., Goodwin, P., Hartin, C., P. Hope, A., Kriegler, E., J. Leach, N., Marchegiani, D., A. McBride, L., Quilcaille, Y., Rogelj, J., J. Salawitch, R., Samset, B.H., Sandstad, M., N. Shiklomanov, A., B. Skeie, R., J. Smith, C., Smith, S., Tanaka, K., Tsutsui, J. and Xie, Z. (2020) 'Reduced Complexity Model Intercomparison Project Phase 1: Introduction and evaluation of global-mean temperature response', *Geoscientific Model Development*, 13(11), pp. 5175–5190. Available at: https://doi.org/10.5194/GMD-13-5175-2020.

O'Neill, B.C. (2003) 'Economics, Natural Science, and the Costs of Global Warming Potentials', *Climatic Change*, 58(3), pp. 251–260. Available at: https://doi.org/10.1023/A:1023968127813.

O'Neill, B.C., Tebaldi, C., Van Vuuren, D.P., Eyring, V., Friedlingstein, P., Hurtt, G., Knutti, R., Kriegler, E., Lamarque, J.F., Lowe, J., Meehl, G.A., Moss, R., Riahi, K. and Sanderson, B.M. (2016) 'The Scenario Model Intercomparison Project (ScenarioMIP) for CMIP6', *Geoscientific Model Development*, 9(9), pp. 3461–3482. Available at: https://doi.org/10.5194/GMD-9-3461-2016.

O'Sullivan, M., Spracklen, D.V., Batterman, S.A., Arnold, S.R., Gloor, M. and Buermann, W. (2019) 'Have synergies between nitrogen deposition and atmospheric CO2 driven the recent enhancement of the terrestrial carbon sink?', *Global Biogeochemical Cycles*, 33(2), pp. 163–180.

Pan, Y., Birdsey, R.A., Fang, J., Houghton, R., Kauppi, P.E., Kurz, W.A., Phillips, O.L., Shvidenko, A., Lewis, S.L. and Canadell, J.G. (2011) 'A large and persistent carbon sink in the world's forests', *Science*, 333(6045), pp. 988–993.

Park, S.W., Kim, J.S., Kug, J.S., Stuecker, M.F., Kim, I.W. and Williams, M. (2020) 'Two Aspects of Decadal ENSO Variability Modulating the Long-Term Global Carbon Cycle', *Geophysical Research Letters*, 47(8). Available at: https://doi.org/10.1029/2019GL086390.

Parsons, L.A. (2020) 'Implications of CMIP6 Projected Drying Trends for 21st Century Amazonian Drought Risk', *Earth's Future*, 8(10), p. e2020EF001608-e2020EF001608. Available at: https://doi.org/10.1029/2020EF001608.

Pedregosa, F., Varoquaux, G., Gramfort, A., Michel, V., Thirion, B., Grisel, O., Blondel, M., Prettenhofer, P., Weiss, R., Dubourg, V., Vanderplas, J., Passos, A. and Cournapeau, D. (2012) 'Scikit-learn: Machine Learning in Python', *MACHINE LEARNING IN PYTHON* [Preprint].

Peng, S., Terrer, C., Smith, B., Ciais, P., Han, Q., Nan, J., Fisher, J.B., Chen, L., Deng, L. and Yu, K. (2024) 'Carbon restoration potential on global land under water resource constraints', *Nature Water*, 2(11), pp. 1071–1081. Available at: https://doi.org/10.1038/s44221-024-00323-5.

Perry, S.J., McGregor, S., Sen Gupta, A., England, M.H. and Maher, N. (2020) 'Projected late 21st century changes to the regional impacts of the El Niño-Southern Oscillation', *Climate Dynamics*, 54(1–2), pp. 395–412. Available at: https://doi.org/10.1007/S00382-019-05006-6/FIGURES/10.

Phillips, O.L., Aragão, L.E., Lewis, S.L., Fisher, J.B., Lloyd, J., López-González, G., Malhi, Y., Monteagudo, A., Peacock, J. and Quesada, C.A. (2009) 'Drought sensitivity of the Amazon rainforest', *Science*, 323(5919), pp. 1344–1347.

Piao, S., Wang, X., Wang, K., Li, X., Bastos, A., Canadell, J.G., Ciais, P., Friedlingstein, P. and Sitch, S. (2020) 'Interannual variation of terrestrial carbon cycle: Issues and perspectives', *Global Change Biology*, 26(1), pp. 300–318. Available at: https://doi.org/10.1111/GCB.14884.

Pierrehumbert, R.T. (2014) 'Short-Lived Climate Pollution', *Annual Review of Earth and Planetary Sciences*, 42(1), pp. 341–379. Available at: https://doi.org/10.1146/annurev-earth-060313-054843.

Pongratz, J., Reick, C.H., Raddatz, T. and Claussen, M. (2010) 'Biogeophysical versus biogeochemical climate response to historical anthropogenic land cover change', *Geophysical Research Letters*, 37(8).

Pongratz, J., Schwingshackl, C., Bultan, S., Obermeier, W., Havermann, F. and Guo, S. (2021) 'Land Use Effects on Climate: Current State, Recent Progress, and Emerging Topics', *Current Climate Change Reports 2021*, 1, pp. 1–22. Available at: https://doi.org/10.1007/S40641-021-00178-Y.

Raoult, N., Jupp, T., Booth, B. and Cox, P. (2023) 'Combining local model calibration with the emergent constraint approach to reduce uncertainty in the tropical land carbon cycle feedback', *Earth System Dynamics*, 14(4), pp. 723–731. Available at: https://doi.org/10.5194/esd-14-723-2023.

Rayner, N.A.A., Parker, D.E., Horton, E.B., Folland, C.K., Alexander, L.V., Rowell, D.P., Kent, E.C. and Kaplan, A. (2003) 'Global analyses of sea surface temperature, sea ice, and night marine air temperature since the late nineteenth century', *Journal of Geophysical Research: Atmospheres*, 108(D14).

Reichstein, M., Camps-Valls, G., Stevens, B., Jung, M., Denzler, J., Carvalhais, N. and Prabhat (2019) 'Deep learning and process understanding for data-driven Earth system science', *Nature*, 566(7743), pp. 195–204. Available at: https://doi.org/10.1038/s41586-019-0912-1.

Riahi, K., Bertram, C., Huppmann, D., Rogelj, J., Bosetti, V., Cabardos, A.-M., Deppermann, A., Drouet, L., Frank, S., Fricko, O., Fujimori, S., Harmsen, M., Hasegawa, T., Krey, V., Luderer, G., Paroussos, L., Schaeffer, R., Weitzel, M., van der Zwaan, B., Vrontisi, Z., Longa, F.D., Després, J., Fosse, F., Fragkiadakis, K., Gusti, M., Humpenöder, F., Keramidas, K., Kishimoto, P., Kriegler, E., Meinshausen, M., Nogueira, L.P., Oshiro, K., Popp, A., Rochedo, P.R.R., Ünlü, G., van Ruijven, B., Takakura, J., Tavoni, M., van Vuuren, D. and Zakeri, B. (2021) 'Cost and attainability of meeting stringent climate targets without overshoot', *Nature Climate Change*, 11(12), pp. 1063–1069. Available at: https://doi.org/10.1038/s41558-021-01215-2.

Rogelj, J., den Elzen, M., Höhne, N., Fransen, T., Fekete, H., Winkler, H., Schaeffer, R., Sha, F., Riahi, K. and Meinshausen, M. (2016) 'Paris Agreement climate proposals need a boost to keep warming well below 2 °C', *Nature*, 534(7609), pp. 631–639. Available at: https://doi.org/10.1038/nature18307.

Rogelj, J., Forster, P.M., Kriegler, E., Smith, C.J. and Séférian, R. (2019) 'Estimating and tracking the remaining carbon budget for stringent climate targets', *Nature*, 571(7765), pp. 335–342. Available at: https://doi.org/10.1038/s41586-019-1368-z.

Rogelj, J., Huppmann, D., Krey, V., Riahi, K., Clarke, L., Gidden, M., Nicholls, Z. and Meinshausen, M. (2019) 'A new scenario logic for the Paris Agreement long-term temperature goal', *Nature*, 573(7774), pp. 357–363. Available at: https://doi.org/10.1038/s41586-019-1541-4.

Rogelj, J., Popp, A., Calvin, K.V., Luderer, G., Emmerling, J., Gernaat, D., Fujimori, S., Strefler, J., Hasegawa, T. and Marangoni, G. (2018) 'Scenarios towards limiting global mean temperature increase below 1.5 C', *Nature Climate Change*, 8(4), pp. 325–332.

Rogelj, J., Shindell, D., Jiang, K., Fifita, S., Forster, P., Ginzburg, V., Handa, C., Kheshgi, H., Kobayashi, S. and Kriegler, E. (2018) 'Mitigation pathways compatible with 1.5 C in the context of sustainable development', in *Global warming of 1.5 Global Warming of 1.5°C. An IPCC Special Report on the impacts of global warming of 1.5°C above pre-industrial levels and related global greenhouse gas emission pathways, in the context of strengthening the global response to the threat of climate change, sustainable development, and efforts to eradicate poverty*. Cambridge, United Kingdom and New York, NY, USA: Cambridge University Press, pp. 93–174.

Schmidt, G. (2024) 'Climate models can't explain 2023's huge heat anomaly — we could be in uncharted territory', *Nature*, 627(8004), pp. 467–467. Available at: https://doi.org/10.1038/d41586-024-00816-z.

Séférian, R., Nabat, P., Michou, M., Saint-Martin, D., Voldoire, A., Colin, J., Decharme, B., Delire, C., Berthet, S. and Chevallier, M. (2019) 'Evaluation of CNRM earth system model, CNRM-ESM2-1: Role of earth system processes in present-day and future climate', *Journal of Advances in Modeling Earth Systems*, 11(12), pp. 4182–4227.

Seland, Ø., Bentsen, M., Olivié, D., Toniazzo, T., Gjermundsen, A., Graff, L.S., Debernard, J.B., Gupta, A.K., He, Y.-C. and Kirkevåg, A. (2020) 'Overview of the Norwegian Earth System Model (NorESM2) and key climate response of CMIP6 DECK, historical, and scenario simulations', *Geoscientific Model Development*, 13(12), pp. 6165–6200.

Sellar, A.A., Jones, C.G., Mulcahy, J.P., Tang, Y., Yool, A., Wiltshire, A., O'connor, F.M., Stringer, M., Hill, R. and Palmieri, J. (2019) 'UKESM1: Description and evaluation of the UK Earth System Model', *Journal of Advances in Modeling Earth Systems*, 11(12), pp. 4513–4558.

Shine, K.P., Berntsen, T.K., Fuglestvedt, J.S., Skeie, R.B. and Stuber, N. (2007) 'Comparing the climate effect of emissions of short- and long-lived climate agents', *Philosophical Transactions of the Royal Society A: Mathematical, Physical and Engineering Sciences*, 365(1856), pp. 1903–1914. Available at: https://doi.org/10.1098/rsta.2007.2050.

Shukla, P.R., Skea, J., Calvo Buendia, E., Masson-Delmotte, V., Pörtner, H.O., Roberts, D.C., Zhai, P., Slade, R., Connors, S. and Van Diemen, R. (2019) 'IPCC, 2019: Climate Change and Land: an IPCC special report on climate change, desertification, land degradation, sustainable land management, food security, and greenhouse gas fluxes in terrestrial ecosystems'.

Smith, C.J., Forster, P.M., Allen, M., Leach, N., Millar, R.J., Passerello, G.A. and Regayre, L.A. (2018) 'FAIR v1.3: a simple emissions-based impulse response and carbon cycle model', *Geoscientific Model Development*, 11(6), pp. 2273–2297. Available at: https://doi.org/10.5194/gmd-11-2273-2018.

Smith, C.J., Kramer, R.J., Myhre, G., Alterskjær, K., Collins, W., Sima, A., Boucher, O., Dufresne, J.-L., Nabat, P., Michou, M., Yukimoto, S., Cole, J., Paynter, D., Shiogama, H., O'Connor, F.M., Robertson, E., Wiltshire, A., Andrews, T., Hannay, C., Miller, R., Nazarenko, L., Kirkevåg, A., Olivié, D., Fiedler, S., Lewinschal, A., Mackallah, C., Dix, M., Pincus, R. and Forster, P.M. (2020) 'Effective radiative forcing and adjustments in CMIP6 models', *Atmospheric Chemistry and Physics*, 20(16), pp. 9591–9618. Available at: https://doi.org/10.5194/acp-20-9591-2020.

Smith, M.A., Cain, M. and Allen, M.R. (2021) 'Further improvement of warming-equivalent emissions calculation', *npj Climate and Atmospheric Science 2021 4:1*, 4(1), pp. 1–3. Available at: https://doi.org/10.1038/s41612-021-00169-8.

Smith, S.M., Lowe, J.A., Bowerman, N.H.A., Gohar, L.K., Huntingford, C. and Allen, M.R. (2012) 'Equivalence of greenhouse-gas emissions for peak temperature limits.', *Nature Climate Change*, 2(July), pp. 535–538.

Sonntag, S., Ferrer González, M., Ilyina, T., Kracher, D., Nabel, J.E.M.S., Niemeier, U., Pongratz, J., Reick, C.H. and Schmidt, H. (2018) 'Quantifying and Comparing Effects of Climate Engineering Methods on the Earth System', *Earth's Future*, 6(2), pp. 149–168. Available at: https://doi.org/10.1002/2017EF000620.

Sonntag, S., Pongratz, J., Reick, C.H. and Schmidt, H. (2016) 'Reforestation in a high-CO2 world—Higher mitigation potential than expected, lower adaptation potential than hoped for', *Geophysical Research Letters*, 43(12), pp. 6546–6553. Available at: https://doi.org/10.1002/2016GL068824.

Stehfest, E. (2014) 'Integrated Assessment of Global Environmental Change with IMAGE 3.0, Model description and policy applications'. The Hague. Available at: https://www.pbl.nl/sites/default/files/downloads/pbl-2014-integrated_assessment_of_global_environmental_change_with_image30_735.pdf (Accessed: 1 July 2024).

Swart, N.C., Cole, J.N., Kharin, V.V., Lazare, M., Scinocca, J.F., Gillett, N.P., Anstey, J., Arora, V., Christian, J.R. and Hanna, S. (2019) 'The Canadian earth system model version 5 (CanESM5. 0.3)', *Geoscientific Model Development*, 12(11), pp. 4823–4873.

Tachiiri, K., Hajima, T. and Kawamiya, M. (2019) 'Increase of the transient climate response to cumulative carbon emissions with decreasing CO2 concentration scenarios', *Environmental Research Letters*, 14(12). Available at: https://doi.org/10.1088/1748-9326/ab57d3.

Tanaka, K., Boucher, O., Ciais, P., Johansson, D.J.A. and Morfeldt, J. (2021) 'Cost-effective implementation of the Paris Agreement using flexible greenhouse gas metrics', *Science Advances*, 7. Available at: http://advances.sciencemag.org/.

Tanaka, K., Cavalett, O., Collins, W.J. and Cherubini, F. (2019) 'Asserting the climate benefits of the coal-to-gas shift across temporal and spatial scales', *Nature Climate Change* [Preprint]. Available at: https://doi.org/10.1038/s41558-019-0457-1.

Tanaka, K., Johansson, D.J.A., O'Neill, B.C. and Fuglestvedt, J.S. (2013) 'Emission metrics under the 2 °C climate stabilization target', *Climatic Change*, 117(4), pp. 933–941. Available at: https://doi.org/10.1007/s10584-013-0693-8.

Tanaka, K., Kriegler, E., Bruckner, T., Hooss, G., Knorr, W., Raddatz, T. and Tol, R. (2007) *Aggregated Carbon cycle, atmospheric chemistry and climate model (ACC2): description of forward and inverse mode*.

Tanaka, K. and O'Neill, B.C. (2018) 'The Paris Agreement zero-emissions goal is not always consistent with the 1.5 °C and 2 °C temperature targets', *Nature Climate Change 2018 8:4*, 8(4), pp. 319–324. Available at: https://doi.org/10.1038/s41558-018-0097-x.

Tanaka, K., Peters, G.P. and Fuglestvedt, J.S. (2010) 'Policy Update: Multicomponent climate policy: why do emission metrics matter?', *Carbon Management*, 1(2), pp. 191–197. Available at: https://doi.org/10.4155/cmt.10.28.

Tanaka, Katsumasa, O'neill, Brian C, Rokityanskiy, Dmitry, Obersteiner, M., Tol, Richard S J, Tanaka, K, Rokityanskiy, · D, Obersteiner, · M, Tol, · R S J, O'neill, B C, Rokityanskiy, D and Tol, R S J (2009) 'Evaluating Global Warming Potentials with historical temperature', *Climatic Change 2009 96:4*, 96(4), pp. 443–466. Available at: https://doi.org/10.1007/S10584-009-9566-6.

Tokarska, K.B., Arora, V.K., Gillett, N.P., Lehner, F., Rogelj, J., Schleussner, C.-F., Séférian, R. and Knutti, R. (2020) 'Uncertainty in carbon budget estimates due to internal climate variability', *Environmental Research Letters*, 15(10), p. 104064. Available at: https://doi.org/10.1088/1748-9326/abaf1b.

Tokarska, K.B., Zickfeld, K. and Rogelj, J. (2019) 'Path Independence of Carbon Budgets When Meeting a Stringent Global Mean Temperature Target After an Overshoot', *Earth's Future*, 7(12), pp. 1283–1295. Available at: https://doi.org/10.1029/2019EF001312.

Tol, R.S.J., Berntsen, T.K., O'Neill, B.C., Fuglestvedt, J.S. and Shine, K.P. (2012) 'A unifying framework for metrics for aggregating the climate effect of different emissions', *Environmental Research Letters*, 7(4), p. 044006. Available at: https://doi.org/10.1088/1748-9326/7/4/044006.

UNFCCC (2018) 'Report of the Conference of the Parties serving as the meeting of the Parties to the Paris Agreement on the third part of its first session, held in Katowice from 3 to 14 December 2018. Addendum 2'.

UNFCCC (2023) *Common metrics / UNFCCC*. Available at: https://unfccc.int/process-and-meetings/transparency-and-reporting/methods-for-climate-change-transparency/common-metrics (Accessed: 13 January 2023).

Uribe, M. del R., Coe, M.T., Castanho, A.D., Macedo, M.N., Valle, D. and Brando, P.M. (2023) 'Net loss of biomass predicted for tropical biomes in a changing climate', *Nature Climate Change*, pp. 1–8.

Van Vuuren, D.P., Stehfest, E., Gernaat, D.E., Doelman, J.C., Van den Berg, M., Harmsen, M., de Boer, H.S., Bouwman, L.F., Daioglou, V. and Edelenbosch, O.Y. (2017) 'Energy, land-use and greenhouse gas emissions trajectories under a green growth paradigm', *Global Environmental Change*, 42, pp. 237–250.

Venter, O., Sanderson, E.W., Magrach, A., Allan, J.R., Beher, J., Jones, K.R., Possingham, H.P., Laurance, W.F., Wood, P., Fekete, B.M., Levy, M.A. and Watson, J.E.M. (2016) 'Sixteen years of change in the global terrestrial human footprint and implications for biodiversity conservation', *Nature Communications*, 7(1), p. 12558. Available at: https://doi.org/10.1038/ncomms12558.

Walker, A.P., De Kauwe, M.G., Bastos, A., Belmecheri, S., Georgiou, K., Keeling, R.F., McMahon, S.M., Medlyn, B.E., Moore, D.J. and Norby, R.J. (2021) 'Integrating the evidence for a terrestrial carbon sink caused by increasing atmospheric CO2', *New phytologist*, 229(5), pp. 2413–2445.

Weedon, G.P., Balsamo, G., Bellouin, N., Gomes, S., Best, M.J. and Viterbo, P. (2014) 'The WFDEI meteorological forcing data set: WATCH Forcing Data methodology applied to ERA-Interim reanalysis data', *Water Resources Research*, 50(9), pp. 7505–7514. Available at: https://doi.org/10.1002/2014WR015638.

Wigley, T.M.L. (1998) 'The Kyoto Protocol: CO2 CH4 and climate implications', *Geophysical Research Letters*, 25(13), pp. 2285–2288. Available at: https://doi.org/10.1029/98GL01855.

Winckler, J., Lejeune, Q., Reick, C.H. and Pongratz, J. (2019) 'Nonlocal effects dominate the global mean surface temperature response to the biogeophysical effects of deforestation', *Geophysical Research Letters*, 46(2), pp. 745–755.

Winckler, J., Reick, C.H., Bright, R.M. and Pongratz, J. (2019) 'Importance of surface roughness for the local biogeophysical effects of deforestation', *Journal of Geophysical Research: Atmospheres*, 124(15), pp. 8605–8618.

Winckler, J., Reick, C.H., Luyssaert, S., Cescatti, A., Stoy, P.C., Lejeune, Q., Raddatz, T., Chlond, A., Heidkamp, M. and Pongratz, J. (2019) 'Different response of surface temperature and air temperature to deforestation in climate models', *Earth System Dynamics*, 10(3), pp. 473–484. Available at: https://doi.org/10.5194/esd-10-473-2019.

Winckler, J., Reick, C.H. and Pongratz, J. (2017) 'Robust identification of local biogeophysical effects of land-cover change in a global climate model', *Journal of Climate*, 30(3), pp. 1159–1176.

Xiong, W., Tanaka, K., Ciais, P., Johansson, D.J.A. and Lehtveer, M. (2023) 'emIAM v1.0: an emulator for Integrated Assessment Models using marginal abatement cost curves', *EGUsphere*, pp. 1–39.

Xiong, W., Tanaka, K., Ciais, P. and Yan, L. (2022) 'Evaluating China's Role in Achieving the 1.5 °C Target of the Paris Agreement', *Energies*, 15(16), p. 6002. Available at: https://doi.org/10.3390/en15166002.

Xu, W., Chang, J., Ciais, P., Guenet, B., Viovy, N., Ito, A., Reyer, C.P.O., Tian, H., Shi, H., Frieler, K., Forrest, M., Ostberg, S., Schaphoff, S. and Hickler, T. (2020) 'Reducing Uncertainties of Future Global Soil Carbon Responses to Climate and Land Use Change With Emergent Constraints', *Global Biogeochemical Cycles*, 34(10), p. e2020GB006589. Available at: https://doi.org/10.1029/2020GB006589.

Yan, R., Wang, J., Ju, W., Goll, D.S., Jain, A.K., Sitch, S., Tian, H., Benjamin, P., Jiang, F. and Wang, H. (2023) 'Interactive effects of the El Niño-Southern Oscillation and Indian Ocean Dipole on the tropical net ecosystem productivity', *Agricultural and Forest Meteorology*, 336, p. 109472. Available at: https://doi.org/10.1016/j.agrformet.2023.109472.

Yeh, S.W., Cai, W., Min, S.K., McPhaden, M.J., Dommenget, D., Dewitte, B., Collins, M., Ashok, K., An, S.I., Yim, B.Y. and Kug, J.S. (2018) 'ENSO Atmospheric Teleconnections and Their Response to Greenhouse Gas Forcing', *Reviews of Geophysics*, 56(1), pp. 185–206. Available at: https://doi.org/10.1002/2017RG000568.

Yukimoto, S., Kawai, H., Koshiro, T., Oshima, N., Yoshida, K., Urakawa, S., Tsujino, H., Deushi, M., Tanaka, T., Hosaka, M., Yabu, S., Yoshimura, H., Shindo, E., Mizuta, R., Obata, A., Adachi, Y. and Ishii, M. (2019) 'The Meteorological Research Institute Earth System Model Version 2.0, MRI-ESM2.0: Description and

Basic Evaluation of the Physical Component', *Journal of the Meteorological Society of Japan. Ser. II*, 97(5), pp. 931–965. Available at: https://doi.org/10.2151/jmsj.2019-051.

Zelinka, M.D., Myers, T.A., McCoy, D.T., Po-Chedley, S., Caldwell, P.M., Ceppi, P., Klein, S.A. and Taylor, K.E. (2020) 'Causes of higher climate sensitivity in CMIP6 models', *Geophysical Research Letters*, 47(1).

Zhang, Y., Dannenberg, M.P., Hwang, T., Song, C., Zhang, Y., Dannenberg, M.P., Hwang, T. and Song, C. (2019) 'El Niño-Southern Oscillation-Induced Variability of Terrestrial Gross Primary Production During the Satellite Era', *JGRG*, 124(8), pp. 2419–2431. Available at: https://doi.org/10.1029/2019JG005117.

Zhang, Y., Wang, X., Lian, X., Li, S., Li, Y., Chen, C. and Piao, S. (2024) 'Asymmetric impacts of forest gain and loss on tropical land surface temperature', *Nature Geoscience*, 17(5), pp. 426–432. Available at: https://doi.org/10.1038/s41561-024-01423-3.

Zheng, X.-T., Hui, C. and Yeh, S.-W. (2017) 'Response of ENSO amplitude to global warming in CESM large ensemble: uncertainty due to internal variability', *Climate Dynamics 2017 50:11*, 50(11), pp. 4019–4035. Available at: https://doi.org/10.1007/S00382-017-3859-7.

Zhu, Q., Riley, W.J., Tang, J., Collier, N., Hoffman, F.M., Yang, X. and Bisht, G. (2019) 'Representing Nitrogen, Phosphorus, and Carbon Interactions in the E3SM Land Model: Development and Global Benchmarking', *Journal of Advances in Modeling Earth Systems*, 11(7), pp. 2238–2258. Available at: https://doi.org/10.1029/2018MS001571.

Zhu, Z., Piao, S., Xu, Y., Bastos, A., Ciais, P. and Peng, S. (2017) 'The effects of teleconnections on carbon fluxes of global terrestrial ecosystems', *Geophysical Research Letters*, 44(7), pp. 3209–3218. Available at: https://doi.org/10.1002/2016GL071743.

Zickfeld, K., Azevedo, D., Mathesius, S. and Damon Matthews, H. (2021) 'Asymmetry in the climate–carbon cycle response to positive and negative CO2 emissions', *Nature Climate Change* [Preprint]. Available at: https://doi.org/10.1038/s41558-021-01061-2.

Zickfeld, K., MacDougall, A.H. and Matthews, H.D. (2016) 'On the proportionality between global temperature change and cumulative CO2 emissions during periods of net negative CO2 emissions', *Environmental Research Letters*, 11(5), pp. 055006–055006.

Ziehn, T., Chamberlain, M.A., Law, R.M., Lenton, A., Bodman, R.W., Dix, M., Stevens, L., Wang, Y.-P. and Srbinovsky, J. (2020) 'The Australian earth system model: ACCESS-ESM1. 5', *Journal of Southern Hemisphere Earth Systems Science*, 70(1), pp. 193–214.